FUNDAMENTAL STUDY OF MEASUREMENT OF LOW CONCENTRATION HYDROGEN SULFIDE IN SERA USING CARBON NANOTUBE

A Thesis Submitted to the College of

Graduate Studies and Research

in Partial Fulfillment of the Requirements

for the Degree of Master of Science

in the Department of Mechanical Engineering

University of Saskatchewan

Saskatoon, Saskatchewan

Canada

By

Junji (Eric) Zhan

PERMISSION TO USE

In presenting this thesis in partial fulfillment of the requirements for a Postgraduate degree from the University of Saskatchewan, I agree that the libraries of this University may make it freely available for inspection. I further agree that permission for copying of this thesis in any manner, in whole or in part, for scholarly purposes may be granted by the professor or professors who supervised my thesis work or, in their absence, by the Head of the Department or the Dean of the College in which my thesis work was done. It is understood that any copying or publication or use of this thesis or parts thereof for financial gain shall not be allowed without my written permission. It is also understood that due recognition shall be given to me and to the University of Saskatchewan in any scholarly use which may be made of any material in my thesis.

Requests for permission to copy or to make other uses of materials in this thesis in whole or part should be addressed to:

Head of the Department of Mechanical Engineering

University of Saskatchewan

Saskatoon, Saskatchewan S7N 5A9

Canada

ABSTRACT

The study presented in this thesis was aimed to gain the fundamental knowledge regarding the mechanism of H_2S measurement in sera by using carbon nanotubes (CNT) and fluorescence response. Characterization techniques such as Raman spectroscopy, X-ray absorption spectroscopy (XAS) and confocal laser scanning microscopy (CLSM) were employed to achieve this goal. The model system used for this study was composed of H_2S, distilled water, two major serum proteins (albumin and globulin), serum, hemoglobin, and CNT.

The results of this study showed that: (1) Two major serum proteins (albumin and globulin) are physically adsorbed on the sidewall of the CNTs; while H_2S is adsorbed on the defect site of the CNTs. (2) Presence of the proteins on the CNTs did not affect the CNT's adsorption of H_2S. (3) Using CLSM with the incident wavelength of 514 nm and the emission wavelength of 530 to 580 nm to acquire the fluorescence response of the H_2S adsorbed on the CNTs is a reliable approach to measure H_2S in sera. (4) Single-wall carbon nanotubes (SWNTs) outperform multi-wall carbon nanotubes (MWNTs) in measurement sensitivity. (5) Presence of hemoglobin in a H_2S solution did not affect the measurement of H_2S with CNTs and CLMS.

The study described in this thesis has provided new knowledge of the interaction behaviors of CNTs with H_2S and major proteins in sera along with the mechanism which governs these behaviors. Such knowledge is very useful to further advance the

CNT approach to sensing H_2S in sera and water solution and to further extend the approach to sensing H_2S in other mammalian tissues such as blood.

ACKNOWLEDGEMENTS

I would like to thank Dr. W. J. (Chris) Zhang who not only served as my supervisor but also encouraged, guided and challenged me throughout completing of this dissertation. I am greatly thankful for his enthusiasm and faith in my capabilities. I would like to extend my appreciation to my co-supervisor Dr. Ramaswami Sammynaiken in Saskatchewan Structural Science Center. He has not only provided his invaluable guidance, but also was patient enough to listen to me at any time I needed expert advice and spent his time discussing spectroscopy theories and spectrum analysis with me. I would also like to thank Dr. Ike Oguocha and Dr. Qiaoqin Yang for their participation as committee members and for their valuable comments. I am also grateful to Dr. Mehdi Nemati for serving as the external examiner and for his valuable suggestions made during the oral defense.

I am greatly indebted to Dr. Xiaochu Wu and Dr. Yongfeng Hu for their valuable comments and help in the process of obtaining the data for the thesis. I am also greatly grateful to Dr. Lingyun Wu in the Department of Pharmacology who allowed me to work in her lab to prepare and test the samples and Mr. Tuanjie Chang for his kind help in the experiment setup. I would also like to thank all the faculty, staff and graduate students for creating an enjoyable learning atmosphere in the Department of Mechanical Engineering.

My special thanks go to Gasotransmitter Research And Training (GREAT) Program for the financial support for my study.

I am greatly thankful to my parents who raised me up in a warm and peaceful atmosphere in full of trusts and encouragements. I deeply thank my father, Mr. Yuntian Zhan, who always supports my study with infinite patience and help. I eternally thank my mother, Ms. Minzhi Wu, who provides any support whenever I need. Thanks for their forever love along with me.

TABLE OF CONTENTS

LIST OF TABLES

LIST OF FIGURES

LIST OF ABBREVIATIONS

AEY: Augur Electron Yield

AFM: Atomic Force Microscopy

ANOVA: Analysis of Variance

AOB: Antioxidant Buffer

BSA: Bovine Serum Albumin

CBS: Cystathionine β-Synthase

CLS: Canadian Light Source

CLSM: Confocal Laser Scanning Microscopy

CNTs: Carbon Nanotubes

CSE: Cystathionine γ-Lyase

CVD: Chemical Vapor Deposition

DWNTs: Double-walled Carbon Nanotubes

EXAFS: Extended X-ray Absorption Fine Structure

FLY: Fluorescence Yield

H_2S: Hydrogen Sulfide

H_2SO_4: Sulfuric Acid

Hb: Hemoglobin

HCL: Hydrochloric Acid

HIPCO: High Pressure Carbon Monoxide Process

HNO_3: Nitric Acid

IgG: Immunoglobulin G

ISE:	Ion-specific Electrode
MWNT:	Multi-Walled Carbon Nanotube
N_2:	Nitrogen
NEXAFS:	Near-edge X-ray Absorption Fine Structure
NSB:	Non-specific Binding
PMT:	Photomultiplier
QCM:	Quartz Crystal Microbalance
RBM:	Radical Breathing Mode
S:	Sulfur
SA:	Streptavidin
SpA:	Staphylococcal Protein A
SSSC:	Saskatchewan Structural Science Center
SWNT:	Single-Walled Carbon Nanotube
SXRMB:	Soft X-ray Micro-characterization Beamline
TEM:	Transmission Electron Microscopy
TEY:	Total Electron Yield
XANES:	X-ray Absorption Near-edge Structure Spectroscopy
XAS:	X-ray Absorption Spectroscopy
XPS:	X-ray Photoelectron Spectroscopy

CHAPTER 1: INTRODUCTION

1.1 H_2S: A General Profile

Hydrogen sulfide (H_2S) is a colorless and flammable gas with a characteristic odor of rotten eggs (ATSDR, 2006). It occurs in nature and is produced by numerous natural and industrial activities. For instance, volcanic sulfur springs, undersea vents, crude petroleum and natural gas contain hydrogen sulfide (Beauchamp *et al*., 1984). It is toxic at a high concentration and usually regarded as both an environmental and industrial pollutant. Thus, most of the previous studies on H_2S were devoted to its toxic effect (Reiffenstein *et al*., 1992).

In human body, it is believed that H_2S is absorbed rapidly through the lungs (Milby *et al*., 1999). H_2S molecule can freely diffuse across membranes, exerting its toxicity by forming sulfides with the active groups of different metalloenzymes and blood pigments; for example, Fe component of cytochrome oxidize can produce sulfide, thereby interrupting cellular respiration activities (Miron *et al*., 1993). The inhalation of high concentration H_2S (greater than 2000 ppm) could lead to unconsciousness (Knezovich *et al*., 1994) and could even be fatal within seconds or minutes in both humans and animals (Reiffenstein *et al*., 1992). Even low concentration H_2S may

change a material from A to B; for example, Ag could become AgS when Ag interacts with H_2S, which is known as "S-pollution" (Canela *et al*., 1998).

1.2 Endogenous H_2S in Mammalian Body

H_2S was found to be endogenously generated from *L-cysteine* in a reaction catalyzed by *cystathionine beta-synthase* (CBS) and/or *cystathionine gamma-lyase* (CSE) in various mammalian cells and tissues (Wang, 2002). For example, rat plasma contains about 50 μM H_2S (Zhao *et al*., 2001), while human blood contains about 10-100 μM of H_2S (Wang, 2003). The level of H_2S in the organ tissue is known to be higher than that in the circulating tissue. For instance, the physiological concentration of H_2S in rat brain tissue is reported to be ~50–160 μM (Hosoki *et al*., 1997).

In some tissues, both CBS and CSE contribute to generating H_2S; while in others only one of them may contribute. It is believed that CSE is the main enzyme responsible for the generation of H_2S in the cardiovascular system (Wang, 2003). On the other hand, CBS seems to play a major role in generating H_2S in the central nervous system (Wang, 2003). By determining the activity and protein levels of CBS in a number of cardiovascular cells and tissues, Geng *et al*. (2004) found that CBS lacked in these tissues. However, CSE and endogenous H_2S were both identified in the rat cardiovascular tissue (Zhao *et al*., 2001). CBS was found highly expressed in rat brain, but only a small amount of CSE could be detected, which led to the conclusion that endogenous H_2S is generated mainly by CBS in brain (Abe *et al*., 1999).

Endogenous hydrogen sulfide may be an indicator for some diseases. For instance, it was found that the level of H_2S was severely decreased by ~55% in the brains of Alzheimer's disease patients (Eto *et al*., 2002). In Down syndrome patient, the expression of cystathionine β-synthase (CBS) was 3 times higher than those in normal individuals (Kamoun *et al*, 2003). Another example is that the chronic exposure to H_2S impaired fetal neuronal development and monoamine neurochemistry in rats (Roth *et al*., 1995). Thus, H_2S may have some functional involvement in neurodegenerative diseases.

These findings increase the interest in understanding the roles of H_2S in mammalian body. It appears to be true that whether H_2S may play a physiological, pathological or a toxicological role depends on its *in-vivo* level. Thus, accurate measurement of H_2S in mammalians with high resolution becomes very important, particularly the resolution being at about 10-20 μM concentration level (Wu *et al*., 2006). Furthermore, measurement of hydrogen sulfide is desired to be taken in real time and a non-invasive (or less-invasive) manner.

1.3 Existing H_2S Measurement Methods

Currently, only a few analytical techniques, such as ion-specific electrode, spectrophotometry and chromatography, are available to measure the H_2S in mammalian tissues. These techniques are developed from the industrial measurement of H_2S in polluted air and water and thus are not quite suitable for the measurement of endogenously generated H_2S in human body and tissues.

Each of these techniques appears to have the following generic procedure (Wu *et al*., 2007): (1) tissues are taken out of the mammalian body and homogenized; (2) homogenized tissues are reacted with chemical additives to generate H_2S; (3) the generated H_2S are measured. These techniques need a bulky amount of tissue samples and there is also a considerable delay between the sample collection and sulfide measurement. Table 1.1 provides a further summary of the advantage and disadvantage of each of these techniques. It can be generally said that these measurement methods are invasive and involve complex steps.

Table 1.1. Comparison of the current methods for H_2S measurement (Ubuka, 2002; Wu, 2006; Wu *et al*., 2007)

Measurement method	Advantages	Disadvantages
Spectrophotometry	• Widely used • Less expensive	• Long experimental time (1.5 days) • Bulky sample • Invasive • *In-vitro*
Chromatography	• Accurate detection • Separates H_2S from mixtures of chemical substances	• Expensive for the first setup • Bulky sample • Invasive • *In-vitro*
Sulfide ion-specific electrode	• Low cost for initial setup • Popular in serum/plasma measurement	• Needs to be calibrated before every measurement • Calibration procedure is complicated • Large amount of sample • Desulfurization of the samples • *In- vitro*

It is worth to mention that sulfide ion-specific electrode (ISE) measurement is the most accurate method currently, among the above three methods, to measure H_2S in the

serum/plasma. However, it employs a harsh chemical condition and needs a relatively large amount of tissue samples. Desulfurization of the samples, which will artificially raise the level of H_2S, is still one of the concerns (Olson, 2009). More details about this technique appear in the next chapter (i.e., Chapter 2).

1.4 A New Method to Measure H_2S in Solutions

Wu *et al*. (2006) developed a new method by using carbon nanotubes (CNT) and fluorescence response of H_2S to measure low concentration H_2S in water solution. The measurement procedure is as follows: CNTs are treated with the solution that contains H_2S to adsorb H_2S. The fluorescence of the treated CNT samples is then examined under the fluorescence microscopy. It is noted that the carbon nanotubes used in the measurement are non-functionalized. It has been found that the fluorescence response of CNTs treated with H_2S solution increased with the increase of H_2S concentration under the specific excitation (514 nm) and emission (530 to 580 nm) wavelength, and the relationship appears to be linear. Compared with the other methods, Wu's method only needs a drop of H_2S solution sample and involves a relatively simple procedure.

Wu also applied this approach to measure the concentration of H_2S in the serum (Wu *et al*., 2007). The linear relationship between the fluorescence response and H_2S concentration was also obtained. The serum is a more complicated system than water solution; besides H_2S, other substances (mainly proteins) are present in the serum. It appears that CNT approach can work in sera without being disturbed by the presence of

the proteins. However, the mechanisms behind this approach as well as interaction among CNT, proteins, H_2S are yet to be known.

1.5 Research Objectives

The overall objective of this thesis research is to study the mechanism which governs the interaction among key proteins in sera or blood, CNT, and hydrogen sulfide. There are four objectives with the present study: (1) examining the interactions between H_2S and CNT under the presence of proteins, (2) understanding the mechanism behind these interactions, (3) examining the difference with CNT structures in these interactions or sensing H_2S in sera, and (4) examining the interactions among hemoglobin, CNT, and H_2S. Motivations for these objectives are presented below.

Regarding Objective (1), one of the most important issues regarding any biosensor system is its specificity, which requires the measurement system to be sensitive to a target bimolecular only but to be insensitive to others. The combined CNT and fluorescence approach appears to be able to measure the low concentration H_2S in sera without being disturbed by the proteins in sera. Thus, the specificity of Wu's approach seems to be excellent. However, in the previous study (Wu *et al*., 2008), hemoglobin, which is an important protein in blood, was found to bind with the non-functionalized multi-wall carbon nanotubes (MWNTs); but such binding is insensitive under the specific wavelength chosen to measure H_2S. Other studies (Shim *et al*., 2002; Chen *et al*., 2003; Chen *et al*., 2004) have also shown that the proteins can be non- specifically adsorbed on as-grown or non-functionalized CNTs, and the adsorption of proteins on

non-functionalized CNTs seems to be a general phenomenon. However, the preliminary study done by Wu *et al*. (2007) showed that the proteins in the serum did not appear to bind with CNTs. Therefore, there are mixed results regarding the interactions between proteins and carbon nanotubes, and this situation warrants a further study.

In this thesis, the characterization techniques, such as Raman spectroscopy, X-ray absorption spectroscopy (XAS) and confocal laser scanning microscopy (CLSM), are employed to examine the interaction between CNTs and proteins. Two major proteins, serum albumin and serum globulin, are being studied, and their effects on the measurement of H_2S will be examined.

Regarding Objective (2), it was proposed that in the adsorption of H_2S with carbon nanotubes, both physical and chemical adsorptions occur (Wu *et al*., 2007). In physical adsorption, the surface, pore volume, and pore size are very important. Chemical adsorption usually occurs under aqueous conditions; it results in the formation of surface oxygen containing complexes, and elemental sulfur (Bandosz, 2002). Wu *et al.* (2007) hypothesized in that the defect sites of carbon nanotubes are likely responsible for adsorbing H_2S in chemical adsorption. This thesis will study this hypothesis.

Raman spectroscopy has become a very powerful tool for the characterization of carbon nanotubes (Dresselhaus *et al*, 2005). Raman spectra are sensitive to the modification of nanotube surface, such as the attachment of chemical species, the change of the defects and the functionalization of nanotubes (Filho *et al*., 2003). The adsorption of H_2S on

carbon nanotubes in the situations of the presence and absence of proteins will be studied by Raman spectroscopy.

Regarding Objective (3), in the previous study (Wu *et al*., 2007), multi-wall carbon nanotubes (MWNTs) were used to measure H_2S in solutions. Different types and sizes of carbon nanotubes (CNT) show different structures, mechanical and electrical characteristics. In this thesis, single-wall carbon nanotube (SWNT) and two different sizes of MWNT will be examined for their performance on H_2S measurement.

Regarding Objective (4), the study presented in the previous work (Wu *et al*., 2008) showed that hemoglobin can bind with non-functionalized MWNT in water solution; however such binding was insensitive to fluorescence response of H_2S. But when different amounts of hemoglobin were put into sera to scavenge H_2S, a change in fluorescence response was observed, which appeared to contradict with the result obtained in water. Wu *et al.* (2008) hypothesized that the foregoing phenomenon is due to the presence of H_2S in sera; as such, the more hemoglobin is added into the serum, the more H_2S will be taken away and thus less fluorescence response is expected. This hypothesis can be stated in a more general way that hemoglobin in the serum will not affect fluorescence response under confocal laser scanning microscopy.

1.6 Thesis Organization

In Chapter 2, the state of knowledge of using carbon nanotubes and fluorescence response to measure H_2S in solution is reviewed, and the background of various

techniques that were used in the study is discussed. To broaden the scientific significance of the study, the literature regarding the interactions between CNTs and proteins is reviewed as well. Chapter 2 is thus expected to provide dual roles: further justification of the objectives of the study described in Chapter 1 and provision of background information and knowledge needed for the subsequent chapters.

In Chapter 3, materials and methods common to each study are described. This chapter is designed to avoid redundant description of materials and methods. Specialized features to each study are, however, presented along with separate chapters that are devoted to them.

The comparative study of single-wall carbon nanotubes (SWNTs) and multi-wall carbon nanotubes (MWNTs) for measuring H_2S in sera is described in Chapter 4. In Chapter 5, interactions of two major proteins (serum albumin and serum globulin) in sera with SWNTs and MWNTs are studied, and their effects on the measurement of H_2S are examined. Interaction of hemoglobin with H_2S and CNT in sera is studied in Chapter 6. In Chapter 7, adsorption of H_2S on CNTs in the presence of proteins and absence of proteins is studied by using Raman spectroscopy. Chapter 8 draws conclusions from each study, states contributions of the thesis, and presents recommendation for future work.

CHAPTER 2: BACKGOUND AND LITERATURE REVIEW

2.1 Carbon Nanotube and its Relevance to H_2S Measurement

Carbon nanotubes (CNT) have been of scientific interest since its discovery in 1991 (Iijima, 1991). A single-wall carbon nanotube (SWNT) can be seen as a graphite sheet rolled into a cylinder, and a multi-wall carbon nanotube (MWNT) is comprised of a group of concentric tubes (Dai, 2002); as shown in Figure 2.1. The diameter of a SWNT is on the order of a nanometer, and the diameter of a MWNT can range from a few nanometres to several hundred nanometres. Generally, there are three main methods to produce CNTs (Dai, 2001): 1) arc-discharge; 2) laser ablation; 3) chemical vapour deposition (CVD). If a perfect nanotube is obtained it would be light, flexible, thermally stable, and chemically inert. Depending on the twist direction of the graphite sheet, nanotubes can be metallic or semiconducting.

(a) 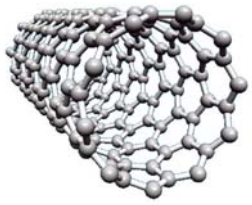 (b) 

Figure 2.1. (a) SWNT, (b) MWNT

The idea of using carbon nanotube to measure H_2S in solution comes from the fact that activated carbon is widely used to adsorb H_2S in the water treatment and purification process (Wu *et al.*, 2006). Adsorption of H_2S onto activated carbon surfaces included both reversible and irreversible processes (Bandosz, 2002). Reversible adsorption is affected mainly by the pore structure, and pore filling is likely the dominant mechanism. The irreversible adsorption of H_2S is affected by chemical reaction. In the presence of activated carbon and water, H_2S can react with oxygen at low temperatures and form sulfur. The irreversible amount of H_2S increases with the increase of surface area. Carbon nanotube has a very large specific surface area and uniform pore size distribution, which makes it a promising material for H_2S adsorption. Its ability for hydrogen storage has been widely known (Liu *et al*., 1999).

Inspired by the mechanism of H_2S adsorption with activated carbon, Wu *et al*. (2007) proposed the mechanism that accounts for the adsorption of H_2S on carbon nanotubes. When carbon nanotubes are in the H_2S solution, a thin water film is formed. Oxygen is dissolved in the film and become reactive points. The H_2S that reaches the carbon nanotubes is also dissolved in the film and partly dissociated into protons (H^+) and hydrosulfide ions (HS^-). HS^- reacts with the oxygen (O_2) to form sulphur (S) and

hydroxyl ions (OH^-). The formed sulfur is further attached to the carbon nanotube. The protons (H^+) neutralize the hydroxyl ions (OH^-) and produce water. The process can be represented by the following equations.

$$H_2S \rightarrow H^+ + HS^- \quad (2.1)$$

$$HS^- + 1/2O_2 \rightarrow S + OH^- \quad (2.2)$$

$$OH^- + H^+ \rightarrow H_2O \quad (2.3)$$

Adsorption of H_2S on carbon nanotubes is not a simple process, and it involves both chemical reactions and physical activities.

2.2 H_2S and Serum

2.2.1 Serum

Serum can be extracted from blood. There are three layers visible in the centrifuged blood (Shier *et al*., 2002): 1) the top golden-yellow color layer called plasma; 2) the middle thin cream color layer called buffy coat, which consists of white blood cells and platelets; and 3) the bottom layer formed by red blood cells. Plasma makes up ~55% of the total blood volume and is the liquid component of blood. It essentially contains 92% water, 8% proteins and trace amounts of other materials such as lipids, hormones, and so on. Albumin, globulin and fibrinogen are the main protein groups in plasma.

Serum is the plasma without fibrinogen and other clotting factors. Since blood cells and fibrinogen show no relation with the generation of H_2S, plasma or serum can be used in measurement of endogenous H_2S instead of the whole blood (Olson, 2009).

2.2.2 H_2S in Water or Sera

H_2S is fairly soluble in water. Dissolved H_2S is a weak acid, and it dissociates into hydrosulfide ion (HS^-) or sulphide ion (S^{2-}) in solution, as shown in Equation 2.4 below:

$$H_2S \rightarrow H^+ + HS^- \rightarrow 2H^+ + S^{2-} \quad (2.4)$$

This reaction is dependent on the pH value of the solutions (Reiffenstein *et al*., 1992). At low pH, the predominant form of the solution is H_2S. At the pH slightly less than 7, there are equal amounts of H_2S and HS^- in the solution. At pH > 7, the amount of HS^- increases rapidly. At pH = 8, HS^- is about ten times that of H_2S. Therefore, HS^- is the dominant species in the solution for pH > 7 (Carroll, 1998). At the physiological pH level (pH = ~7.4), there is essentially no S^{2-} in serum/plasma, and approximately, one-third of the total H_2S will be in the undissociated form (H_2S) and two-thirds as hydrosulfide ion (HS^-) (Dombkowski *et al*., 2004).

2.3 Sulfide Ion-specific Electrode for Measuring H_2S in Serum or Plasma

Currently, sulfide ion-specific electrode (ISE) is one of the major methods for H_2S measurement in the plasma or serum. In ISE measurement, a typical sulfide calibration curve is required before the measurement. The calibration curve is obtained by

measuring the standard solution which is prepared through a series of dilution of known concentration of Na_2S solution. The electrode potentials (mV) of the standard solution are plotted on the linear axis (x axis) and their concentrations on the log axis (y axis). The electrode potential of an unknown sample can be measured, and its value is read against the linear calibration curve to obtain its concentration. Figure 2.2 shows a typical sulfide calibration curve.

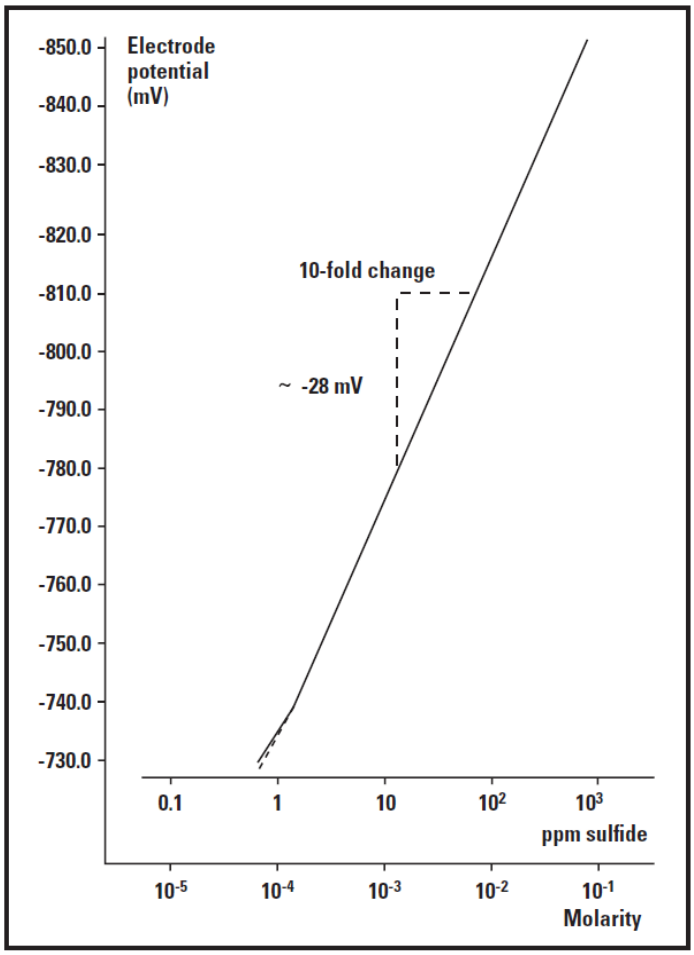

Figure 2.2. Sulfur ion-specific electrode typical calibration curve (Lazar Research Laboratories, 2009).

In order to implement ISE measurement in serum/plasma, the sulfide in the sample must be in the form of S^{2-}. This is usually accomplished by two methods called direct method

and indirect method. In the direct method, the sample is directly placed in an antioxidant buffer (AOB) that is comprised of a strong alkali and an antioxidant. The strong alkali transfers all the H_2S and HS^- ions into S^{2-}, and the antioxidant prevent S^{2-} further oxidized into SO_3^{2-} or SO_4^{2-}. Sulfide is recorded 20-30 min after the plasma/serum is mixed with AOB. In the indirect method, strong acid like hydrochloric acid (HCl) or sulfuric acid (H_2SO_4) is added into the sample to liberate the sulfide. The evolved H_2S gas is carried by a stream of nitrogen (N_2) into the flask filled with AOB. The sulfide concentration is measured by ISE in AOB. The system setup is shown in the Figure 2.3.

Figure 2.3. System setup for ISE indirect method.

Both methods employ a harsh chemical condition and sample modification procedure. Several problems were found, which could affect the measurement. In the direct method, it has been known (Khan *et al.*, 1980) that the direct mixing AOB with serum or plasma resulted in protein desulfurization and produced an elevated sulfide level. Whitfield *et al*. (2008) observed that sulfide was produced directly from bovine serum

albumin (BSA) when mixed with AOB. Further research has shown that much of the sulfide measured with the ISE was actually derived from the desulfurization of cysteine sulfur within the BSA. The development of the indirect method can somehow overcome the protein desulfurization. However, not only does the system setup become more complicated but also does the system require to be tightly sealed; any leak of the liberated H_2S would affect the measurement (the system is usually put under water to monitor the leak of the gas). The strong acidic used to liberate H_2S in the serum or plasma may also alter the properties of samples. Recent studies have shown that acid-labile sulfide present in the serum or plasma would be liberated during the process along with H_2S, which can cause errors to the final measurement (Ubuka, 2002).

2.4 Confocal Laser Scanning Microscopy for H_2S Measurement

The carbon nanotube method for measuring H_2S is based on the theory that the fluorescence intensity is proportional to the concentration of chemical species and to the intensity of the incident radiation. Chemical species are excited to higher electronic energy states by light, heat or chemical reaction. Fluorescence will be emitted when they dispose of the excess energy and return to the ground vibration and electronics states (Greyson, 1990). The intensity of the fluorescence is directly associated with the concentrations of the luminescent species in the medium being tested, and it follows Beer's law.

$$\frac{I}{I_0} = \exp(-abC) \tag{2.5}$$

where I is the intensity of transmitted light, and I_0 is the intensity of incident light. *a, b* and C are the absorbance, cell path length and concentration, respectively. The fraction of light adsorbed is then calculated by

$$1-\frac{I}{I_0}=1-\exp(-abC) \tag{2.6}$$

The total amount of the light absorbed (I_a) is found by

$$I_a = I_0 - I = I_0[1-\exp(-abC)] \tag{2.7}$$

In low concentration, one can expand $[1-\exp(-abC)]$ and drop the higher order terms, leading to

$$I_a = I_0 abC \tag{2.8}$$

Since the intensity of fluorescence (I_f) is proportional to the amount of the light adsorbed, we have

$$I_f = KI_a \tag{2.9}$$

Substituting equation (2-4) into (2-5), we get

$$I_f = KI_0 abC \tag{2.10}$$

Compared to the conventional laser microscopy, a pinhole is used in a confocal laser scanning microscopy (Sheppard *et al*, 1997). A mixture of emitted fluorescence light and reflected incident light from the specimen is collected by the objective. A beam splitter then separates the mixture light by only allowing the fluorescent light to pass through and reflecting the incident light. Before the fluorescence light is able to be detected by a photomultiplier (PMT) that transfers the light signal into electrical signal to be processed by the computer, a pinhole is placed to block the out-of-focus light (the

light above or below the objective focal plane that is not confocal with the pinhole), which only allows the light on the focal plane to be detected. Such a mechanism greatly improves the resolution and signal to noise ratio of the detection (Amos *et al*., 2003).

Wu *et al*. (2007) has successfully used confocal laser scanning microscopy to measure the low concentration of H_2S in water solution and sera. The incident light was set at 514 nm to excite the H_2S adsorbed on CNTs, and the emission light was set at a range from 530 to 580 nm to collect the emitted fluorescence of sulfur. The intensities of the fluorescence increase with the increasing H_2S concentration, and the relationship is linear (Figure 2.4). The result is in good match to the above theory.

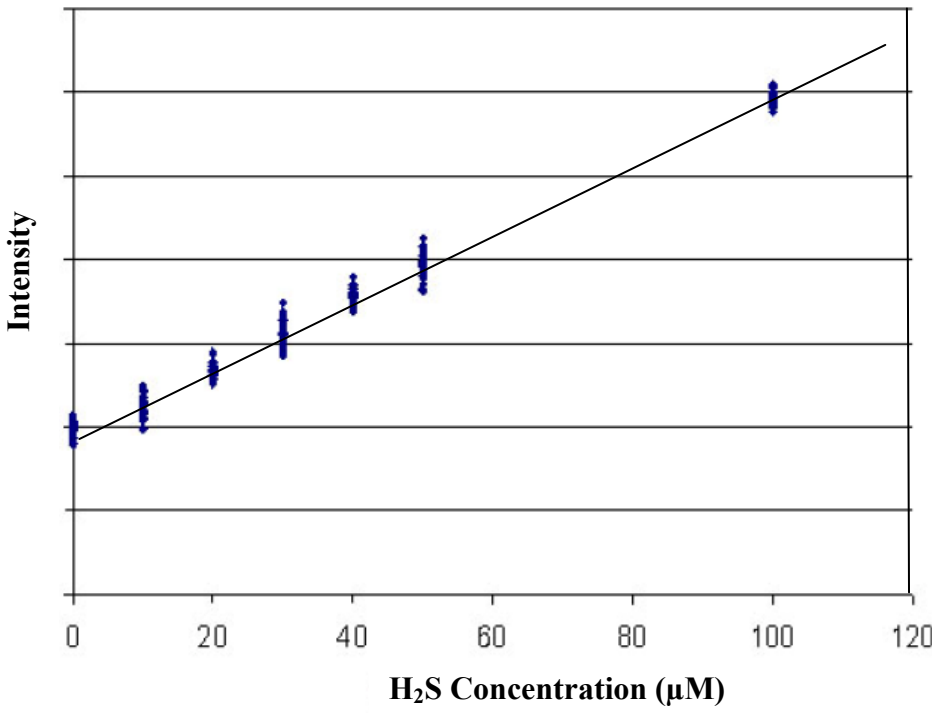

Figure 2.4. Confocal laser scanning microscopy fluorescence of the carbon nanotubes treated with different concentrations of H_2S in water (0 μM, 10 μM, 20 μM, 30 μM, 40 μM, 50 μM, and 100 μM) (used by the permission of Wu, 2007).

2.5 X-ray Absorption Spectroscopy for Sulfur Measurement

2.5.1 X-ray Absorption Spectroscopy (XAS)

When the X-rays hit a sample, the electromagnetic radiation interacts with the electrons in the atom. The radiation will be scattered or absorbed by the electrons (Figure 2.5).

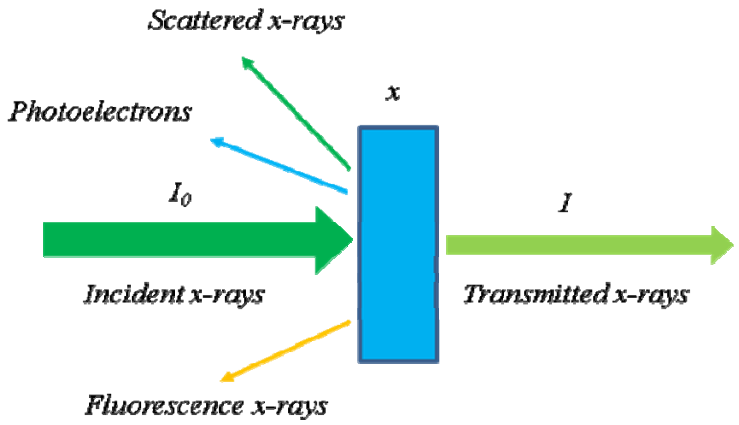

Figure 2.5. Diagram representation of X-rays interaction with the sample.

An X-ray beam of intensity I_0 passing through a sample of thickness x will be reduced to I according to the expression (George *et al.*, 2009):

$$\log_e\left(\frac{I_0}{I}\right) = \mu x \tag{2.11}$$

where μ is the x-ray absorption coefficient and x is the thickness of the sample. μ depends strongly on the type of the atom and the density of the material, it is approximately given by:

$$\mu = \frac{\rho Z^4}{AE^3} \tag{2.12}$$

where ρ is the density of the sample, Z is the atomic number, A is the atomic mass, and E is the X-ray energy.

For a given element, at a certain energy level where the absorption increases drastically and gives rise to an absorption edge. Each such edge occurs when the energy of the incident X-ray photons is just sufficient enough to excite a core electron of the absorbing atom to a continuum state to produce an emitted photoelectron, and leave a core hole behind (Figure 2.6). The energies of the absorbed radiation at these edges correspond to the binding energies of electrons in the K, L, M shells. For example, the absorption edges for sulfur occur at 2472 eV (K-edge), 230.9 eV (L_1-edge), 163.6 eV (L_2-edge) and 162.5 eV (L_3-edge), and correspond to the creation of photoelectron from the 1s, 2s, $2p_{1/2}$ and $2p_{3/2}$ core level respectively (Thompson *et al*., 2001). The core hole is then filled by the decay of the higher orbital electron with the emission of fluorescence photon, or Auger electron. These are two competing processes (Auger ratio + Fluorescence ratio = 1), with the Auger process being favored for the low Z atom and the fluorescence process favored for the high Z atom (Jalilehvand, 2006). By measuring fluorescence photons or Auger electrons, the absorption spectra can be obtained.

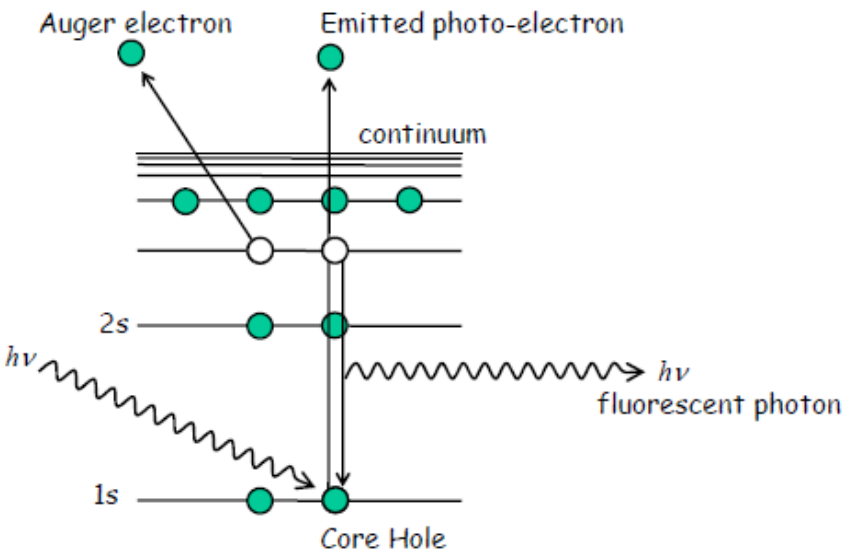

Figure 2.6. Schematic representation of the basic theory of XAS (adapted from Hemraj-Benny *et al*., 2006)

The XAS spectra are generally reported as total electron yield (TEY), Auger electron yield (AEY) and fluorescence yield (FLY) as a function of the incident X-ray photon energy. Since the penetration depth of fluorescence photos is much greater than electrons, a deeper bulk analysis can be achieved by FLY measurement. In contrast, the escape depth of the electrons is quite small, Auger electron detection (AEY) is more surface sensitive and provides the surface information (Stöhr, 1992). Total electron yield (TEY) detection measures the integral over the entire range of the emitted electrons, the technique is less surface sensitive than Auger yield (AEY) and provides surface and near surface information (for example, ~70 nm for sulfur K-edge and ~5 nm for sulfur L-edge) (Sarret *et al*., 1999). For the sulfur K-edge, FLY detection has been used mostly due to its high signal to noise ratio, while for the sulfur L-edge, TEY detection is preferred because of the low fluorescence yield (Kasrai *et al*., 1996).

The X-ray source for measuring X-ray absorption spectrum (XAS) is usually from synchrotron radiation, which covers all wavelengths of the electromagnetic spectrum with the intensity of more than 100 times higher than the conventional X-ray tubes (Attwood, 2007). To produce synchrotron radiation, charged electrons from a linear accelerator with a speed close to the light are injected into the storage ring under high vacuum. The ring consists of straight parts and curved parts. Magnetic fields, from the bend magnets around the ring, force the accelerated electrons to follow the ring in the curved section. A radio frequency cavity (called RF-cavity) in the ring occasionally kicks the electrons to restore their energy.

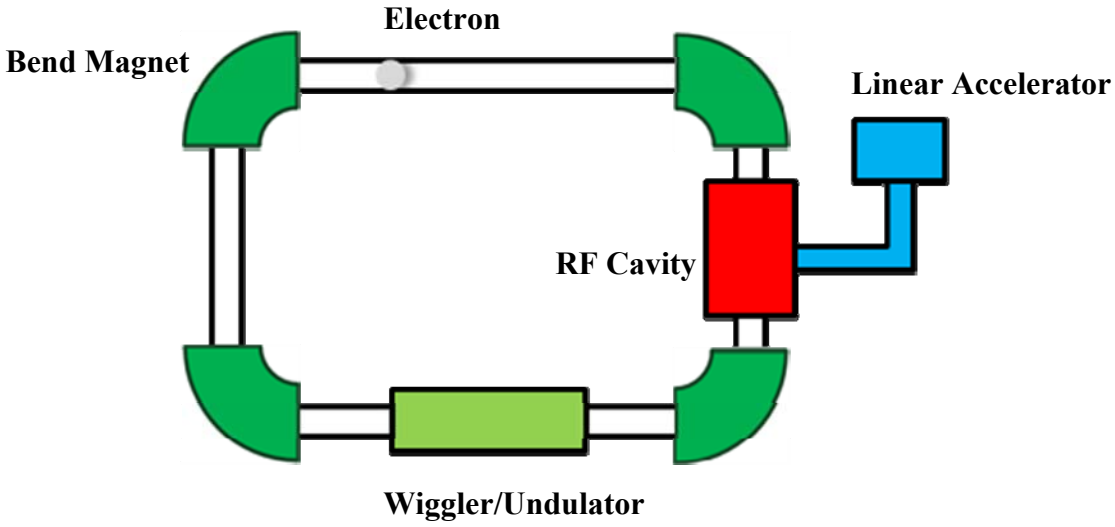

Figure 2.7. Illustration of the basic structure of synchrotron ring (beamlines are off the bend magnet or undulator).

When the high energy electrons (e.g. 2.9 GeV in Canadian Light Source, CLS) changes momentum in curved parts (bending magnet or undulator), they lose a part of their energy and produce synchrotron radiation, and the emitted radiation is tangential to the curved section. The synchrotron radiation can also be generated by insertion devices (like, wigglers or undulators) in the straight parts of the ring. Unlike bend magnets, the properties of the insertion devices can be adjusted to optimize the radiation for specialized purposes. Wigglers are like undulators but are able to provide a stronger magnetic field and give out radiation with a more uniform intensity distribution (Koningsberger *et al*., 1988). The synchrotron radiation has a broad distribution in energy and space. Beamlines guide the synchrotron radiation out of the ring. They select the suitable X-ray beam for experiments and protect the users from radiation exposure. Beamlines usually combine X-ray optical components, detector systems, experiment

station, and computer system (Mills, 2002). Beamlines and beamline components select the energy, shape the beam and tailor the X-rays for the experiments.

2.5.2 Sulfur X-ray Absorption Spectra

A typical X-ray absorption spectrum can be considered to have three energy regions (Figure 2.8). (1) The pre-edge region, the lowest energy part, is the region before the sharply rising absorption edge. (2) The near edge region (the one which is of interest to the present study), defined as the range between the absorption edge up to ~40 eV above the edge. The incident X-ray energy E is higher than that of the absorption edge E_0. The emitted photoelectron has relatively low kinetic energy: $E_k = E - E_0$. The near edge region is usually named as Near-edge X-ray Absorption Fine Structure (NEXAFS) or X-ray Absorption Near-edge Structure (XANES). The XANES spectral region of interest for analytical purposes is normally within the region about ±10 eV around the edge (Jalilehvand, 2006). (3) The extended X-ray absorption fine structure (EXAFS) region is the oscillatory part of an X-ray absorption spectrum, which occurs at ~40 – 1000 eV above the edge. In this region the emitted photoelectron gains high kinetic energy and is scattered from the neighbouring atoms. The backscattered wave interferes constructively or destructively with the outgoing wave, which provides the information of the number and identity of the neighbouring atom, and the distance from the adsorbing atom (Solomon & Hanson, 1999)

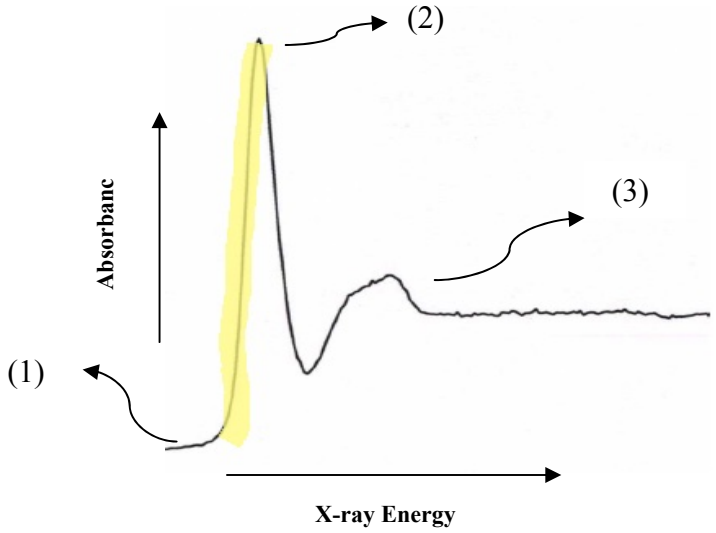

Figure 2.8. XAS spectrum contains three regions: (1) Pre-edge, (2) XANES, (3) EXAFS.

This thesis study was interested in sulfur XANES spectrum. There are rich features in sulphur XANES spectrum which is element specific and provides a sensitive probe for sulfur chemical states characterization (Solomon *et al*, 2003). A higher oxidation state of the sulfur atom will reduce the shielding of the nuclear charge and raise the binding energy of the core orbital. There is a large shift of about 13 eV from sulfides (S^{2-}) to sulfate ($SO4^{2-}$) at Sulfur K-edge (George *et al.,* 1989). Thus, sulfur XANES is very sensitive to the sulfur oxidation states. Pickering *et al*. (1998) used sulfur K-edge XANES to determine the sulfur forms in blood and serum. They found that even for two compounds as similar as cysteine and methionine, a noticeable difference could be detected in their S K-edge XANES spectra. Sulfur K-edge XANES has also been used to examine the biodesulfurization process in oil refineries (Grossman *et al*., 1999). Sulfur K-edge provides valuable information to help understand the mechanisms for

detoxification and heavy metal regulation in living organisms, and sulfur metabolism in the biological system (Rompel *et al*., 1998; Akabayov *et al*., 2005).

Through the sulfur K-edge XANES study, it is expected to answer some remaining questions regarding using CNTs to measure H_2S in sera. They are in particular: 1) How do the proteins in the serum interact with CNTs? 2) Will the interaction between CNTs and proteins cause the desulfurization of proteins and thus affect the accurate measurement of H_2S in the serum? The second question was motivated by the finding discussed in Section 2.3 that the protein desulfurization in sulfide ion-specific electrode (ISE) measurement can happen, which can lead to the false report of the sulfide level in the serum (Khan *et al*, 1980).

2.6 Raman Spectroscopy for CNT Characterization

Raman spectroscopy has become one of the most powerful tools for carbon nanotube characterization (Jorio *et al*., 2003). Raman scattering is the inelastic scattering of light, and the process includes three steps: (1) an electron is excited from the valence band to the conduction band by absorbing a photon; (2) the excited electron is scattered by emitting (or absorbing) phonon; (3) the electron relaxes to the valence band by emitting a photon (Ferraro *et al*., 2003).

Raman spectra are for the scattered photon whose energy is smaller than the energy of the incident photon. By measuring the intensity of the scattered light as a function of

frequency downshift (losing energy) of the scattered light, which is plotted as Raman spectra, an accurate measure of the phonon frequencies of the material can be obtained. Raman scattering can occur for phonon emission or by phonon absorption, and these two processes are called the Stokes process and anti-Stoke process, respectively; see Figure 2.9.

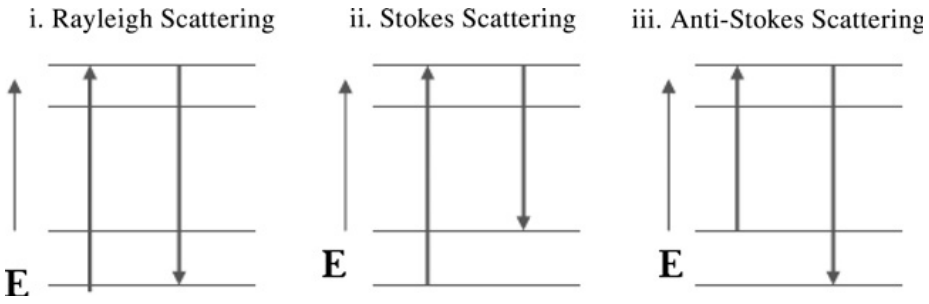

Figure 2.9. Raman energy level diagram (adapted from Skoog *et al*., 1998).

Raman spectrum measurement needs a minimum or none sample preparation, and the acquisition of the spectrum only takes minutes. The whole process is simple and can be done at room temperature and under ambient pressure, and it is non-destructive. Figure 2.10 shows the spectrum of SWNT, which is used in our study.

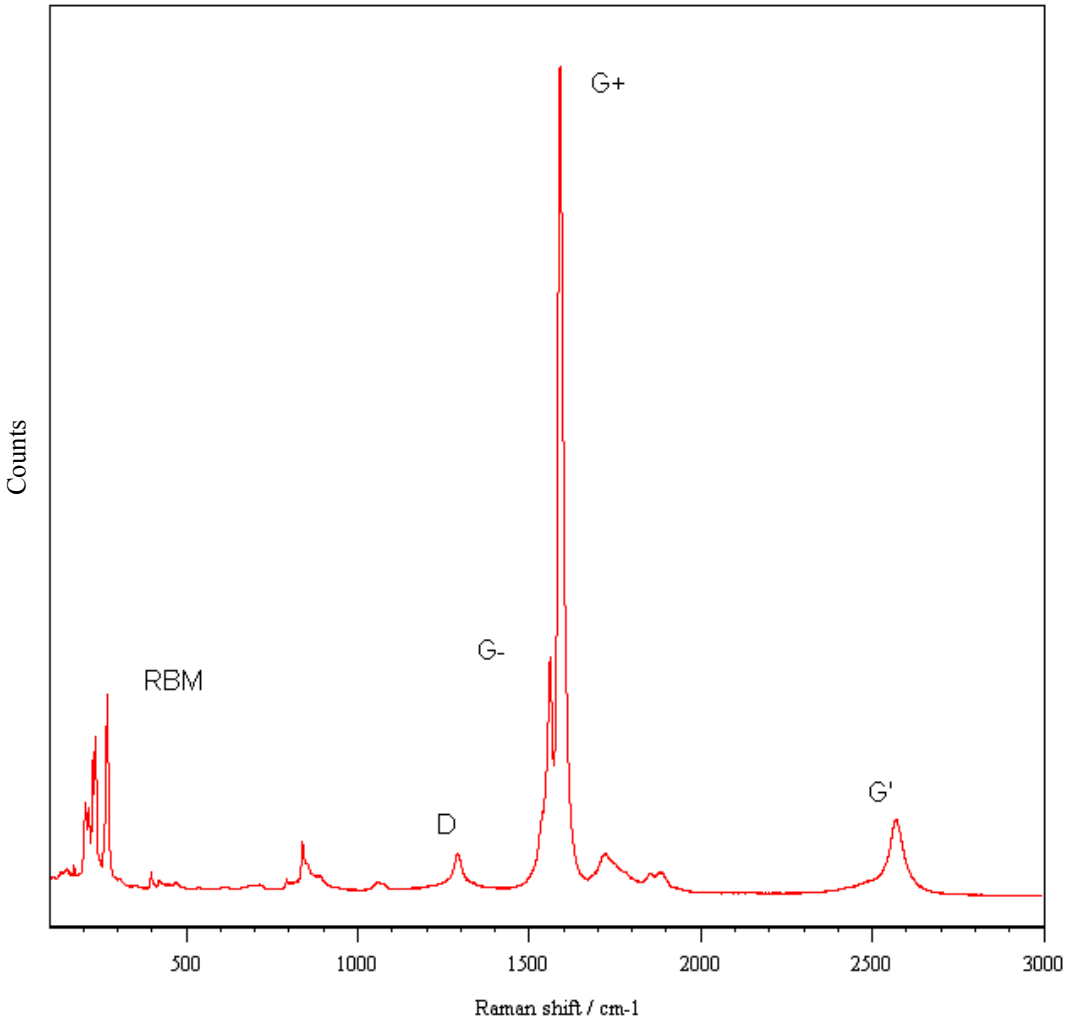

Figure 2.10. Raman spectrum of SWNT acquired with a Renishaw Invia Microscope showing the radial breathing mode (RBM), D band, G band and G' band.

There are several important features exhibited in the CNT Raman spectrum (Figure 2.10). 1) Low frequency peaks < 200 cm^{-1} are assigned to radical breathing mode (RBM). RBM corresponds to the coherent vibration of C atoms in the radical direction, and its atomic displacement is shown in Figure 2.11. It is unique to carbon nanotubes and can be used to identify the existence of SWNTs in the samples. RBM frequency is also inversely proportional to the diameter of nanotube and can be used to characterize

the diameter distribution in the samples (Jorio *et al*., 2001). The relation between RBM frequency (ω_{RBM}) and nanotube diameter (d_t) can be expressed as (Jorio *et al*., 2001):

$$\omega_{RBM} = \frac{A}{d_t} + B \tag{2.13}$$

where parameter A and B are determined experimentally.

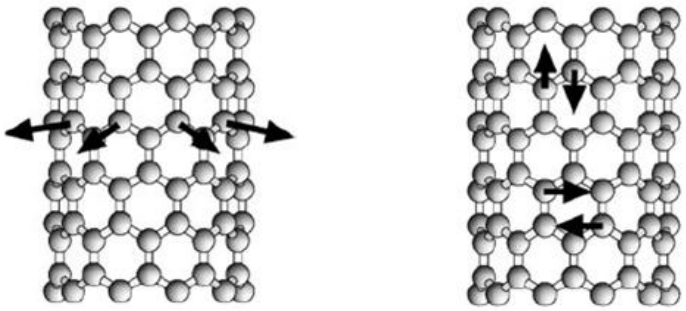

RBM G-band

Figure 2.11. Atomic displacements associated with the RBM mode and G-band mode vibrations.

2) a large feature ω_D at ~1350 cm^{-1} is assigned to D band, corresponding to the defect-induced mode in nanotube; and its first overtone occurs at ~2 ω_D (between 2450 and 2700 cm^{-1}), called G' band. The D and G' band have a strong dispersive behaviour as regard to laser excitation energy. The D band frequency changes about 53 cm^{-1} and G' band changes about 106 cm^{-1} as a result of changing the laser energy by 1 eV (Dresselhaus *et al*., 2002). The position and linewidth of D band can be used to distinguish various forms of carbon material; for instance, amorphous carbon has a very broad linewidth (> 100 cm^{-1}), crystalline graphite forms have a typical position at 1305-1330 cm^{-1} and a width of about 30-60 cm^{-1}; however, SWNT has the position at 1285-

1300 cm^{-1} and a linewidth of 10-30 cm^{-1}, and MWNT are similar to crystalline graphite-like forms (Arepalli *et al*., 2004).

3) Another important feature is called G band which occurs between 1500 and 1600 cm^{-1}, which is related to the tangential mode vibration of the carbon atoms. The atomic displacement of the G band is shown in Figure 2.11. The G band is non-dispersive and its frequency is not sensitive to the laser excitation energy (Dresselhaus *et al*., 2002). The G band consists of two main components, one peaked at about 1570 cm^{-1} (G^-) and the other peaked at about 1590 cm^{-1} (G^+). The G^- feature is associated with the vibration of carbon atom along the circumferential direction of the SWNT, and its lineshape is highly sensitive to whether SWNT is metallic or semiconducting (Jorio *et al*., 2003). The G^+ feature is associated with the vibration of carbon atom along the nanotube axis and its frequency is sensitive to charge transfer from dopant additions to SWNTs , in particular upshift for acceptors and downshift for donors (Jorio *et al*., 2003).

Recent studies have shown that changes in the D and G band of Raman spectra can be used to probe and monitor structural modification to the nanotube (Filho *et al*., 2003). The introduction or reduction of defects can be probed through the analysis of frequency, linewidth, and intensity of the disorder-induced D-band (Brown *et al*., 2001). The high frequency G band is associated with the vibration of carbon atom along the nanotube axis, it has been used to identify the electronic properties (metallic/semiconducting) of carbon nanotubes, and its frequency is known to be very sensitive to the interaction of chemical species to the sidewall of carbon nanotubes

(Corio *et al*., 2004; Dresselhaus *et al*., 2005). G'-band is the overtone of defect-induced D-band. However G'-band is not defect-dependent; in contrast, it exhibits great sensitivity to the small perturbation to the electronic structure or the environment around the nanotubes, which is very similar to the feature of G-band (Brown *et al*., 2001; Corio *et al*., 2003). The G'-band has been used to study the compressive and tensile strains applied on the carbon nanotubes (Thomsen *et al*., 1999; Dharap *et al*, 2004), and the attachment of chemical species on the sidewall of carbon nanotubes (Proctor *et al*, 2006; Guo *et al*, 2007). Sample impurity and functionalization can also be investigated using the D/G band intensity ratio from Raman spectrum (Alvarez *et al*., 2000).

Because MWNTs contain an ensemble of carbon nanotubes with diameters ranging from small to very large, most of the characteristic features that are observed in SWNT Raman spectra which differ from graphite spectra are not so evident in MWNT Raman spectra (Benoit *et al*., 2002); see Figure 2.12 for Raman spectrum of MWNT used in our study. For example, RBM Raman feature is usually too weak to be observable in MWNT Raman spectra due to the large diameter tube (Zhao *et al*., 2002). The splitting of G^+ and G^- in G band cannot be observed either, due to the different diameter distribution within in the MWNT (Rao *et al*., 2000). MWNT Raman spectra more resemble graphite spectra. However, for MWNTs with very small innermost nanotubes (~1 nm), their RBM peaks and G band splitting can be observed at the isolated MWNT level.

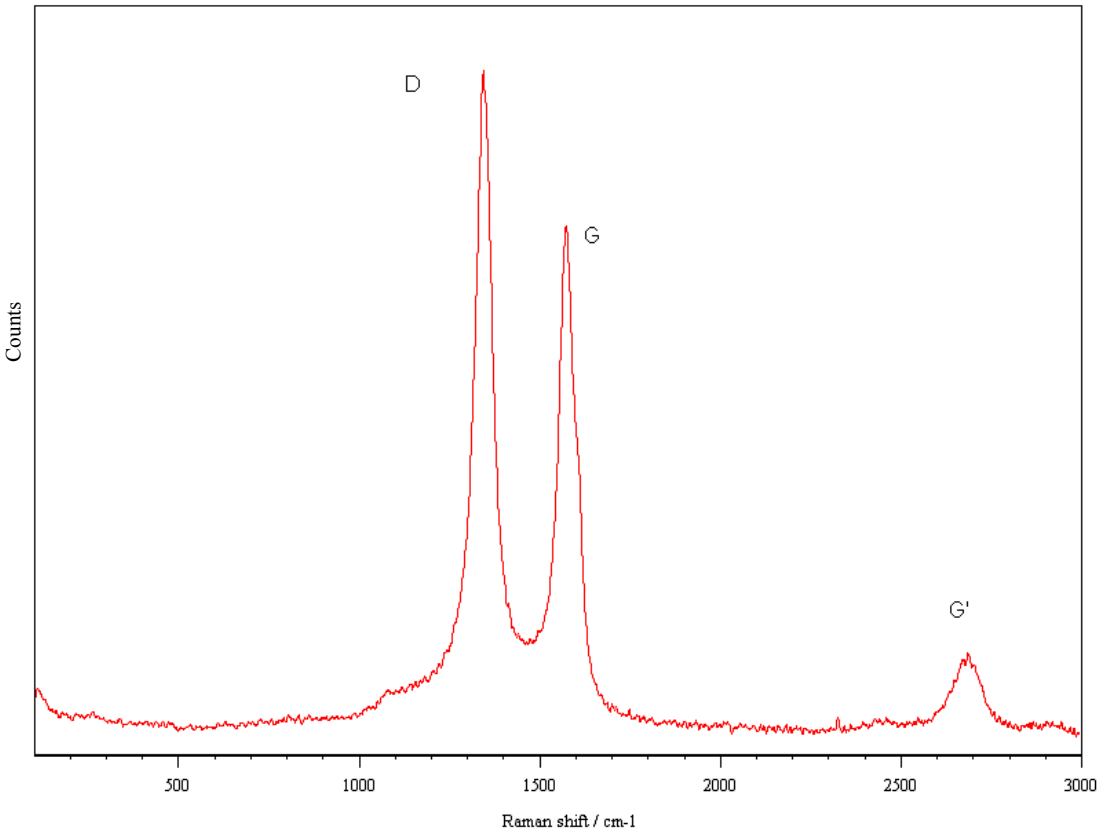

Figure 2.12. Raman spectrum of MWNT acquired with Renishaw Invia Microscope showing D band, G band and G' band.

2.7 Interaction of Carbon Nanotubes with Proteins

In the method to use carbon nanotubes to measure H_2S in sera, one of the main concerns is whether the presence of proteins in the serum would affect the measurement. The questions are: how would the proteins interact with carbon nanotubes and how would such interaction further affect the adsorption of H_2S and fluorescence measurement?

Balavoine *et al.* (1999) reported that streptavidin, a water-soluble protein which has become very useful in biochemical assays due to its high affinity to biotin, can strongly

interact with as-grown MWNTs. The tubes were seen covered by the streptavidin under the electron microscope. Their study also found that the streptavidin-coated nanotubes retained streptavidin-biotin binding properties. Thus, CNTs showed the promise for being used as a bioreactive docking matrix. Further in their work, protein HupR was also studied and found to strongly attach to the as-grown MWNTs as well.

Chen *et al*. (2001) reported a simple approach to noncovalent functionalization of SWNTs and subsequent immobilization of various proteins onto nanotubes with a high degree of control and specificity for various applications. The successful immobilization of both ferritin and streptavidin onto the functionalized SWNTs were observed in the transmission electron microscopy (TEM) and atomic force microscopy (AFM). The non-functionalized SWNTs were found to be free of ferritin and streptavidin.

Shim *et al*. (2002) reported that streptavidin can bind to SWNTs even without functionalization with the help of AFM. Fibrinogen, on the other hand, was found not to be strongly adsorbed on the as-grown SWNTs. This may be attributed to the much larger size of fibrinogen (~340 kDa) relative to the diameter of SWNTs (~2 nm). In contrast, streptavidin is a relatively small protein with weight of ~60 kDa.

Chen *et al*. (2003, 2004) used AFM and quartz crystal microbalance (QCM), electronic transport measurement and X-ray photoelectron spectroscopy (XPS) to study the adsorption behavior of various types of proteins, such as streptavidin (SA), avidin, BSA, α-glucosidase (GCD), staphylococcal protein A (SpA) and human immunoglobulin G

(IgG) with the as-grown SWNTs. AFM revealed the adsorption of all the proteins on the sidewalls of SWNTs. QCM measurement further confirmed the observation. Thus, they suggested that the non-specific binding (NSB) of the proteins on as-grown SWNTs is a general phenomenon, and such bindings may be attributed to the hydrophobic interaction between the proteins and nanotube surface. Such phenomenon was undesirable for the author's application of using CNTs to detect specific biomolecules such as antigen, antibody and specific protein-protein conjugation. A functionalization method was developed to prevent such non-specific bindings. The experiments have shown that SWNTs treated with polyethylene oxide (PEO) provided excellent protein resistance. The binding partner was further linked on top of PEO-functionalized nanotubes to re-enable binding of CNTs to the selected targets. The specific protein-protein, antigen-antibody binding, such as SA-biotin, and SpA-IgG, were achieved by using the new method, and the non-specific bindings were found to be suppressed.

Kam *et al*. (2005) used a combination of the treatment of refluxing and sonication in nitric acid (HNO_3) to produce short (50-500 nm) individual or small bundles of SWNTs with oxygen-containing groups (e.g., -COOH) along the sidewalls and ends of the tubes. They reported that the functionalized SWNTs are capable of transporting proteins such as BSA and SA (with weight less than 80 kDa) and oligonucleotides into cells.

Salvador-Morales *et al*. (2006) studied the binding of proteins to the nitric acid (HNO_3) purified carbon nanotubes in human plasma and serum. They found that when double-walled carbon nanotubes (DWNTs) were exposed to the human serum and plasma, only

a few proteins, such as fibrinogen and apolipoprotein A1, can bind to DWNT in large quantity. Other proteins, including apolipoprotein AIV and C-III, were found to bind to DWNT in low quantity.

In the study of using carbon nanotubes to measure H_2S in aqueous media, Wu *et al*. (2008) reported that hemoglobin can bind with non-functionalized MWNTs in the aqueous solution. The binding was observed by Raman spectra. Such binding did not affect the adsorption of H_2S on MWNTs and was insensitive to the fluorescence response of H_2S which is attached to MWNTs.

Table 2.1 summarizes the recent studies on the interaction between CNTs and proteins.

Table 2.1. Interaction of CNTs with proteins: an overview

Protein	**Binding**	**CNT**	**Test Method**	**Mechanism**	**Author**
Streptavidin, HupR	Yes	MWNT (as-grown)	TEM	Hydrophobic interaction	Balavoine *et al*. (1999)
Streptavidin, ferritin	No	SWNT (as-grown)	TEM, AFM	Functionalization is required to achieve selective binding of proteins on CNTs	Chen *et al*. (2001)
Streptavidin	Yes	SWNT (as-grown)	AFM	Hydrophobic interaction, and electrostatic interaction	Shim *et al*. (2002)
Fibrinogen	No			Too large (~340 Kda, 45nm) to be absorbed by SWNT (~2nm), in contrast to Streptavidin (~60 Kda)	
BSA, SA, Avidin, GCD, SpA	Yes, Irreversible	SWNT (as-gown)	AFM, QCM, and electronic sensing	Hydrophobic interaction and electrostatic interaction. NSB of protein on SWNT is a general phenomenon.	Chen *et al*. (2003)
BSA, HSA, hCG, α-hCG, hIgG, avidin	Yes, irreversible. (the adsorption of hCG against further adsorption of IgG)	SWNT (as-grown)	AFM, QCM, ,electronic sensing and XPS	Hydrophobic interaction	Chen *et al*. (2004)
Fibrinogen, Apolipoprotein A1	Yes, (other proteins in serum/plasma, No)	DWNT (HNO_3 purified)	Mass spectrometry and sequence analysis	N/A	Salvador-Morales *et al*. (2006)
BSA, SA	Yes	SWNT (functionalized)	AFM	Functional group (e.g., -COOH) introduced by acid oxidization.	Kam *et al*. (2005)
Hemoglobin	Yes	MWNT (non-functionalized)	Raman spectroscopy	N/A	Wu *et al*. (2008)

It can be seen from Table 2.1 that there are mixed results regarding proteins interacting with CNTs. Some suggested that CNT functionalization, such as chemical coating, acid oxidization, ammonia treatment and so on, were necessary for the binding of proteins to CNTs. Others suggested that the proteins were ready to bind to as-grown CNTs and the functionalization was developed to prevent such undesired bindings (Chen *et al*., 2003, 2004).

In a previous study, the mixed results were obtained as well. The preliminary study done by Wu *et al*. (2007) reported that the proteins did not bind to non-functionalized MWNTs in the serum. However, Wu *et al*. (2008) reported that hemoglobin can bind with non-functionalized MWNTs in water solution. Therefore, a further study on the interactions between proteins and CNTs is needed, especially the study on how the interactions may affect the measurement of H_2S by using CNTs.

CHAPTER 3: MATERIALS AND METHODS

3.1 Introduction

In this chapter, materials and methods common to all the experiments conducted in this thesis study are described. They may be used for one or more experiments to study the problems as defined in Chapter 1. The materials include carbon nanotubes, sera, proteins, and H_2S. The methods are related to the facilities including Raman spectroscopy, confocal laser scanning microscopy, and Sulfur K-edge X-ray Absorption Near-edge Spectroscopy,

3.2 Materials

3.2.1 Carbon Nanotube

SWNT and MWNT with two different sizes but the same type were used in the studies. All the CNT samples were in powder forms. SWNTs were purchased from Carbon Nanotechnologies Inc. (Houston, USA) (see Figure 3.1). According to the manufacturer, they were produced by a high pressure carbon monoxide process (HIPCO). The average diameter of the SWNT sample is approximately 1.0 nm, and the specific surface area of the sample is around 1000 m^2/g.

Two MWNT samples with different outer diameters (10-20 nm and 60-100 nm, respectively) were purchased from Shenzhen Nanotechnologies Co. Ltd (Shenzhen, China) (see Figure 3.2). According to the manufacturer, they were produced by a chemical vapor deposition (CVD) process. The specific area of the 10-20 nm MWNT (named MW10) is around 160-180 m^2/g, and the specific area of the 60-100 nm MWNT (named MW100) is around 60-70m^2/g.

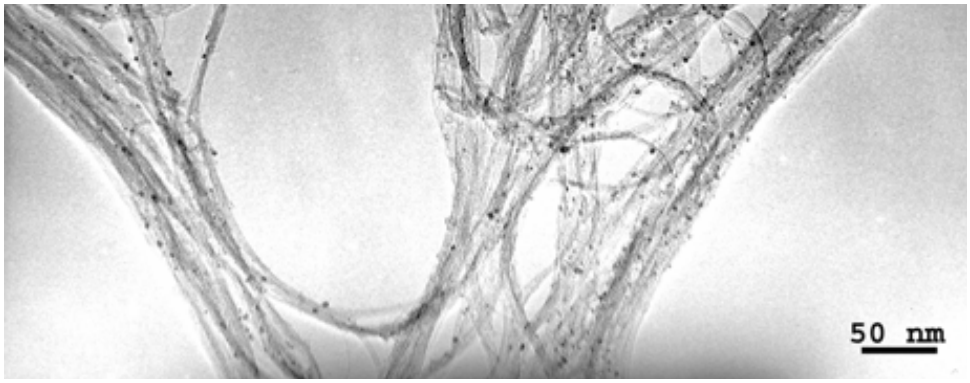

Figure 3.1. TEM image of SWNT provided by the vendor (CNI Inc.) upon purchase of SWNT.

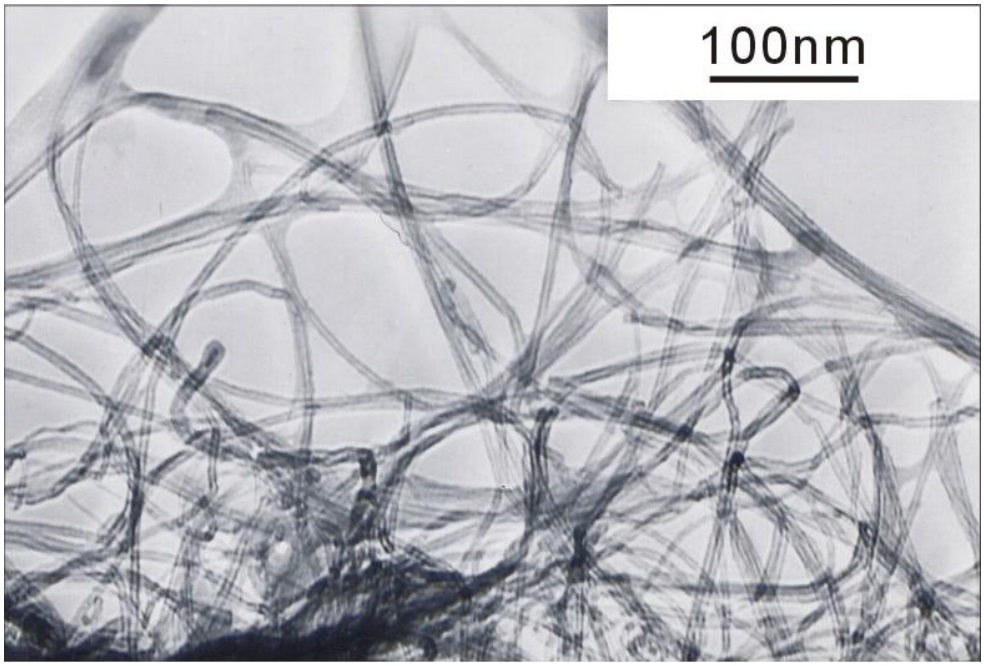

Figure 3.2. TEM image of MW10 provided by the vendor (Shenzhen Nanotechnologies Co. Ltd) upon purchase of MW10.

According to the manufacturers, all the CNT samples have been purified. The purity of the SWNT sample is >85% and that of the MWNT samples is >90%. No further purification and functionalization processes were performed on these CNT samples.

CNT samples prepared for Raman spectroscopy or confocal laser scanning microscopy or Sulfur K-edge X-ray Near-edge Absorption Spectroscopy were first immersed into the solutions, including distilled water, proteins, and sera, for 1 hour, and then taken out and dried on the glass slide at the room temperature.

3.2.2 H_2S Water Solution Sample Preparation

Hydrogen sulfide solutions were prepared at Dr. Lingyun Wu's laboratory at the Department of Pharmacology, University of Saskatchewan. Hydrogen sulfide gas-

saturated solution (90 mM) was prepared by bubbling pure hydrogen sulfide gas into 40 ml distilled water at 30ºC and 10 psi for 30 min. The H_2S gas-saturated solution was freshly prepared on the day of the measurement. NaOH solution (300 ml) was used to trap the extra H_2S gas. The equipment was gas-tight sealed. The lower concentrations (μM level) of hydrogen sulfide water solutions were diluted from 90 mM H_2S solution.

3.2.3 Protein and Serum Samples Preparation

Two serum proteins, namely bovine serum albumin (BSA) (Cat. # A7906) and bovine gamma-globulin (γ-Globulin) (Cat. # G5009), were purchased from Sigma-Aldrich. They are in white powder forms. Protein solutions were made by solving proteins in distilled water. BSA solution with concentration of 30 mg/mL and γ-Globulin solution with concentration of 15 mg/mL, which are close to their real concentration in the serum, were prepared. The protein solutions with different concentrations of H_2S (50 μM, 100 μM, 200 μM) were prepared by adding a dedicated amount of H_2S solution into the protein solutions, and the low concentration solutions were obtained by diluting from the high concentration solutions. Fetal bovine serum (Cat. #F2442) was purchased from Sigma-Aldrich. Using the sulfide ion-specific electrode (Model LIS-146AGSCM, Lazar Research Lab, Inc.) measurement, the bovine serum contains around 30 μM H_2S.

3.3 Methods

3.3.1 Confocal Laser Scanning Microscopy Fluorescence Measurement

Confocal Laser Scanning Microscopy (Leica TCS SP2), at the Department of Comparative Biomedical Science, Louisiana State University, was used to acquire the

fluorescence of CNT samples treated with various solutions as described before (e.g., serum solution, H_2S water solution, etc.). The incident light was set at 514 nm to excite sulfide and the emission light was collected with a bandpass filter at a range from 530 to 580 nm to collect the emitted fluorescence of sulfide. For each CNT sample, thirty different spots were scanned, and their average was recorded.

3.3.2 Raman Spectroscopy CNT Spectrum Measurement

Raman spectroscopy (Renishaw inVia Raman Microscope) at Saskatchewan Structural Science Center (SSSC) was used to acquire the Raman spectra of carbon nanotubes treated with various solutions. Lecia 50x objective was used to focus the laser beam on the samples. For SWNT samples, excitation laser with 785 nm wavelength was used, laser power was set at 0.1%, and cosmic ray removal function was turned on. For MWNT samples, excitation laser with 514 nm wavelength was used, cosmic ray removal function was turn on and 12 accumulations were used. For each CNT sample, 3 different spots on each sample were scanned under Raman spectroscopy.

3.3.3 Sulfur K-edge X-ray Near-edge Absorption Spectroscopy Measurement

Sulfur K-edge X-ray near-edge absorption spectroscopy (XANES) was used to understand (1) the mechanism behind two basic proteins (BSA and γ-Globulin) that may bind with CNTs and (2) the desulfurization of these proteins. The motivation for (1) is that whether proteins in the serum are attached to CNT is still unknown (see discussion in Chapter 1). The motivation for (2) is a couple of reports of desulfurization of proteins and peptides, such as desulfurization of BSA (Khan *et al*., 1980; Whitfield *et al*., 2008) in the ISE measurement process, desulfurization of amino acid L-cysteine on nickel

surface but non-desulfurization of amino acid L-cysteine on copper surface (Yagi *et al*., 2003).

The rationale for the use of XANES (1) and (2) is the knowledge that sulfur K-edge XANES is very sensitive to the chemical forms of sulfur in the samples (e.g., in the CNT samples) and sulfur is the basic element in BSA and γ-Globulin. Therefore, it may be possible to discover some knowledge for (1) and (2) by examining the forms of sulfur that may be attached on the CNT before and after it interacts with CNTs by using sulfur K-edge XANES.

The sulfur K-edge XANES measurements were carried out on the Soft X-ray Micro-characterization Beamline (SXRMB) at Canadian Light Source (CLS). Double crystal monochromator Si (111) was used to achieve high resolution measurement. The CNT samples and proteins samples (used for control) were mounted on the carbon tapes and put in the high vacuum chamber for the measurement.

The Sulfur K-edge XANES spectra of the samples were obtained by using fluorescence yield detection (FLY) that provides a deeper penetration and relatively better signal to noise ratio at sulfur K-edge (Jalilehvand, 2006). The X-ray energy was calibrated by setting the elemental sulfur (S_8) K-edge, which has (0) oxidation state, white-line point to 2472 eV. The edge position was determined using derivative curves. A linear background subtraction was performed by extrapolating a background line from the pre-

edge region (Hay *et al*., 2004). Spectra were finally normalized to the height of the jump edge of sulfur.

3.3.4 Sulfide ion-specific electrode (ISE) measurement

Sulfide ion-specific electrode (ISE) instrument was used to measure H_2S in solutions, and the purpose of the ISE measurement in this thesis study was to provide a means to verify the proposed approach to measure H_2S with CNT and fluorescence response.

The ISE Model LIS-146AGSCM (Lazar Research Lab, Inc., Las Angeles, CA) with Lazar Model 601A (Lazar Research Lab, Inc) digital pH/millivolt meter was used by following the manufacturer's procedure to measure H_2S in the experiments. Standards solutions, between 10^{-6} to 10^{-2} M, were prepared from Na_2S stock solution, which was freshly prepared on the day of the measurement. The standardization curve was obtained by plotting millivolt (Y axis) vs. sulfide ion concentration(X axis) on semi log paper and drawing the best straight line through points. The linear range of the sulfide sensitive electrode was found to be greater than 10 μM, which is sufficient for all the experiments in the study.

CHAPTER 4: MEASUREMENT OF HYDROGEN SULFIDE IN SERA

4.1 Introduction

Multi-wall carbon nanotube (MWNT) with confocal laser scanning microscopy was successfully used to measure H_2S concentration in both water and sera in the previous studies (Wu *et al*., 2007). Wu *et al*. (2006) also reported that different forms of MWNT may affect the measurement of H_2S in water solution. In this chapter, a study is described on the effects of single-wall carbon nanotube (SWNT) and two different sizes of MWNT on the measurement of H_2S in sera.

4.2 Materials and Methods

The bovine serum was used. A calculated amount of H_2S was added to the serum to increase the level of H_2S to 1mM, which was verified by the sulfide ion-specific electrode. The serum samples with the concentrations of H_2S ranging from 30 μM, 40 μM, 50 μM, 60 μM, 70 μM, 80 μM, 90 μM, to 100 μM H_2S were prepared by diluting the 1mM H_2S serum sample. Confocal Laser Scanning Microscopy (CLSM) was used to acquire fluorescence response of CNT treated with these serum samples.

4.3 Results and Discussion

4.3.1 SWNT Results

The fluorescence intensity of the SWNT samples treated with 30 µM, 40 µM, 50 µM, 60 µM, 70 µM, 80 µM, 90 µM, 100 µM serum solutions, respectively, is shown in Figure 4.1. The intensity plotted in the figure is the average value of thirty spot measurements on each sample. From the figure, it can be seen that the intensity of the fluorescence increases with the increase of the H_2S concentration.

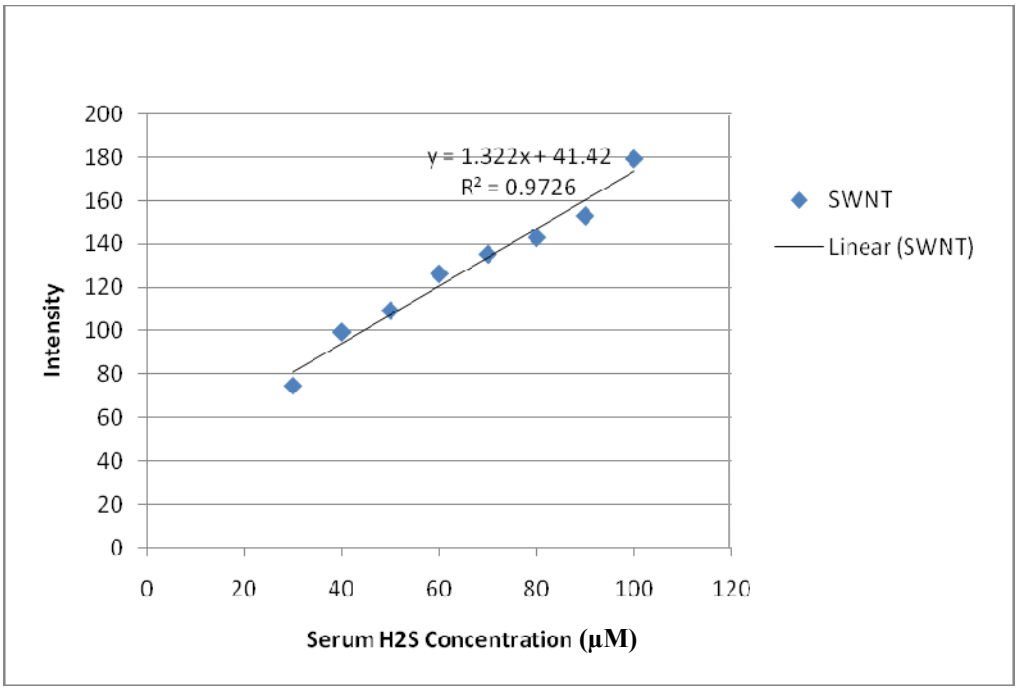

Figure 4.1. Fluorescence intensity of SWNT samples treated with the serum samples with H_2S concentration of 30 µM, 40 µM, 50 µM, 60 µM, 70 µM, 80 µM, 90 µM, 100 µM.

The linear regression analysis was further performed, which results in the following model:

$$y = 1.322x + 41.420 \quad (4.1)$$

where *y:* the fluorescence intensity of SWNT samples; *x:* the concentration of H_2S in the serum. The regression statistic output (Table 4.1), ANOVA results (Table 4.2), line fit plot (Figure 4.2), and residual plot (Figure 4.3) were also obtained.

Table 4.1. SWNT Regression statistics output.

Regression Statistics	
Multiple R	0.986
R Square	0.973
Adjusted R Square	0.968
Standard Error	5.866

Table 4.2. ANOVA for the linear relationship between H_2S concentration in the serum and the fluorescence intensities.

	Df	*SS*	*MS*	*F*	*Significance F*
Regression	1	7340.140	7340.141	213.310	6.466E-06
Residual	6	206.464	34.411		
Total	7	7546.604			

	Coefficients	*Standard Error*	*t Stat*	*P-value*	*Lower 95%*	*Upper 95%*
Intercept	41.420	6.238	6.640	0.000563	26.155	56.684
H_2S	1.322	0.0905	14.605	6.47E-06	1.101	1.544

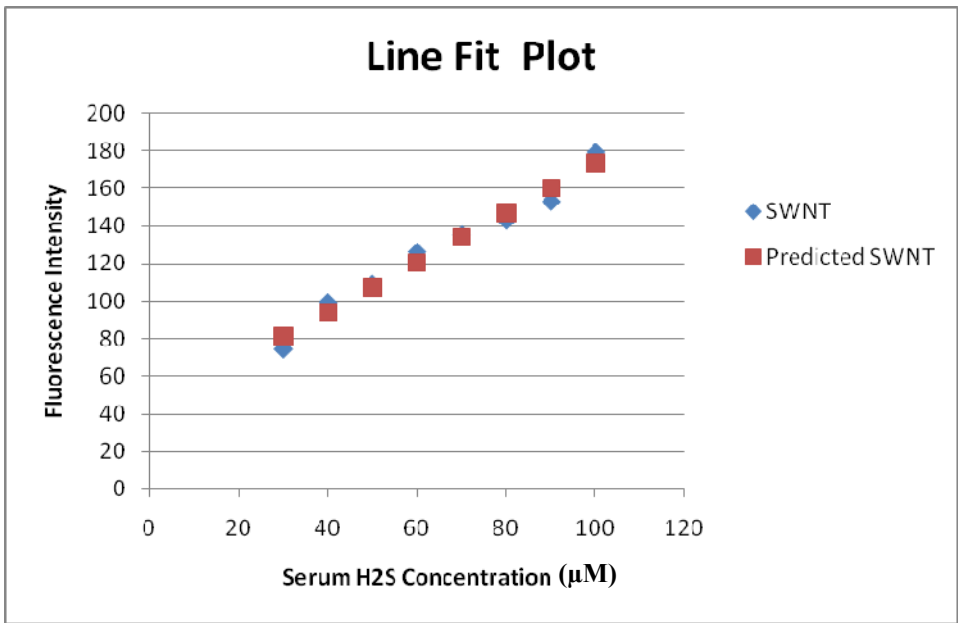

Figure 4.2. Line fit plot. X-axis shows the H_2S concentration in serum. Y-axis gives the fluorescence intensity. The small blue diamonds represent the measurement values for each H_2S concentration. The small red squares represent the values predicted by linear regression model for each H_2S concentration.

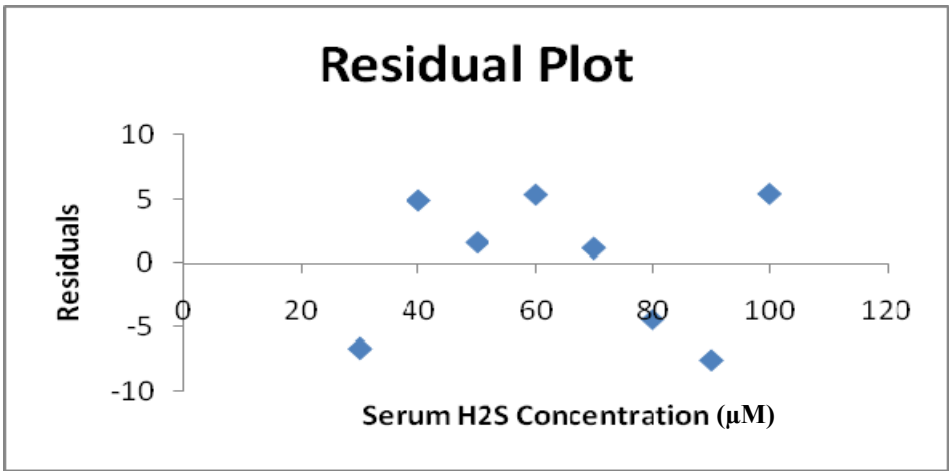

Figure 4.3. Residual plot. The small blue diamonds illustrate the residual value between the fluorescence intensity measured and the fluorescence intensity given by the regression model. The residuals look random provides the proof that linear model fits the experiment.

It can been seen from the regression statistics output table (Table 3.1), the coefficient of determination R^2 = 0.9726, which measures the proprtion of variance of Y that is explained by X, and correlation efficient R = 0.9862 (the maximum correlation between Y and a linear combination of X), are close to one, which indicates that the linear regression model, Eq. (4.1), is excellent. From ANOVA (Table 4.2), the significance level assicoatied with F-test is less than 0.01, and thus reject the null-hypothesis that independent variable has no linear effect on the dependant variable. Therefore, there is an excellent linear relationship between H_2S concentration and fluroscence response, and it can be represencted by Eq. (4.1).

4.3.2 MWNT Results

4.3.2.1 MW10 Results and Regression Analysis

The result of MW10 measurement is shown in Figure 4.4. From this figure, it can be seen that the fluorescence intensity of the MW10 samples increases with the increase of the H_2S concentration in the serum. To establish the reltionship between the fluroescence intensity and H_2S concentration, the linear regression analysis was conducted. The regression statistic output (Table 4.3), ANOVA results (Table 4.4), line fit plot (Figure 4.5), and residual plot (Figure 4.6) were also obtained after the analysis.

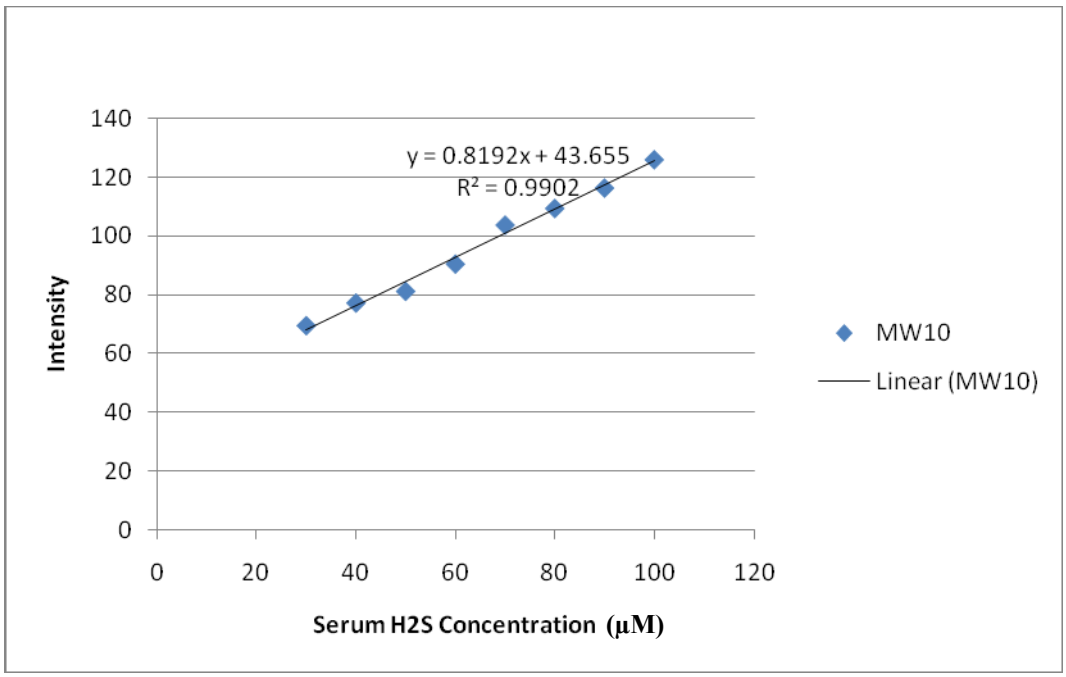

Figure 4.4. Fluorescence intensities of MW10 samples treated with the serum samples with H_2S concentration of 30 µM, 40 µM, 50 µM, 60 µM, 70 µM, 80 µM, 90 µM, 100 µM.

Table 4.3. MW10 Regression statistics output.

Regression Statistics	
Multiple R	0.995
R Square	0.990
Adjusted R Square	0.989
Standard Error	2.154

Table 4.4. ANOVA for the linear relationship between H_2S concentration in serum and MW10 fluorescence intensities.

	Df	*SS*	*MS*	*F*	*Significance F*
Regression	1	2818.834	2818.834	607.696	2.931E-07
Residual	6	27.831	4.639		
Total	7	2846.666			

	Coefficients	*Standard Error*	*t Stat*	*P-value*	*Lower 95%*	*Upper 95%*
Intercept	43.655	2.290	19.059	1.35E-06	38.050	49.259
H_2S	0.819	0.0332	24.651	2.93E-07	0.738	0.901

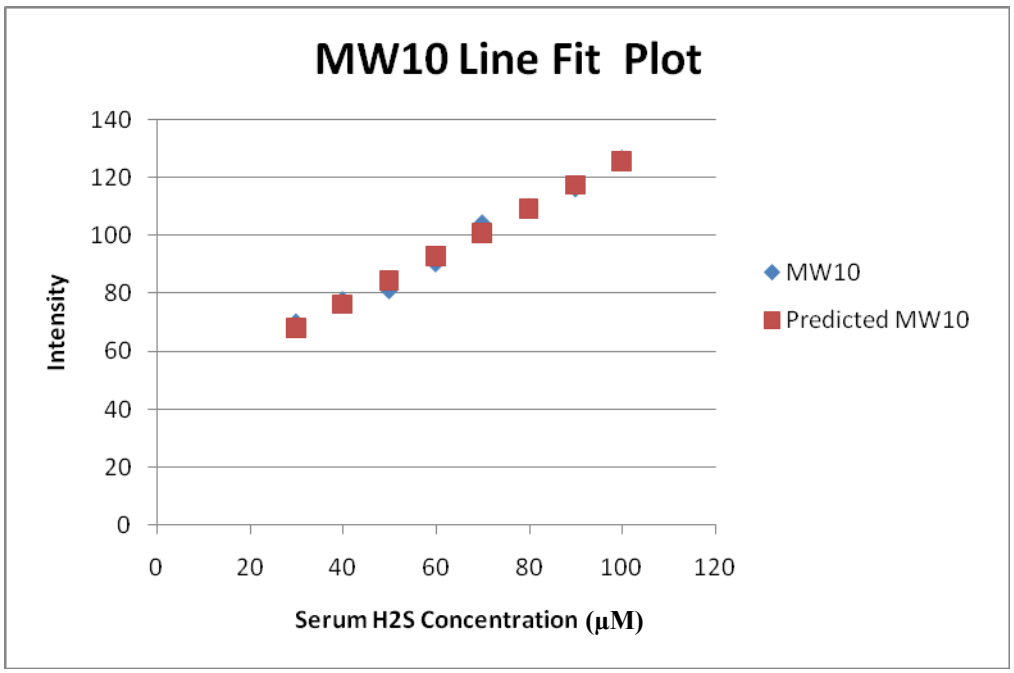

Figure 4.5. MW10 line fit plot. X-axis shows the H_2S concentration in serum. Y-axis gives the fluorescence intensity. The small blue diamonds represent the measurement values for each H_2S concentration. The small red squares represent the values predicted by regression model for each H_2S concentration.

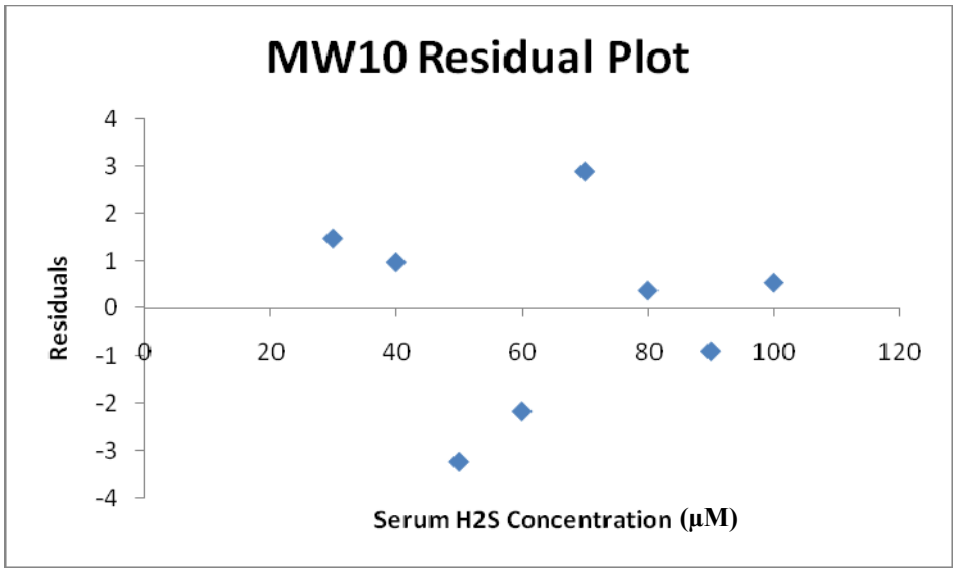

Figure 4.6. MW10 Residual plot. The small blue diamonds illustrate the residual value between the fluorescence intensity measured and the fluorescence intensity given by the regression model. The residual plot looks random provides the proof that linear model fits the experiment.

It can be seen from Table 4.3 that R^2 = 0.9726, and from ANOVA (Table 4.4) the significance level is less than 0.01, which indicate that there is an excellent linear relationship between H_2S concentration and fluorescence response. This relationship can be represented by the following linear model:

$$y = 0.819x + 43.655 \quad (4.2)$$

where y: the fluorescence intensity of MW10 samples; x: the concentration of H_2S in the serum.

4.3.2.2 MW100 Results and Regression Analysis

The fluorescence intensity of the MW100 samples versus the concentration of H_2S in the serum is shown in Figure 4.7. The results of statistical data analysis are shown in Figure 4.8, Figure 4.9, Table 4.5, and Table 4.6, respectively. The regression analysis indicates that the relationship between the fluorescence intensity and H_2S is linear, and it fits the following linear model quite well.

$$y = 0.899x + 39.671 \quad (4.3)$$

where y: The fluorescence intensity of MW100 samples; x: The concentration of H_2S in the serum.

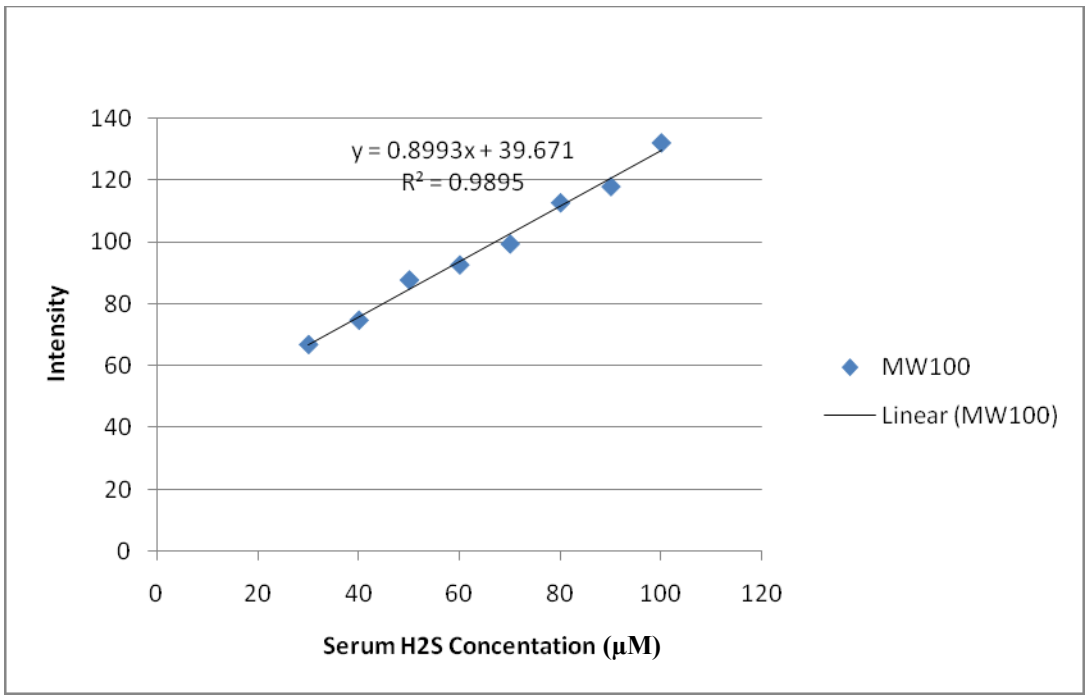

Figure 4.7. Fluorescence intensities of MW100 samples treated with the serum samples with H_2S concentration of 30 µM, 40 µM, 50 µM, 60 µM, 70 µM, 80 µM, 90 µM, 100 µM.

Table 4.5. MW100 Regression statistics output.

Regression Statistics	
Multiple R	0.995
R Square	0.989
Adjusted R Square	0.987
Standard Error	2.455

Table 4.6. ANOVA table.

	Df	*SS*	*MS*	*F*	*Significance F*
Regression	1	3396.602	3396.602	563.697	3.665E-07
Residual	6	36.153	6.026		
Total	7	3432.756			

	Coefficients	*Standard Error*	*t Stat*	*P-value*	*Lower 95%*	*Upper 95%*
Intercept	39.671	2.610	15.197	5.12E-06	33.284	46.059
Serum+H2S	0.899	0.0379	23.742	3.67E-07	0.807	0.992

Figure 4.8. MW100 line fit plot. X-axis shows the H_2S concentration in serum. Y-axis gives the fluorescence intensity. The small blue diamonds represent the measurement values for each H_2S concentration. The small red squares represent the values predicted by regression model for each H_2S concentration.

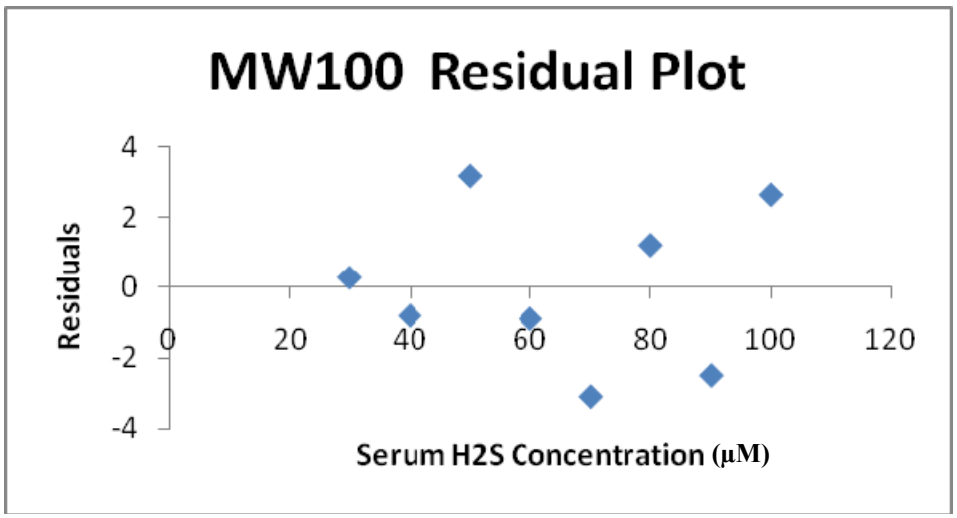

Figure 4.9. MW100 Residual plot. The small blue diamonds illustrate the residual values between the fluorescence intensity measured and the fluorescence intensity given

by the regression model. The residual plot looks random provides the proof that linear model fits the experiment.

4.3.3 Comparison of SWNT and MWNT

From the experiment results and regression analysis, the fluorescence responses of both the SWNT and MWNT samples increase with the increase of the H_2S concentration in sera with an excellent linearity. Thus, both SWNTs and MWNTs are promising to be used to measure H_2S in the serum.

Figure 4.10 plots three relationships, expressed by Eq. (4.1) to Eq. (4.3), together. From this figure, it can be seen that SWNT is more sensitive than the MWNT. However, between the two MWNT samples with different sizes of the tubes, there is no significant difference.

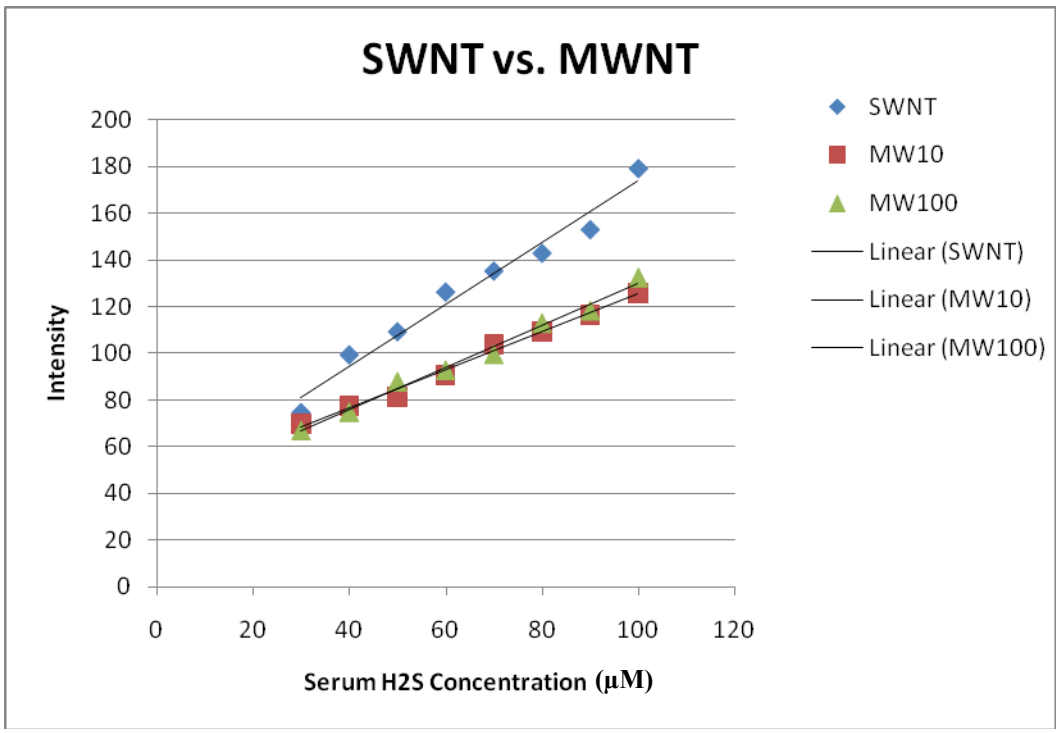

Figure 4.10. Comparisons of SWNTs and MWNTs treated with sera with different concentration of H_2S.

The forgoing results may be attributed to the different surface areas in the SWNTs and MWNTs. A single-wall carbon nanotube (SWNT) can be seen as a sheet of graphite rolled into a cylinder, and a multi-wall nanotube (MWNT) is composed of several sheets of graphite. In SWNTs, all the atoms are exposed to the surface. Therefore, SWNT usually has a much larger specific surface area than MWNT. The unit surface areas of the SWNTs and MWNTs used in this experiment are shown in Table 4.7, which is extracted from the specifications of CNTs provided by the manufacturers.

Table 4.7. Specific surface area of SWNTs and MWNTs

Type	Manufacturer	Specific Surface Area	Quantity used
SWNT	Carbon Nanotechnologies Inc.	800 - 1000 m^2/g	3 mg
MW10	Shenzhen Nanotechnologies Co. Ltd	160-180 m^2/g	3 mg
MW100	Shenzhen Nanotechnologies Co. Ltd	70-90 m^2/g	3 mg

In the experiments, the same amount of SWNT, MW10 and MW100 were used for each measurement. It can be seen from Table 4.7 that the SWNT has its specific surface area six times larger than the MW10 and 10 times larger than the MW100. It is noted that although the MW10 has its specific surface area 2 times larger than the MW100, such difference does not seems to be significant to affect the sensitivity of measurement.

To confirm the conclusion above, SWNT, MW10 and MW100 samples were also used to measure different concentrations of H_2S water solutions. The same experiment conditions and procedures were applied. The results are shown in Figure 4.11. It can be seen from Figure 4.11 that the SWNT has a higher sensitivity than both the MW10 and

MW100. In fact, the pattern of the measurement as shown in Figure 4.11 is quite consistent with that shown in Figure 4.10.

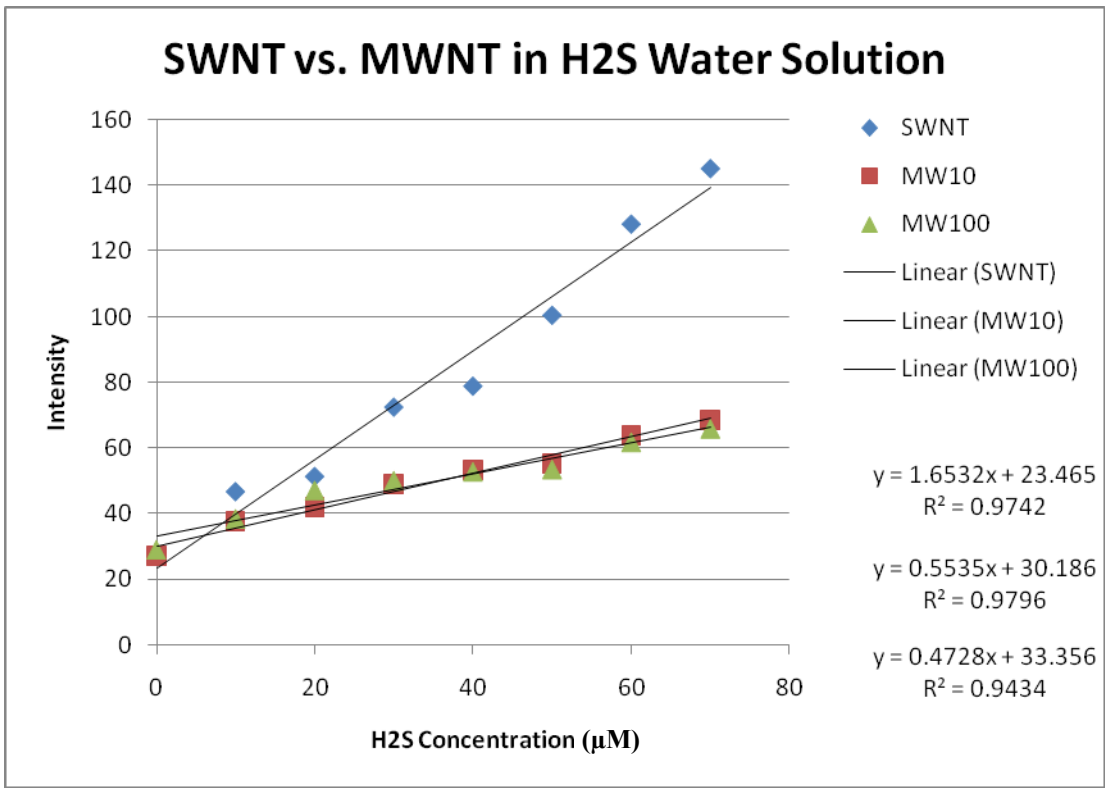

Figure 4.11. SWNT, MW10 and MW100 treated with different concentration of H_2S water solution.

4.4 Conclusions

This experiment used a SWNT and two MWNTs with different tube sizes to study the effect of the structure of the CNT on the measurement of H_2S in the serum and water solution using confocal laser scanning microscopy as a means to get fluorescence response. The following are conclusions drawn from the experimental results:

(1) There is an excellent linear relation between the fluorescence intensity of CNTs treated with sera and the H_2S concentration in sera as well as in distilled water. The approach to use CNT and CLSM for sensing H_2S in the serum and in water solutions is therefore excellent.

(2) The measurement resolution for H_2S in the serum has achieved 10 μM by using both the SWNT and MWNT.

(3) SWNT seems more promising than MWNT in the sensitivity of measurement. However, the response sensitivity of the two types of nanotubes is closer in sera than in water.

CHAPTER 5: INTERACTION OF CARBON NANOTUBES WITH PROTEINS AND HYDROGEN SULFIDE

5.1 Introduction

One of the most important issues regarding the sensor system is its specificity – i.e. the capability of the sensor to recognize a target element only, while to be insensitive to other elements. In the CNT-based approach to measuring H_2S in sera, the target molecule is H_2S; however, the serum is a complicated system, which includes many other substances, mainly proteins. The question is: does the presence of proteins affect the specificity of H_2S measurement? The answer to this question demands us to understand how the proteins in sera interact with carbon nanotubes, and how the interaction between CNTs and the proteins may or may not affect the measurement. In this chapter, a study on two major proteins in the serum (serum albumin and serum globulin), their interactions with the SWNT and MWNT and their effects on the measurement of H_2S, is described.

5.2 Material and Methods

The protein solutions with different concentrations of H_2S (BSA 30 mg/mL solutions with 50 μM, 100 μM and 200 μM H_2S, γ-Globulin 15 mg/mL with 50 μM, 100 μM and

200 μM H_2S) were prepared. Different concentrations of pure BSA solutions (25 mg/mL, 30 mg/mL and 35 mg/mL) and γ-Globulin solutions (10 mg/mL, 15 mg/mL and 20 mg/mL) were also prepared as control samples. The 3mg each of SWNT and MWNT samples (MW10) were treated with all the foregoing solutions, respectively, getting all the treated CNT samples ready for Raman spectroscopy measurement and confocal laser scanning microscopy measurement.

Interactions between the proteins (BSA and γ-Globulin) and CNT was further studied with the sulfur K-edge XANES spectroscopy. CNT samples treated with the proteins solutions were prepared. The pure BSA and γ-Globulin samples were also prepared as control samples.

5.3 Results and Discussion

5.3.1 Raman Spectroscopy Measurement of BSA and γ-Globulin

Figure 5.1 shows the Raman spectra of MWNT treated with distilled water, pure γ-Globulin solution, and pure BSA solution, respectively. The defect-induced D-band at ~1345 cm-1, the tangential mode G-band at ~1572 cm-1, and G'-band (the overtone of D-band) at ~2690 cm-1 are well observed in all spectra. The spectra analysis shows that the MWNTs treated with BSA or γ-Globulin both lead to the frequency downshift of the G-band (around 5 cm^{-1}) and upshift of G'-band (around 6 cm^{-1}) in comparison with the control samples (MWNTs treated with distilled water). Interestingly, the D-band features of MWNTs are not affected. Table 5.1 summarizes the peak positions of D-band, G-band and G'-band of MWNT samples.

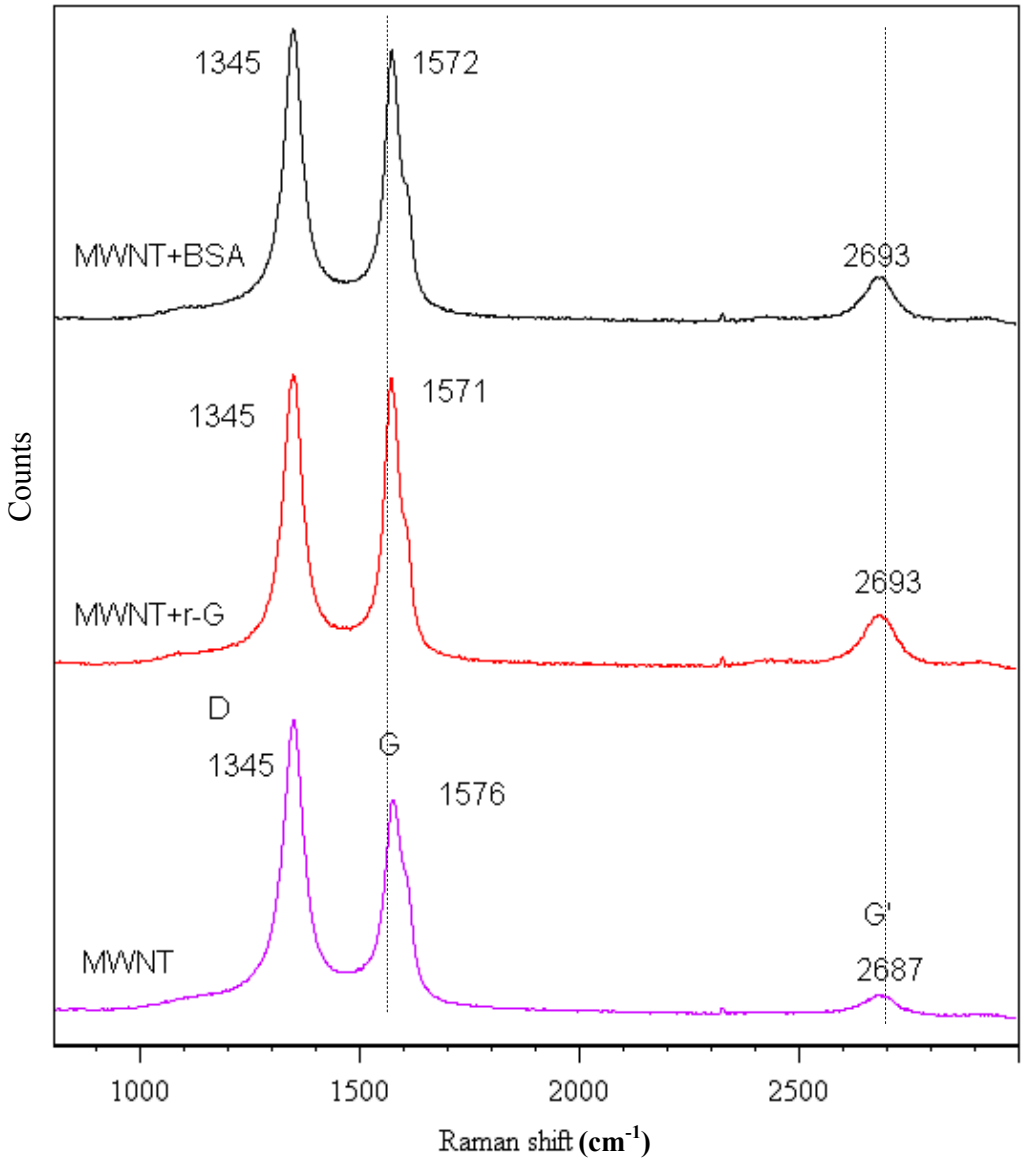

Figure 5.1. Raman spectra of MWNT treated with distilled water, γ-globulin (MWNT+ r-G), and BSA (MWNT+BSA). The dominant D-band, G-band and G'-band features are indicated in wavenumber cm^{-1}.

Table 5.1. Band positions of MWNT treated with distilled water, BSA (MWNT+BSA), and γ-globulin (MWNT+ r-G).

CNT	D	G	G'
MWNT 1	1345	1576	2687
MWNT 2	1345	1575	2688
MWNT 3	1346	1576	2687
MWNT+BSA 1	1345	1572	2693
MWNT+BSA 2	1344	1572	2693
MWNT+BSA 3	1345	1571	2694
MWNT+r-G 1	1345	1571	2694
MWNT+r-G 2	1345	1572	2693
MWNT+r-G 3	1346	1571	2693

As discussed before in Chapter 2, G-band and G'-band is sensitive to the interaction of chemical species to the sidewall of carbon nanotubes, and to the small perturbation to the electronic structure or the environment around the nanotubes. Hence, the frequency shifts of MWNTs treated with proteins may be associated with the interaction of proteins on CNTs, and this may further indicate that the adsorptions of proteins are on the sidewall of MWNTs. The zero affection on the D-band may indicate that the interaction of proteins does not affect the defect sites of MWNTs. The results may suggest that the proteins are adsorbed on the sidewall of nanotubes rather than the defect sites of the nanotubes.

The Raman spectra of SWNT treated with distilled water, BSA solution and γ-Globulin solution were also obtained. Figure 5.2 shows the Raman spectra of SWNT samples. In comparison with the MWNT Raman spectra, more unique features, such as RBM mode which can be used to evaluate the diameter distribution of SWNTs (Dresselhaus *et al*.,

2005) and the split G^+/G^- features of G-band which can be used to identify semiconducting/metallic properties of SWNTs (Jorio *et al*., 2003), are observed in the SWNT spectra.

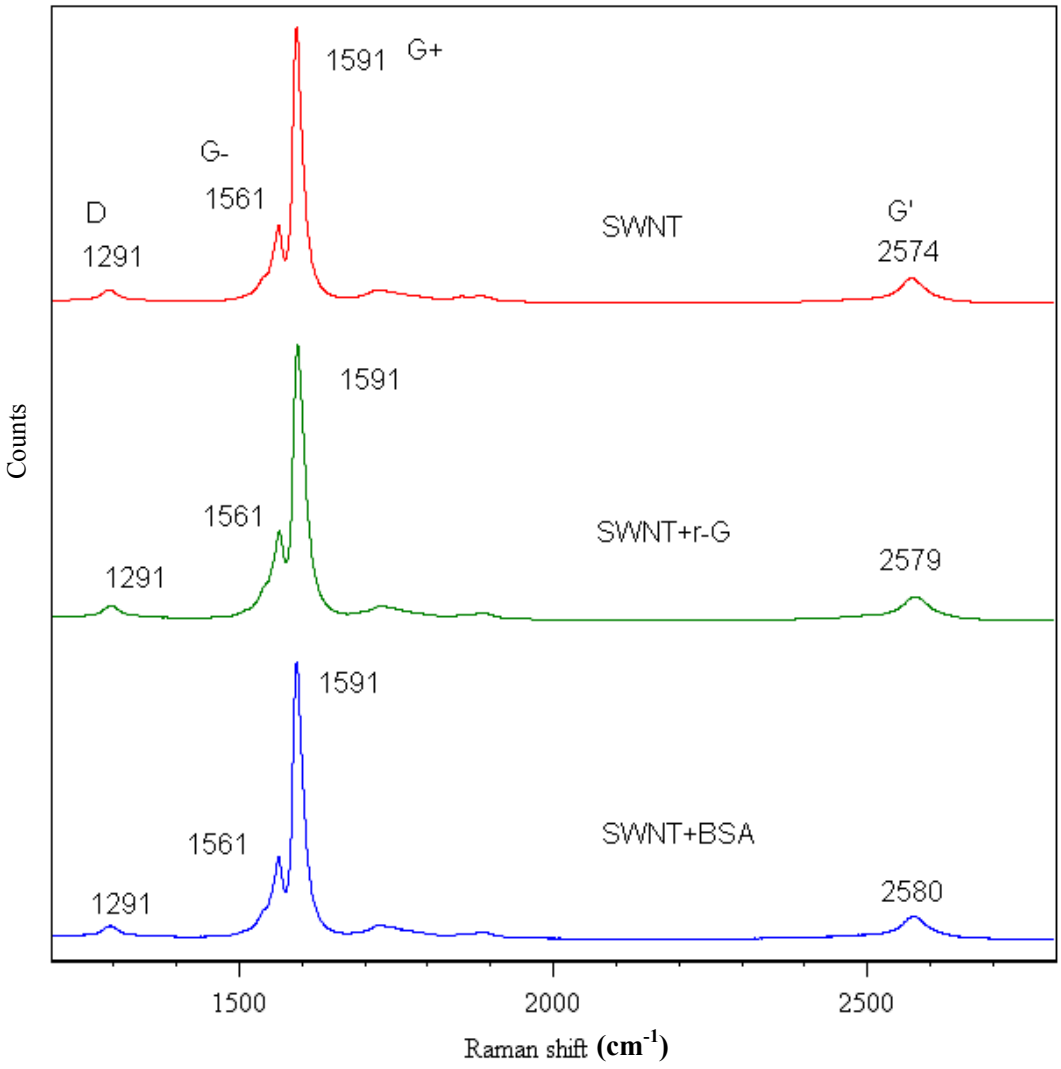

Figure 5.2. Raman spectra of SWNT treated with distilled water, γ-globulin, and BSA solution. The frequencies for the D-band, G-band (G^- and G^+) and G' band are indicated on the spectra.

The analysis of the lineshape of G^+-band and G^--band indicates that the SWNT samples used in the experiment have a semiconducting characteristic. The peak positions of D-band, G-band and G'-band of SWNT samples are summarized in Table 5.2. Unlike the MWNT spectra, there were no frequency shift observed on G-band of SWNTs treated with proteins compared to the control samples, similarly the upshift of G'-band (about 6 cm^{-1}) were observed in both SWNT samples. As discussed before, G'-band is very sensitive to the electronic structure or the environment change around the nanotubes which are very similar to G-band. Thus, the shifts of the G'-band may reflect the interactions of proteins with SWNTs. Similar to the MWNT spectra, the D-band of SWNTs remain undisturbed. Thus, the results may indicate that the interactions of proteins on SWNTs happen more likely on the sidewall of nanotubes rather than on the defect sites of the nanotubes. It is very interesting to see that unlike MWNTs there is no change observed on the G-band of SWNTs. This is perhaps related to the structural difference between MWNT and SWNT in that MWNT has interlayers but SWNT does not.

Table 5.2. Band positions of SWNT treated with distilled water, BSA (SWNT+BSA), and γ-globulin (SWNT+ r-G).

CNT	D	G-	G+	G'
SWNT 1	1291	1561	1591	2574
SWNT 2	1290	1561	1591	2573
SWNT 3	1291	1561	1590	2574
SWNT+BSA 1	1291	1561	1591	2580
SWNT+BSA 2	1292	1560	1590	2579
SWNT+BSA 3	1291	1561	1591	2580
SWNT+r-G 1	1291	1561	1591	2579
SWNT+r-G 2	1291	1560	1590	2579
SWNT+r-G 3	1290	1561	1591	2580

The results of Raman spectra analysis can be summarized in the following. First, the interactions of proteins with MWNTs and SWNTs can be observed through Raman spectra. In MWNTs, the carbon nanotubes treated with BSA and γ-Globulin led to the frequency downshift (about 5 cm^{-1-}) of G-band and upshift of G'-band (around 6 cm^{-1}). In SWNTs, no frequency shift was observed on G-band; similarly, the upshifts (about 6 cm^{-1}) of G'-band were observed. The difference among SWNTs and MWNTs may be attributed to the inherent structural differences of SWNT and MWNT, and may also be attributed to the different wavelength of laser (resonance to achieve better signal to noise ratio), which was employed to obtain the spectra. The band shifts between carbon nanotubes treated with BSA and γ-Globulin are almost identical, which may be due to the resolution limit of Raman spectroscopy used.

Second, the interactions of the proteins on CNTs affect the G-band and G'-band of MWNTs but only G'-band of SWNT, both G-band and G'-band are sensitive to the electronic structure or environment changes around the nanotubes, and have been used to study the attachment of chemical species to the sidewall of the nanotubes. Neither D-band of MWNT nor of SWNT was affected by the proteins. The results may indicate that the interaction/adsorption of the proteins on CNTs probably happen on the sidewall of the nanotubes rather than the defect sites of the nanotubes, which is in agreement with the hypothesis stated in Chapter 2.

5.3.2 Confocal Laser Scanning Microscopy Measurement of BSA and γ-Globulin

The results of CLSM fluorescence measurement of CNTs treated with pure protein solutions and CNTs treated with protein solutions with different concentration of H_2S

are presented in this section. The fluorescence responses of MWNT treated with 25 mg/mL, 30 mg/mL and 35 mg/mL of BSA solutions are shown in Figure 5.3. It can be seen from this figure that the fluorescence intensities do not change significantly with the change of BSA concentrations. It seems that BSA is not sensitive under the specific wavelength chosen to measure H_2S.

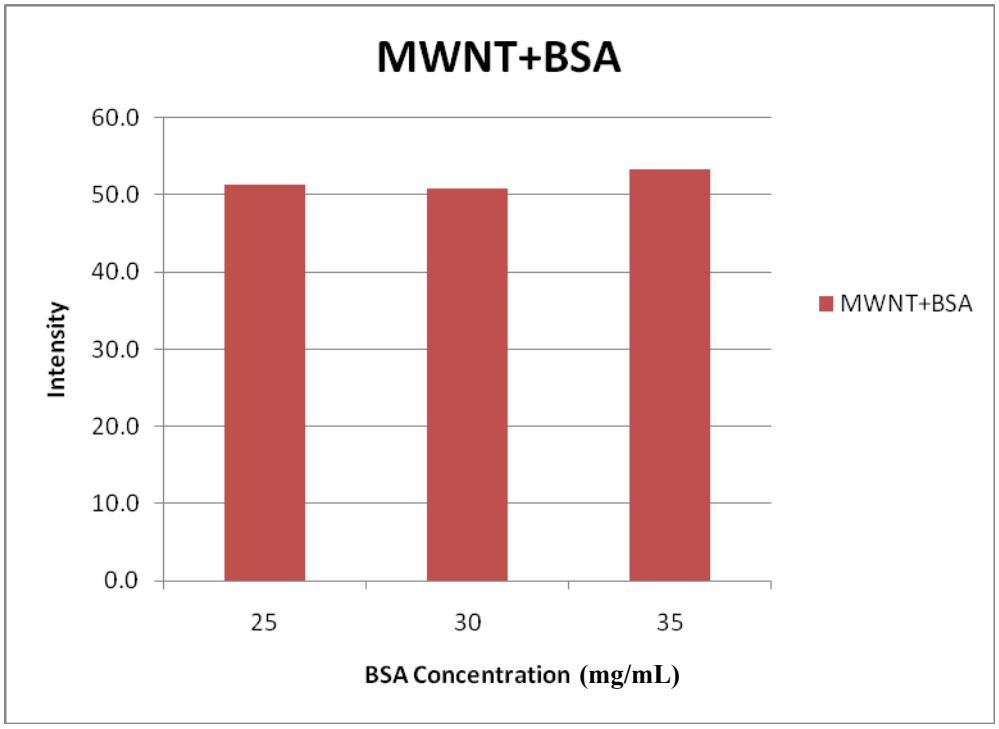

Figure 5.3. Fluorescence intensity of MWNTs treated with different concentration of BSA solutions (25 mg/mL, 30 mg/mL, 35 mg/mL).

In the next experiment, the concentration of BSA (30 mg/mL) was kept unchanged, and H_2S was added to the BSA solution. The fluorescence intensities of MWNT treated with BSA solutions with different concentrations of H_2S (50 μM, 100 μM, 200 μM) are shown in Figure 5.4. The pure BSA (30 mg/mL) solution was used as control sample.

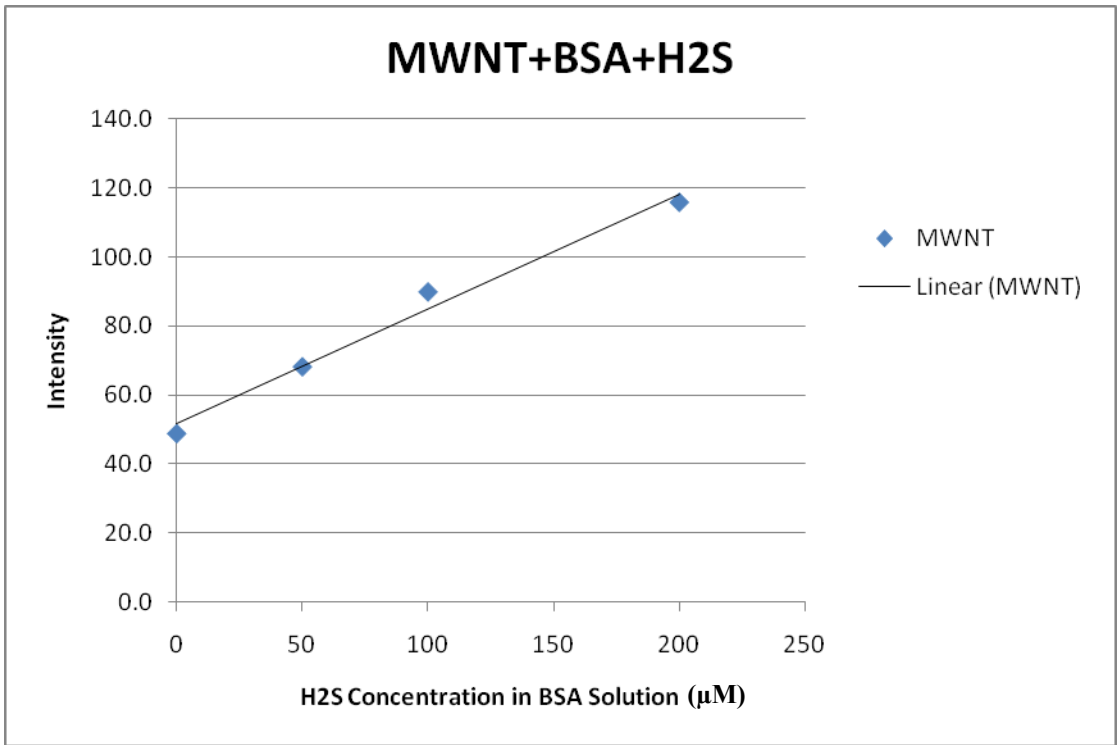

Figure 5.4. Fluorescence intensity of MWNT treated with BSA solutions with different concentration of H_2S (0, 50 μM, 100 μM, 200 μM).

It can be seen from Figure 5.4 that the fluorescence intensities increase as the concentrations of H_2S in BSA solutions increase, and it appears to be linear. As discussed in the previous experiment, the BSA would not change the fluorescence intensities. Thus, the change of fluorescence responses here must come from H_2S. Therefore, the results from both experiments suggest that the fluorescence responses of MWNTs are sensitive to the H_2S concentration in the protein solutions, and the BSA seems not to affect the adsorption of H_2S by MWNT and the measurement of H_2S.

The fluorescence measurement of MWNTs treated with γ-Globulin, and γ-Globulin solutions with different concentrations of H_2S were also conducted (Figure 5.5).

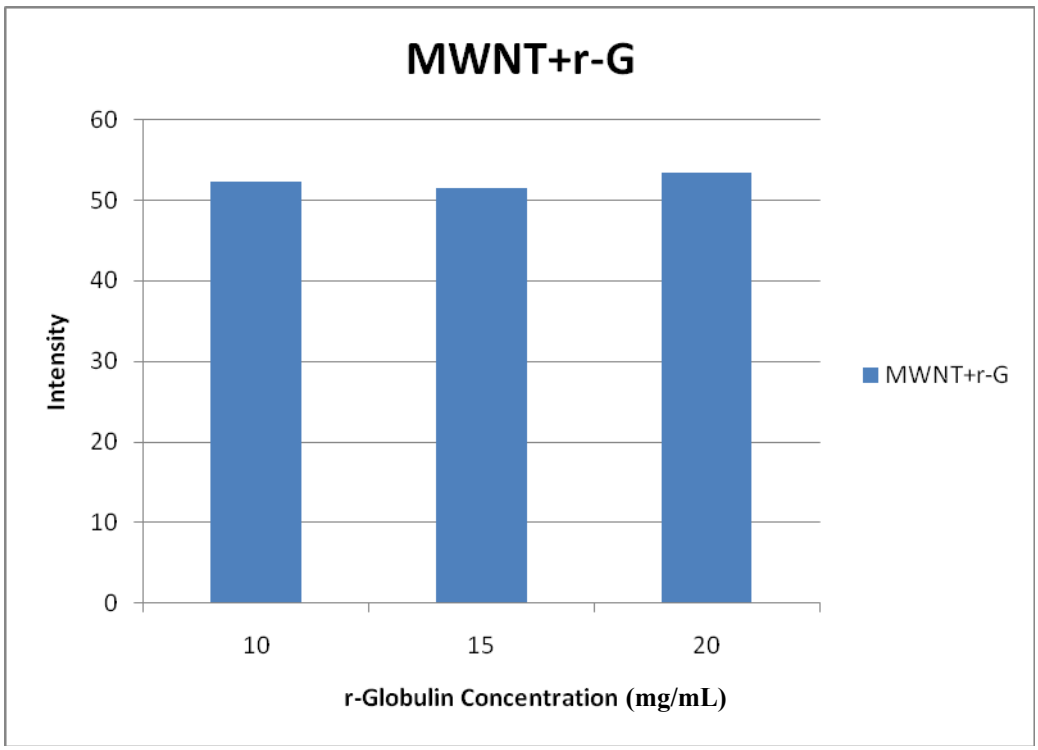

Figure 5.5. Fluorescence intensity of MWNT samples treated with different concentration of γ-Globulin solutions (10 mg/mL, 15 mg/mL, 20 mg/mL).

It can be seen from Figure 5.5 that the intensities of fluorescence do not change significantly as the γ-Globulin concentrations increase. In the next experiment, H_2S was added to the 15 mg/mL γ-Globulin solution. The fluorescence intensities of MWNT treated with γ-Globulin solutions (15 mg/mL) with different concentration of H_2S (50 μM, 100 μM, 200 μM) are shown in Figure 5.6, where pure γ-Globulin solution (15mg/mL) was used as control samples.

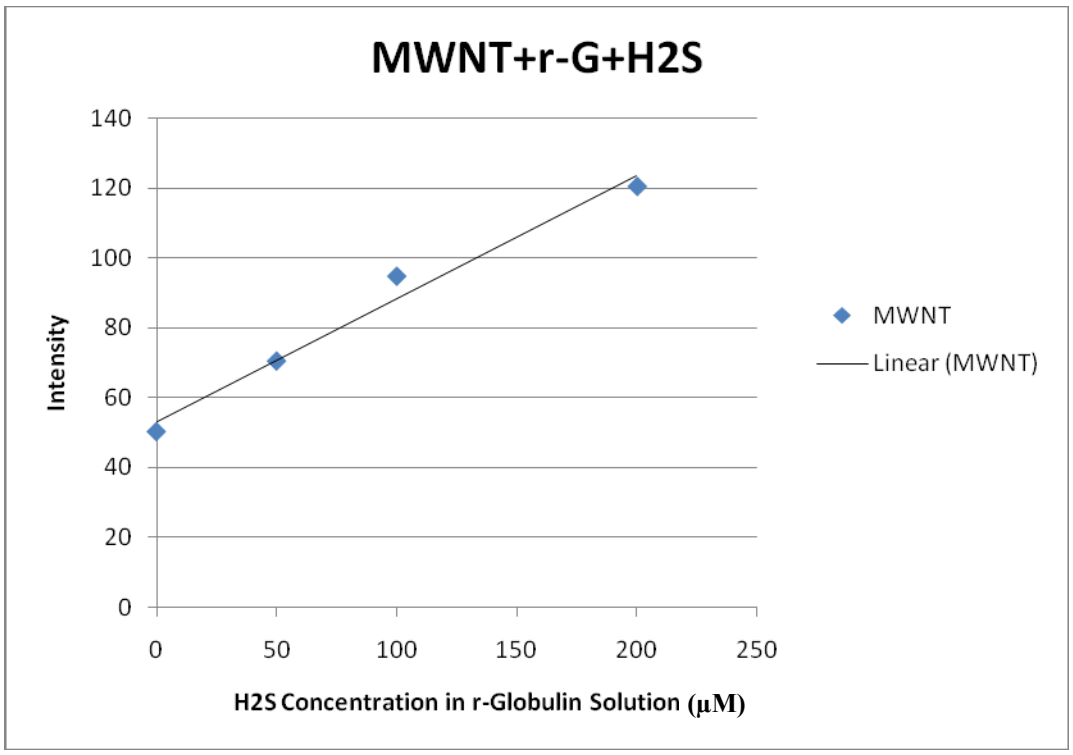

Figure 5.6. Fluorescence intensity of MWNT samples treated with γ-Globulin (15 mg/mL) solutions with different concentration of H_2S (0, 50 μM, 100 μM, 200 μM).

It can be seen from Figure 5.6 that the fluorescence intensities increase with the increase of H_2S concentrations in γ-Globulin solution, and it appears to be linear. Thus, this suggests that CNTs can be used measure to H_2S in γ-Globulin solution, and the presence of γ-Globulin seems not to affect adsorption of H_2S by CNTs and the measurement of H_2S.

The same experiments with SWNT were performed, and the results are consistent with the MWNT experiments. Thus, it can be concluded that: First, the fluorescence responses of CNTs treated with BSA and γ-Globulin do not change with the change of proteins' concentration. Thus, both proteins are insensitive to the CLSM fluorescence

measurement under the specific wavelength chosen to measure H_2S. Second, the fluorescence intensities increase with the H_2S concentrations in protein solutions increase, and the relationship between the intensity of fluorescence and the concentration of H_2S appears to be linear. The results suggest that the fluorescence measurement are sensitive to the H_2S concentration in BSA and γ-Globulin solution, and the presences of BSA and γ-Globulin seem not to affect the adsorption of H_2S by CNTs and the measurement of H_2S.

5.3.3 Sulfur X-ray Near-edge Absorption Spectroscopy Measurement

BSA includes a great number of sulfur-containing amino acids, precisely 35 cysteines and 5 methionines; 34 out of 35 cysteines are engaged in the formation of 17 disulfide bonds. Accordingly, the sulfur (S) K-edge XANES spectrum of BSA is expected to exhibit a main contribution from the disulfide bonds (Ascone, 2008). The S K-edge spectrum of the pure BSA sample is shown in Figure 5.7, and the spectrum is dominated by the disulfide bonds, which is in agreement with the expectation. The spectrum of the pure SWNT sample was also obtained for the control purpose (see Figure 5.7). As expected, no sulfur existence on the pure SWNT was observed.

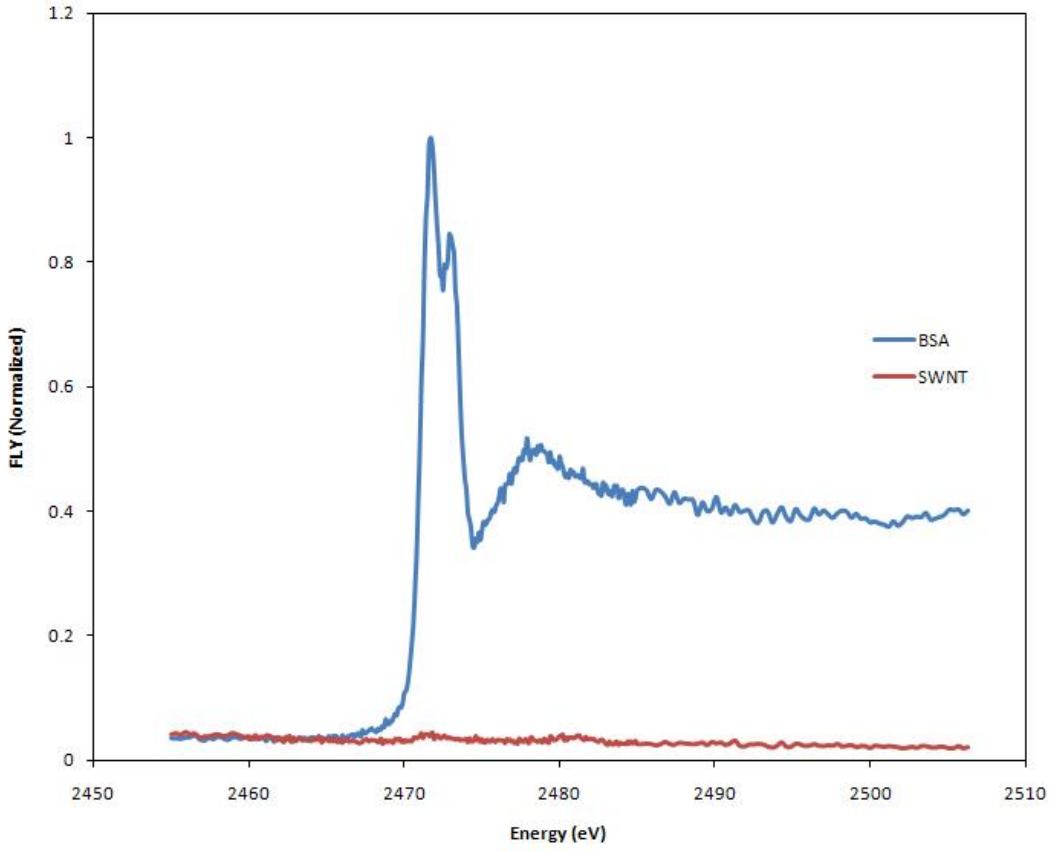

Figure 5.7. Sulfur K-edge XANES spectra of pure BSA and pure SWNT, disulfide bridges dominate the BSA spectrum, no clear measurement of sulfur species is obtained on pure SWNT.

After recording the XANES spectra of pure BSA and pure SWNT, the acquisition of XANES spectra of CNT treated with BSA (named SWNT+BSA) was conducted. Figure 5.8 compares the spectra of SWNT+BSA, BSA and SWNT. It can be seen from this figure that the spectrum of SWNT+BSA is almost identical to the spectrum of BSA. This suggests that the sulfur signal of SWNT+BSA sample comes from the protein. This also provides the evidence that BSA is presented on CNT. From Figure 5.8, no new features or peaks appear on the SWNT+BSA spectrum in comparison with the BSA

spectrum, which implies that CNT scarcely perturbs the environment of the sulfur in the protein. Thus, CNTs would not cause the dissociation or desulfurization of BSA.

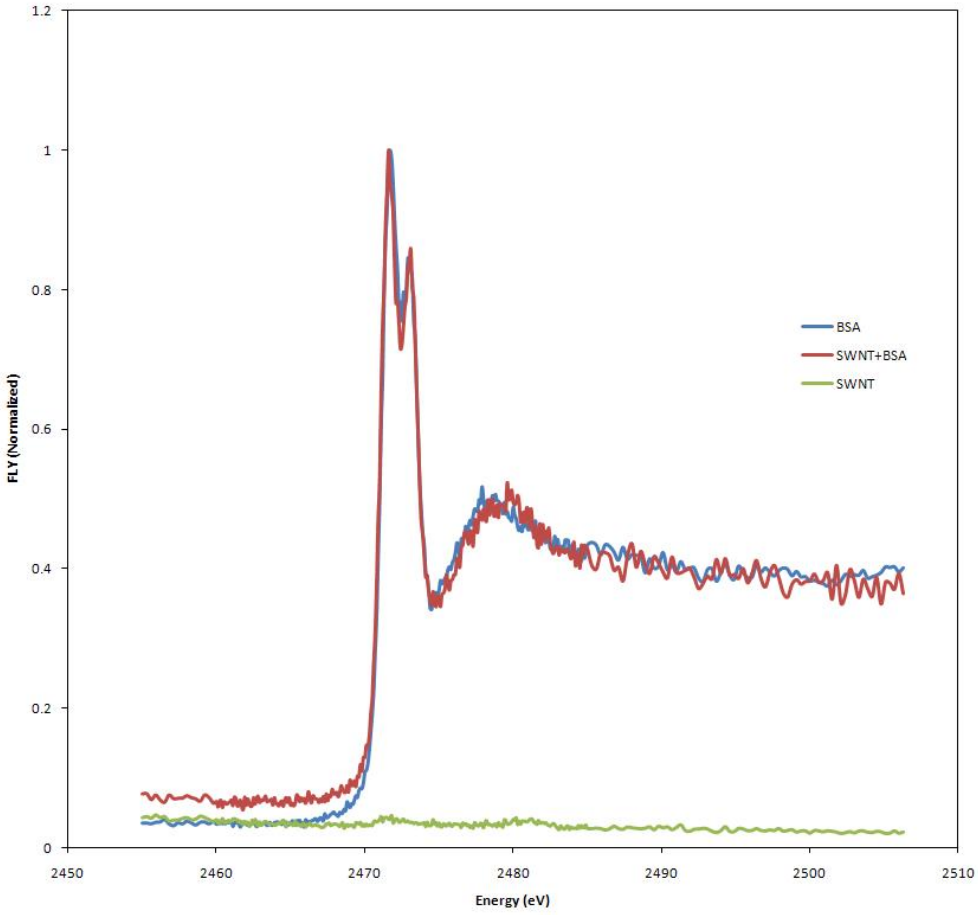

Figure 5.8. Sulfur K-edge XANES spectrum of SWNT treated with BSA (SWNT+BSA) compared to pure BSA and SWNT spectra. The spectrum of SWNT+BSA is almost identical to BSA spectrum, which indicates (1) BSA is adsorbed on CNTs (2) CNT is not able to dissociate or desulfurize BSA. BSA is likely physically adsorbed on CNTs.

The interaction between γ-Globulin and MWNT were studied under sulfur K-edge XANES. The spectrum of pure MWNT was obtained first, which is shown in Figure 5.9, and no sulfur were found present on the MWNT as expected. The spectrum of γ-Globulin is a bit different from the one of BSA. This may be attributed to the different

sequences sulfur-containing amino acids in γ-Globulin in comparison with that in BSA; in particular, more methionines and less cysteines were included in γ-Globulin than BSA according to Bellacchio *et al*. (2001).

It can be seen from Figure 5.9 that the spectrum of MWNT treated with γ-Globulin (named MWNT+r-G) is almost identical to the pure γ-Globulin spectrum; this suggests that γ-Globulin is present on MWNT. No new features were observed from the MWNT+r-G spectrum in comparison with the pure γ-Globulin spectrum, which confirms that the chemical form of γ-Globulin is intact after interaction with CNTs.

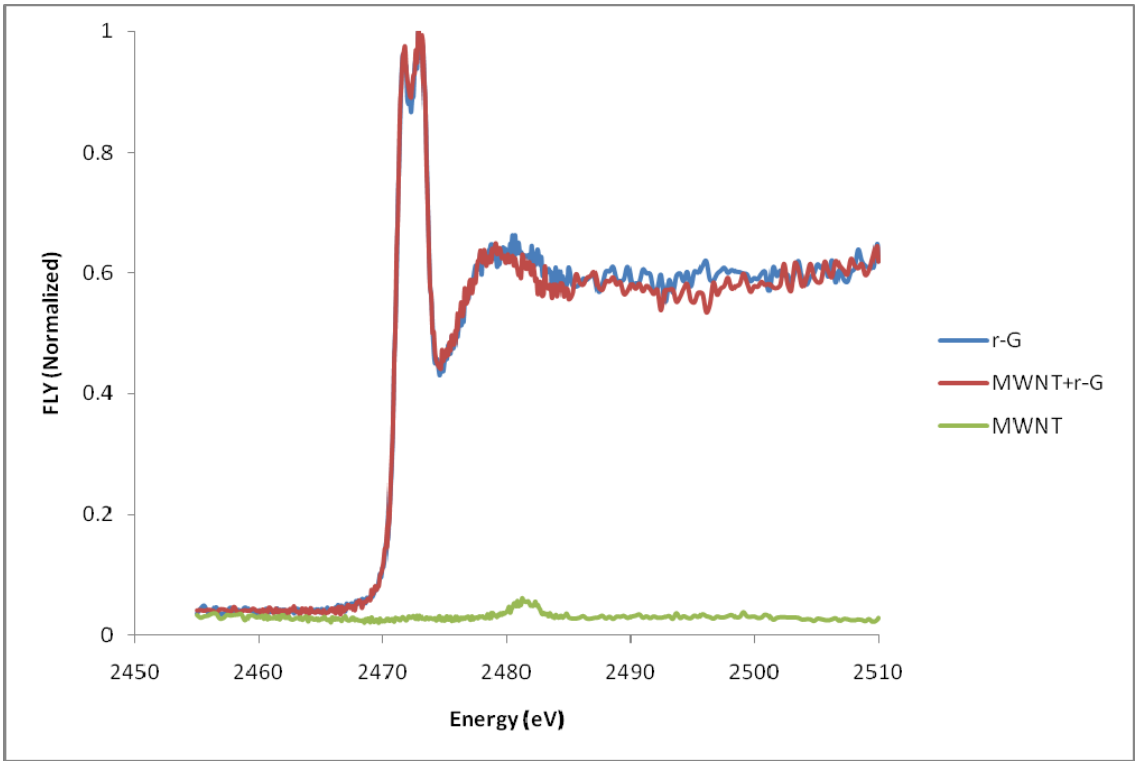

Figure 5.9. Sulfur K-edge XANES spectra of MWNT treated with γ-Globulin (MWNT+r-G), pure MWNT and pure γ-Globulin.

5.4 Conclusions

In this chapter, we used various characteristic techniques, Raman spectroscopy, confocal laser scanning microscopy and sulfur X-ray near-edge absorption spectroscopy, to examine the interaction between proteins (BSA and gamma-globulin) and both SWNT and MWNT, and their effects on the H_2S measurement. The following conclusions can be drawn.

(1) Both Raman spectrum and sulfur K-edge XANES spectrum measurements revealed that both BSA and γ-Globulin can be absorbed on CNTs. Sulfur K-edge XANES spectra further confirm that CNTs do not perturb the existence form of sulfur inside proteins and thus eliminate the possibility of the dissociation or desulfurization of the proteins by CNTs. The results also indicate that proteins may be just physically absorbed on CNTs. Raman spectra study further revealed that such absorption may happen on the sidewall of the carbon nanotubes rather than the defect sites of the nanotubes.

(2) The confocal laser scanning microscopy fluorescence measurement confirms that BSA and γ-Globulin are insensitive to fluorescence response under the specific excitation wavelength and emission wavelength chosen to acquire fluorescence response. However, when there are H_2S present in the protein solutions, fluorescence intensities increase with the increase of the H_2S concentrations in the protein solutions. The results confirm that the presence of the proteins on CNTs do not affect the adsorption of H_2S on CNTs and the measurement of H_2S.

(3) It seems that the adsorption of proteins on CNTs is a general phenomenon, and it is likely the physical adsorption. Some studies (Balavoine *et al*., 1999; Chen *et al*., 2003, 2004) have suggested that hydrophobic interaction is mainly responsible for the adsorption, but electrostatic interaction may also play an important role.

(4) The interaction of CNTs with the proteins may be probed by Raman spectrum. This can be seen from the frequency downshift of G-band and G'-band as a result of the interaction of the proteins and MWNT. However, unlike MWNT, there is no frequency shift in the G-band of SWNT interacted with proteins but the frequency upshift of G'-band only. The different outcomes with SWNT and MWNT may be attributed to the inherent different characteristics of SWNT and MWNT, which warrants a further study.

CHAPTER 6: INTERACTION OF HEMOGLOBIN WITH CARBON NANOTUBES IN SERA: REVISIT

6.1 Introduction

Hemoglobin is known as a common "sink" for H_2S and can scavenge H_2S *in-vivo* (Wang *et al*., 1998). Hemoglobin takes 97% component of red blood cells in blood and is responsible for the red color of blood. This chapter will present a study on the hypothesis that hemoglobin in the serum will not affect fluorescence response with the incident wavelength of 514 nm and emission window of 530 to 580 nm.

The general idea of the experiment to study this hypothesis was as this; we first determined the amount of hemoglobin that can scavenge H_2S in H_2S water solution. With this knowledge, we then added proper amounts of hemoglobin to the serum that originally contains H_2S to scavenge H_2S in the serum. As a result, we were able to obtain the serum sample that contains H_2S, two other serum samples that do not contain H_2S but contain different amounts of hemoglobin. CNT was then treated by these three samples, and the fluorescence response of the treated CNTs was acquired using CLSM.

6.2 Materials and Methods

The 50 μL of 2 mM, 4 mM and 6 mM hemoglobin samples were added into 300 μL of 100 μM H_2S water solutions, respectively, ready for the ISE measurement of H_2S in the three solutions, respectively. After having determined the amount of hemoglobin that can scavenge H_2S, proper amounts of hemoglobin were added to two 300 μL of fetal bovine serum to get two serum samples that do not have H_2S but certain amounts of hemoglobin. One 300 μL of fetal bovine serum (which contains around 30 μM H_2S based on the ISE measurement) was used as a control sample. CNT was then treated with the three serum samples, i.e., one original serum sample and the other two serum samples which contain hemoglobin but no H_2S, ready for fluorescence response acquisition with CLSM.

6.3 Results and Discussion

6.3.1 Hemoglobin in H_2S Water Solution

For the hemoglobin H_2S water solution experiment, ISE measurement showed that (1) 100 μM H_2S water solution sample added with 50 μL of 2 mM hemoglobin still had around 20 μM H_2S; (2) H_2S level of the water solution sample treated with 50 μL of 4 mM hemoglobin had dropped below the lowest level of ISE standard curve, which suggested that no H_2S had remained in the solution; (3) No further potential drop was observed in the sample treated with 50 μL of 6 mM hemoglobin, which suggested that all H_2S had been scavenged by hemoglobin. Thus, we determined that 50 μL of the 4

mM hemoglobin was able to scavenge all the H_2S in 300 μL of the 100 μM H_2S water solution.

6.3.2 Hemoglobin in the Serum

Based on the experiment conducted in the H_2S water solution, 50 μL of 4 mM and 6 mM hemoglobin should be sufficient to scavenge H_2S in the 300 μL serum which contains around 30 μM H_2S. The ISE measurement showed that the H_2S concentration of the serum added with 50 μL of 4 mM hemoglobin dropped below the lowest level of ISE standard curve, which indicated that H_2S in the serum sample had been completely scavenged by hemoglobin. Any further drop was not observed in the ISE measurement in the serum sample when it was added with 50 μL of 6 mM hemoglobin, which agreed with our expectation.

6.3.3 Confocal Laser Scanning Microscopy Fluorescence Measurement

Three 3 mg MWNT samples (MW10) were treated with the 300 μL of the pure bovine serum sample, the serum added with 50 μL of 4mM hemoglobin, and the serum added with 50 μL of 6mM hemoglobin, respectively, named MWNT, MWNT+HB4 and MWNT+HB6 for the convenience of the following discussion.

Figure 6.1 shows the fluorescence intensities of the three CNT samples measured using CLSM. It can be seen from this figure that the fluorescence intensities of MWNT+HB4 and MWNT+HB6 are almost at the same level. However, the MWNT sample treated with the pure serum shows higher fluorescence intensity than the other two.

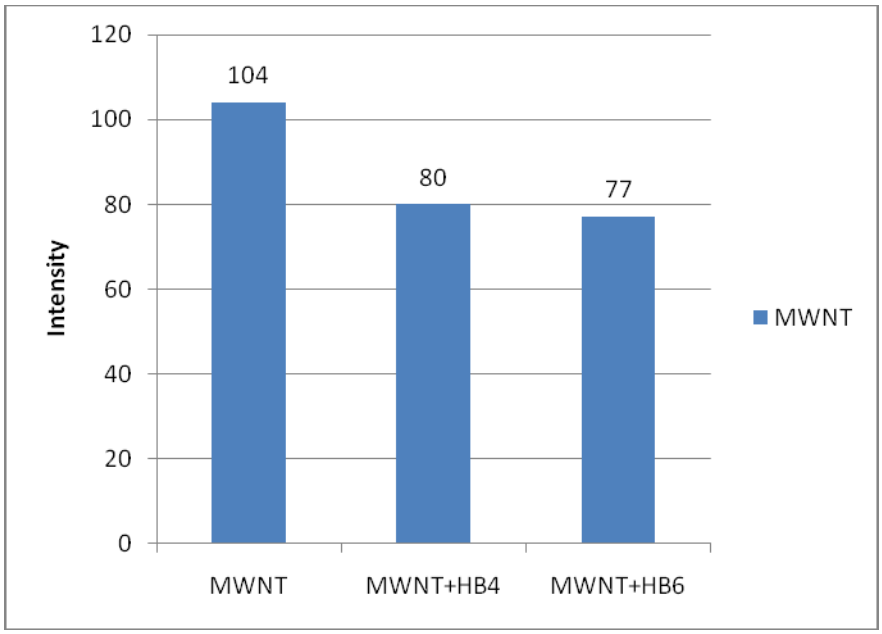

Figure 6.1. The fluorescence intensity of MWNTs treated with the serum (MWNT), the serum added with 50 µL of 4 mM hemoglobin (MWNT+HB4), and the serum with 50 µL of 6 mM hemoglobin (MWNT+HB6).

These results are consistent with our expectation: (1) hemoglobin completely scavenged the H_2S in both serum samples (MWNT+HB4, MWNT+HB6) and the higher fluorescence observed in the serum comes from the H_2S; (2) the two serum samples added with different amounts of hemoglobin have shown almost the same level of intensities, which suggests that both hemoglobin and sulfhemoglobin (a product of hemoglobin and H_2S interaction) does not change the fluorescence intensities of CNT (even though they may bind with CNT).

The results thus positively test the hypothesis. The results also suggest that the existence of hemoglobin and sulfhemoglobin in the serum are insensitive to the fluorescence response of the non-functionalized CNT treated with the H_2S-hemoglobin-serum solution.

6.4 Conclusions

In this chapter, we re-examined the interaction of hemoglobin with non-functionalized MWNT in the serum. In particular, we studied the hypothesis that hemoglobin in the serum will not affect fluorescence response with the incident wavelength of 514 nm and emission window of 530 to 580 nm. The study can conclude: (1) the proposed hypothesis is correct, and (2) the presence of hemoglobin or sulfhemoglobin (which is the product after hemoglobin reacts with H_2S) in the serum are insensitive to the CLSM fluorescence measurement of H_2S in the serum.

It should be noted that hemoglobin does not exist in the serum, so it is not really a concern for the measurement of H_2S in the serum. But hemoglobin does exist in blood, and the current study may provide some knowledge for the direct measurement of H_2S in blood.

CHAPTER 7: RAMAN SPECTROSCOPY STUDY OF HYDROGEN SULFIDE ADSORPTION ON CARBON NANOTUBES

7.1 Introduction

In Chapter 5, we used Raman spectroscopy to study the interaction of proteins with carbon nanotubes. Raman spectra are sensitive to the adsorption of proteins on carbon nanotubes and reveals that proteins are likely physically adsorbed on the sidewall of CNTs rather than the defect sites. In this chapter, a study of the mechanism of adsorption of hydrogen sulfide (H_2S) on carbon nanotubes using Raman spectroscopy will be presented. The study paid a particular attention to the hypothesis proposed by Wu *et al*. (2007) that the adsorption of H_2S on CNTs involves both the physical adsorption and chemisorption and defect sites might be the preferable places where such adsorption occurs.

7.2 Materials and Methods

H_2S solutions with 50 μM, 100 μM and 200 μM were prepared. The 3 mg of SWNT and MWNT samples (MW10) each were treated with 300 μL of 50 μM, 100 μM and 200

μM H_2S water solution to get three treated SWNT samples and three treated MWNT samples.

The 30 mg/mL bovine serum albumin (BSA) (Sigma, Cat. # A-7906) and 15 mg/mL bovine gamma-globulin (γ-Globulin) (Sigma, Cat. #G-5009) solutions were prepared. The protein solutions with 1 mM H_2S were made by adding a calculated amount of H_2S into the BSA and γ-Globulin solutions, respectively. The samples with the lower concentrations of 50 μM, 100 μM, 200 μM H_2S were obtained by diluting 1 mM H_2S solutions, respectively. The 3 mg of SWNT samples each were treated with 300 μL of BSA solutions which contain 100 μM, 200 μM H_2S. The 3 mg of MWNT samples each were treated with 300 μL of γ-Globulin solutions which contain 50 μM, 100 μM, 200 μM H_2S. Both the 3 mg of SWNT and 3 mg of MWNT samples were treated with pure protein solutions as control samples.

7.3 Results and Discussion

7.3.1 Raman Spectra of CNTs Treated with H_2S Water Solutions

Raman spectra of MWNT samples treated with different concentration of H_2S water solution and distilled water are shown in Figure 7.1. The defect-induced D-band at ~1345 cm^{-1}, the tangential mode G-band at ~1572 cm^{-1}, and G'-band (the overtone of D-band) at ~1608 cm^{-1} were well observed in all spectra. Since we hypothesized that H_2S would be likely adsorbed on the defect sites of CNTs, some of the changes on D-band, probably frequency shift, were expected to be observed.

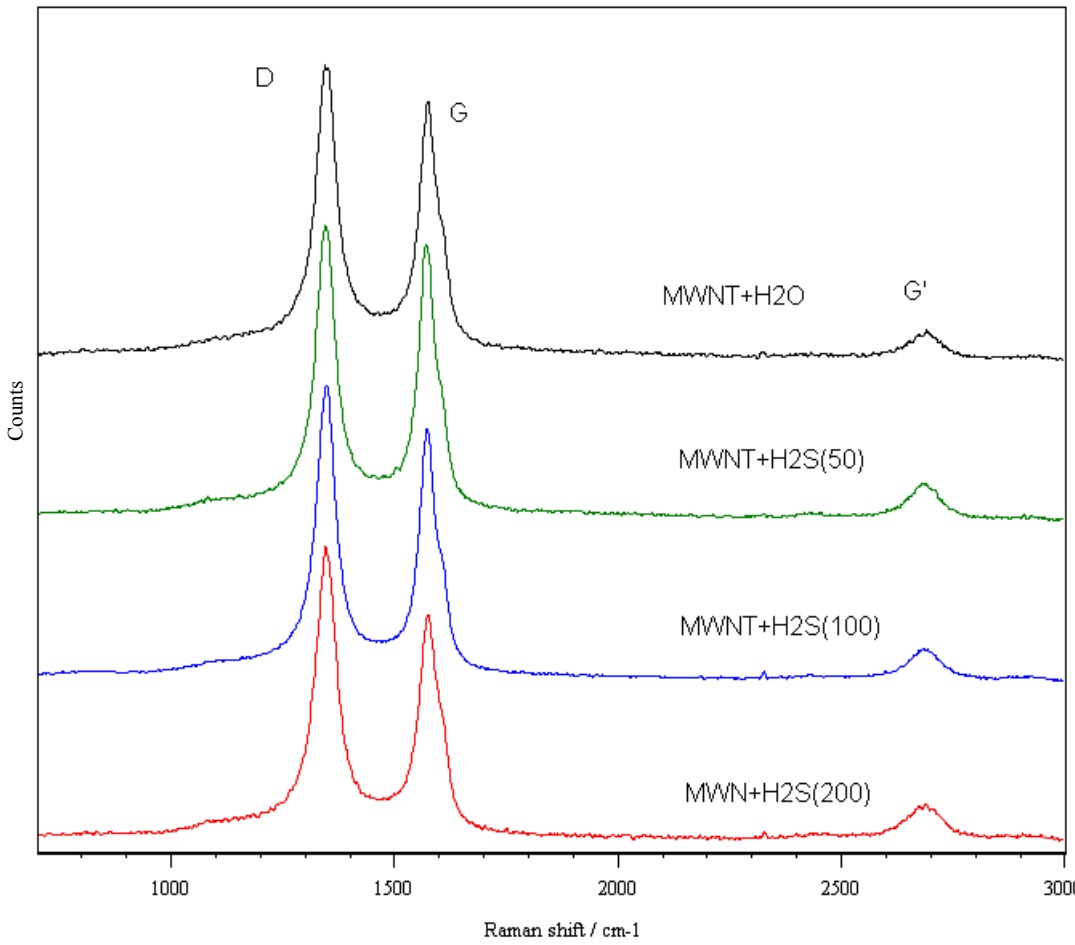

Figure 7.1. Raman spectra of MWNT samples treated with different concentration of H_2S water solutions (50 µM, 100 µM. 200 µM).

The band positions of D-band, G-band and G'-band of all the samples are shown in Table 7.1. No frequency shift was observed among MWNTs treated with distilled water and MWTNs treated with H_2S solution, and among MWNTs treated with different concentrations of H_2S. The results are not in accord with our expectation. Does this mean that Raman spectra are not sensitive to the adsorption of H_2S on CNTs?

Table 7.1. Band positions of MWNT samples treated with different concentration of H_2S water solutions. D-band and G-band intensity ratio is calculated by integrating the area of D and G-band.

H_2S	D	G	G'	D/G
0	1345	1575	2688	1.215
0	1345	1575	2688	1.264
0	1344	1576	2686	1.144
50	1345	1574	2688	1.355
50	1344	1575	2686	1.323
50	1344	1575	2687	1.236
100	1345	1576	2688	1.470
100	1344	1575	2688	1.338
100	1344	1575	2687	1.418
200	1344	1576	2687	1.309
200	1345	1575	2688	1.475
200	1344	1575	2688	1.384

D-band to G-band intensity ratio has been used to measure the degree of defects, impurities and functionalization on CNTs. In the study of Datsyuk *et al*. (2008), they reported that the MWNT samples treated with hydrochloric acid (HCl) and sulfuric acid (H_2SO_4) led to the decrease of D/G band intensity ratio, which may be attributed to the removal of impurities in the carbon nanotubes. However, the MWNT samples treated with nitric acid (HNO_3) resulted in the increase of D/G band intensity ratio. They confirmed that HNO_3 destructed the graphitic integrity and increased the defect population of the CNTs, which led to the introduction of more carboxyl and hydroxyl functional groups on the defect sites. Gao *et al*. (2005) and Sidorov *et al*. (2008) reported that D-band to G-band intensity ratio increased due to the attachment of polymer functional groups on SWNTs and MWNTs. The hydrogenation of MWNTs can also change the D-band to G-band intensity ratio (Tang *et al*., 2010).

In our experiment, the D-band to G-band intensity ratio (D/G) was calculated by integrating the area of D and G-band using the Lorentzian function (Dresselhaus *et al*., 2005). Before Lorentzian curve fitting, baseline subtraction was performed on all the spectra. Figure 7.2 shows the representative graphs of the D and G band curve fitting results of MWNT sample.

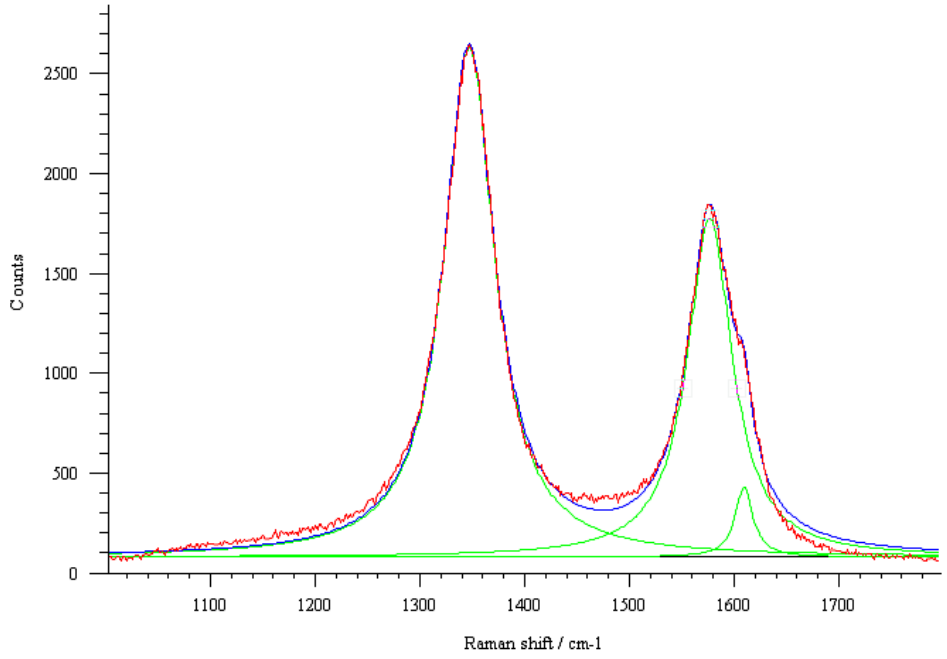

Curve Name	Centre	Width	Height	Area	% Gaussian
Curve 1	1346.95	59.0096	2563.69	237634	0
Curve 2	1577.36	52.374	1700.75	139919	0
Curve 3	1610.19	20.5078	353.291	11380.7	0

Figure 7.2. Representative graph of MWNT D-band and G-band Lorentzian curve fitting result.

D/G intensity ratio of MWNTs treated with different concentration of H_2S water solution was summarized in Table 7.1. The D/G ratio against H_2S concentration is plotted in Figure 7.3, which reveals that the D/G ratio slightly increases with the increase of the H_2S concentration.

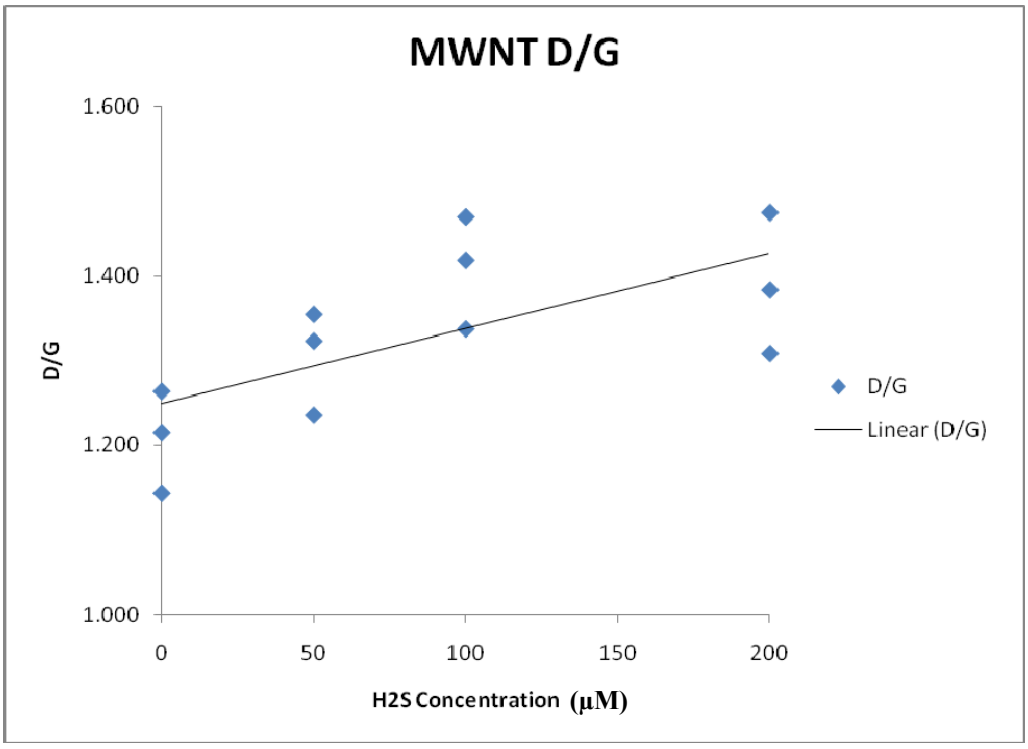

Figure 7.3. D/G ratio of MWNTs treated with different concentration of H_2S solutions. D/G ratio increases with the increase of H_2S concentration.

The similar analysis was done on the Raman spectra of SWNTs treated with different concentrations of H_2S water solution. Figure 7.4 shows the spectra of SWNT treated with distilled water and different concentration H_2S solutions. Table 7.2 summarizes the band positions of D-band, G^- -band and G^+-band, and G'-band of all the SWNT samples. It can be seen from this table that no frequency shift was observed among the SWNT treated with distilled water and SWNT treated with different concentrations of H_2S, which is consistent with MWNT experiments.

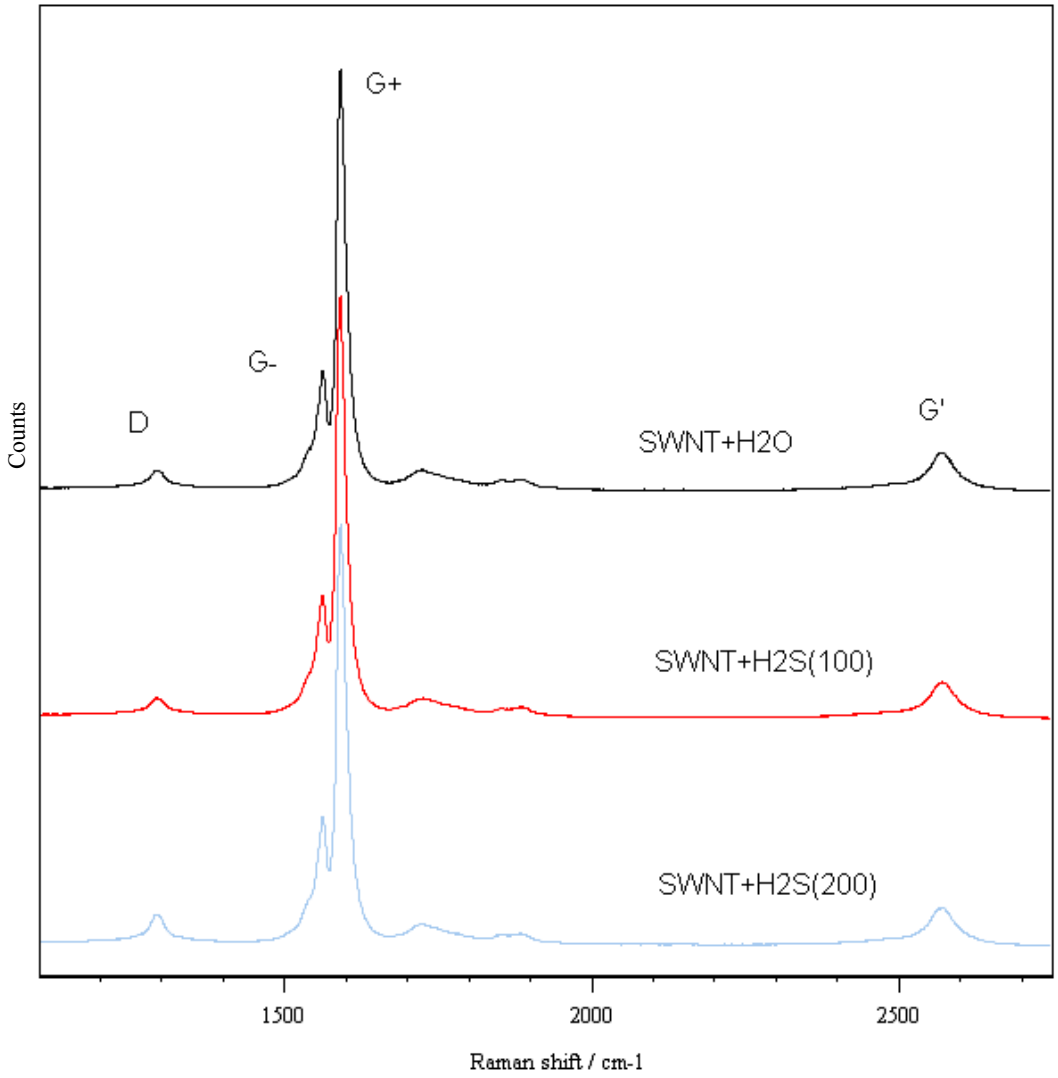

Figure 7.4. Raman spectra of SWNT samples treated with different concentration of H_2S water solutions(100 μM. 200 μM).

Table 7.2. Band positions of SWNT samples treated with different concentration of H_2S water solutions. D-band and G-band intensity ratio is calculated by integrating the area of D and G-band.

H_2S	D	G-	G +	G'	D/G
0	1291	1561	1590	2573	0.0807
0	1291	1561	1590	2574	0.1022
0	1291	1560	1589	2574	0.0934
100	1291	1560	1589	2573	0.0941
100	1291	1560	1589	2574	0.1184
100	1290	1560	1589	2574	0.1023
200	1291	1561	1590	2574	0.1332
200	1290	1561	1590	2574	0.1660
200	1290	1560	1590	2574	0.1569

Similarly, Lorentzian curve fitting was performed on the SWNT Raman spectra to calculate the D-band to G-band intensity ratio (D/G). The D/G ratio is the integrating area ratio of D-band and G-band. Before the curve fitting, baseline subtraction was performed on all the spectra. Figure 7.5 shows the representative graph of SWNT D and G band curve fitting results.

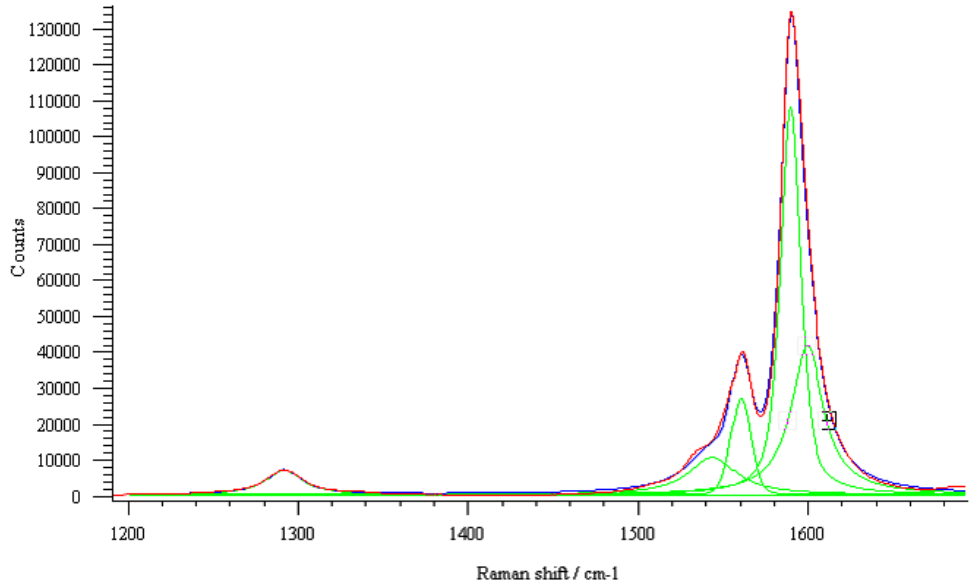

Curve Name	Centre	Width	Height	Area
Curve 1	1291.31	25.8459	6882.16	279406
Curve 2	1560.92	13.5895	26909.7	417707
Curve 3	1589.94	14.0455	108798	2.09704e+006
Curve 4	1544.16	33.7827	10430	553475
Curve 5	1600.05	23.4846	41815.2	1.54254e+006

Figure 7.5. Representative graph of SWNT D-band and G-band Lorentzian curve fitting result.

The D/G intensity ratio of SWNT samples treated with different concentrations of H_2S water solution was shown in Table 7.2. The value of D/G ratio against H_2S concentration was plotted in Figure 7.6, which shows that the D/G ratio increases with the increase of the H_2S concentrations, and the trend seems more apparent in SWNT than in MWNT.

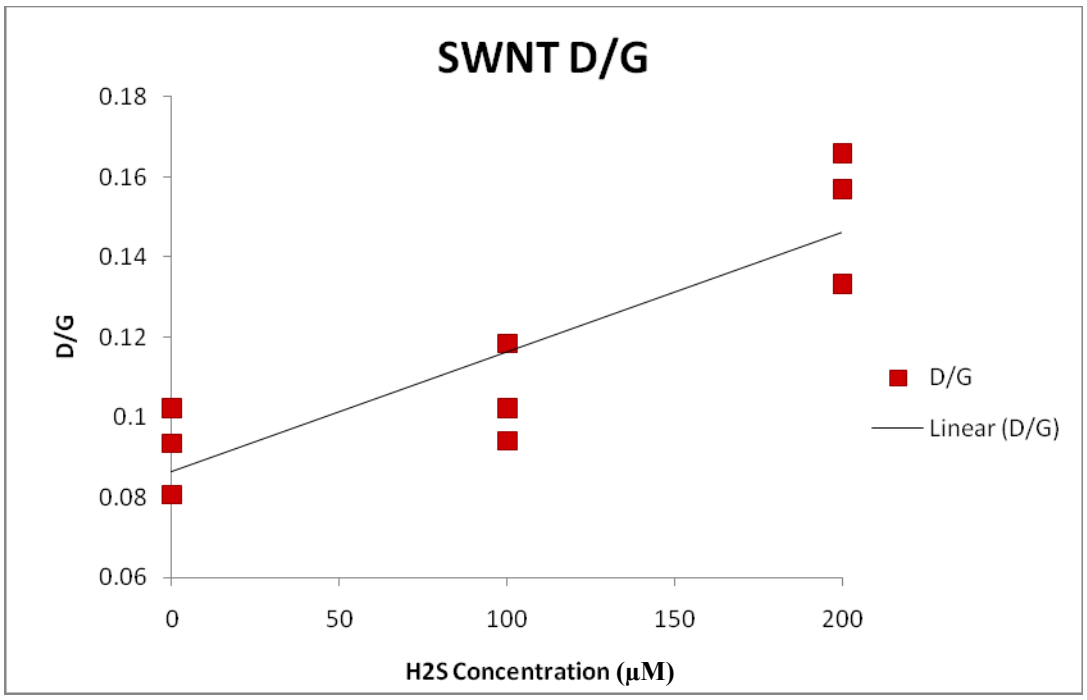

Figure 7.6. D/G ratio of SWNTs treated with different concentration of H_2S solutions. D/G ratio increases with the increase of H_2S concentration.

It is interesting to see that the adsorption of H_2S on CNTs cannot be observed from the frequency shift of main Raman spectra features such as D-band, G-band and G'-band. This is different from the CNT-protein interaction that was described in Chapter 4. However, the D/G ratio increases with the increase of H_2S concentration and such a trend can be seen both in MWNT and SWNT. Thus, we may conclude that this is not an isolated phenomenon; it should be related to the adsorption of H_2S on CNTs. This may indicate that the adsorption of H_2S affect the intensity of D-band rather than the frequency of the D-band. The finding also gives the evidence to support the hypothesis that H_2S is likely adsorbed on the defect sites than on the sidewalls of CNTs (see the physical significance of these bands in Chapter 2).

7.3.2 Raman Spectra of CNTs Treated with Protein Solutions with H_2S

Raman spectra analysis of MWNTs treated with γ-globulin solution with different concentration of H_2S (50μM, 100μM, 200μM) were conducted in this experiment. The band positions of D-band, G-band and G'-band of MWNTs are summarized in Table 7.3. There was no significant frequency shift among the MWNTs treated with pure γ-globulin and the MWNTs treated with γ-globulin solutions which had different concentrations of H_2S. However, we did observe about 4 cm^{-1} downshift of G-band and about 6 cm^{-1} upshift of G'-band compared to the MWNTs treated with distilled water and H_2S water solution, which was consistent with the MWNT-γ-globulin study conducted in Chapter 5.

Table 7.3. Band positions of MWNTs treated with γ-globulin solutions with different concentration of H_2S (50, 100 and 200 μM). D-band and G-band intensity ratio was calculated by integrating the area of D and G-band.

r-G+H_2S	D	G	G'	D/G
0	1345	1571	2693	1.079
0	1345	1572	2694	1.148
0	1344	1571	2693	1.188
50	1346	1572	2693	1.254
50	1344	1570	2692	1.178
50	1345	1571	2694	1.143
100	1345	1571	2694	1.273
100	1345	1572	2692	1.168
100	1346	1572	2692	1.341
200	1344	1571	2693	1.271
200	1346	1572	2694	1.220
200	1344	1572	2693	1.359
H_2O	**1345**	**1575**	**2687**	N/A
H_2S	**1345**	**1576**	**2687**	N/A

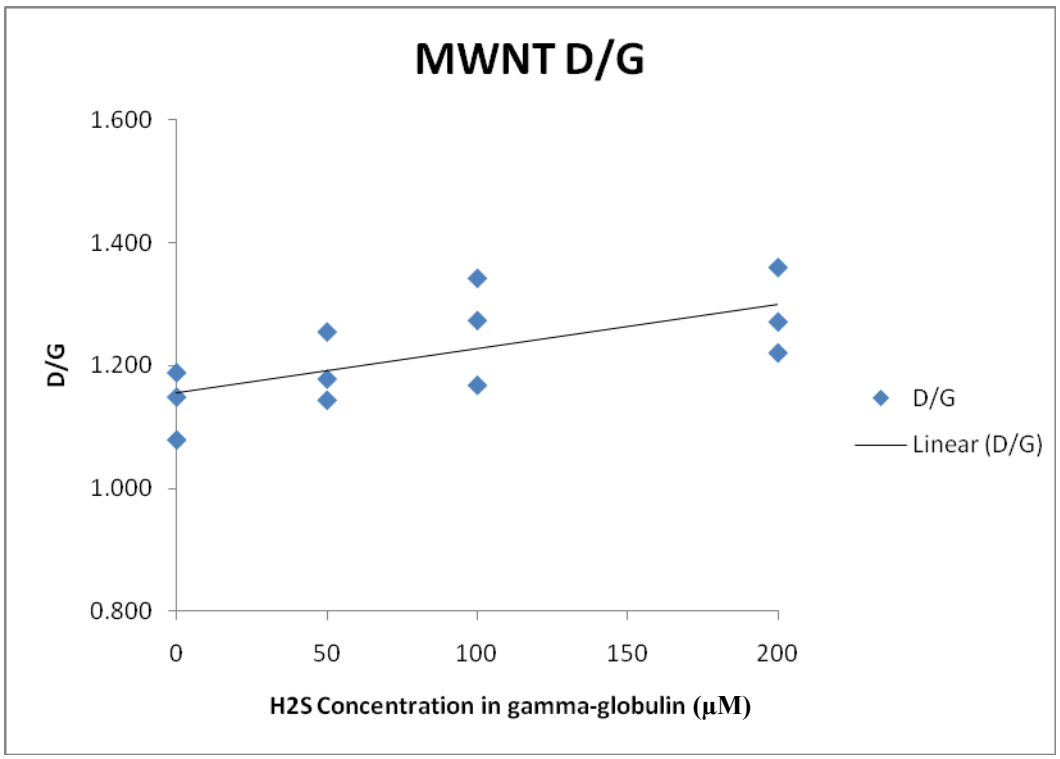

Figure 7.7. D/G ratio of MWNTs treated with γ-globulin with different concentration of H_2S (50, 100, and 200 µM). D/G ratio increases with the increase of H_2S concentration in γ-globulin solution.

D-band to G-band intensity ratio (D/G) analysis was performed on all the spectra, which followed the same procedure as MWNT spectra treated with H_2S water solution. The results are summarized in Table 7.3. The D/G ratio against the H_2S concentration was plotted in Figure 7.7. It can be seen from Figure 7.7 that the D/G ratio increases as the level of H_2S in γ-globulin solution increases. The result is similar to the one found in MWNTs treated with H_2S water solution. As we have concluded that the D/G ratio increase may be related to the adsorption of H_2S on CNTs. The result may suggest that H_2S could be absorbed on MWNTs (probably at the defect sites) at the presence of

protein on the sidewall of MWNTs. Such finding provided further evidence to our hypothesis.

Similar Raman spectra analysis was conducted on the SWNTs samples treated with BSA solutions which had different concentrations of H_2S (0, 100, and 200 μM). Table 7.4 summarized the peak position of D-band, G-band and G'-band of the SWNT spectra. It can be seen that there were no significant frequency shifts among the SWNTs treated with pure BSA solution and SWNTs treated with BSA solution with different concentrations of H_2S. However, we observed about 6 cm^{-1} upshift in G'-band compared to the SWNTs treated with distilled water and H_2S water solution. The observation is consistent with the SWNT-BSA study conducted in Chapter 5.

Table 7.4. Band positions of SWNTs treated with BSA solutions with different concentration of H_2S. D-band and G-band intensity ratio was calculated by integrating the area of D and G-band.

BSA+H_2S	**D**	**G-**	**G+**	**G'**	**D/G**
0	1291	1561	1590	2580	0.0998
0	1290	1561	1591	2581	0.0874
0	1291	1561	1590	2580	0.0897
100	1291	1561	1590	2580	0.1343
100	1292	1560	1590	2579	0.1578
100	1291	1561	1590	2580	0.1287
200	1291	1561	1590	2579	0.1819
200	1291	1560	1590	2580	0.1488
200	1290	1561	1591	2580	0.1604
H_2O	**1291**	**1561**	**1590**	**2574**	N/A
H_2S	**1291**	**1561**	**1590**	**2574**	N/A

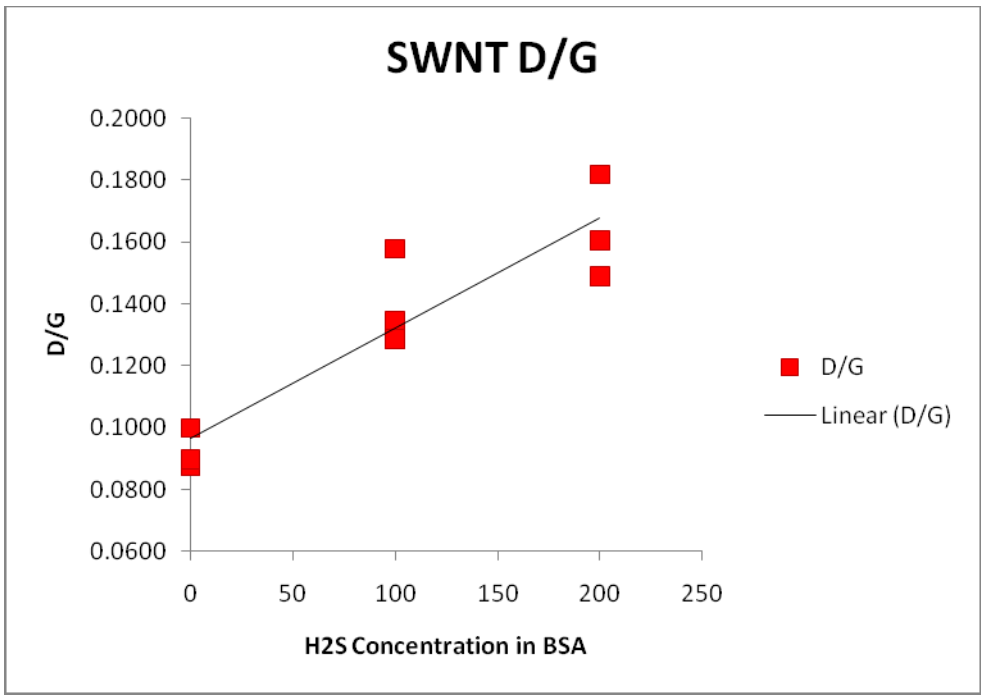

Figure 7.8. D/G ratio of SWNTs treated with BSA solutions with different concentration of H_2S (0, 100, and 200 μM). D/G ratio increases with the increase of H_2S concentration in BSA solution.

D-band to G-band intensity ratio (D/G) analysis was performed on all SWNT spectra, which followed the same procedure as SWNT spectra treated with H_2S water solution. The results are summarized in Table 7.4 and Figure 7.8. It can be seen from Figure 7.8 that the D/G ratio increases as the concentrations of H_2S in BSA solution increase. It is not only similar to the result of SWNT treated with H_2S water solution but also similar to MWNT's; besides, the slope of the increase in SWNT is sharper than that in MWNT. This may suggest SWNT performs better than MWNT for the adsorption of H_2S, which is in agreement with the finding in Chapter 4. Both SWNT and MWNT results indicate that H_2S can be adsorbed on the CNTs at the presence of proteins, and such adsorption may likely happen on the defect sites of CNTs rather than the sidewall of CNTs.

7.4 Conclusions

In this chapter, we used Raman spectroscopy to examine the adsorption of hydrogen sulfide (H_2S) on CNTs both in water solutions and in protein solutions. We can conclude:

(1) The adsorption of H_2S on CNTs either in water solution or in proteins solution cannot be observed from the frequency shift of D-band, G-band or G'-band, which is different from the adsorption of proteins on CNTs. However, the D-band to G-band intensity ratio (D/G) studies reveals that D/G ratio increases with the increase of H_2S concentration. This phenomenon has been observed both in SWNT spectra and MWNT spectra and both in the water solution and in protein solution. This may suggest that such phenomenon is not random, and it may be related to the adsorption of H_2S on CNTs.

(2) The studies (Brown *et al*., 2001; Filho *et al*., 2003; Sullivan *et al*, 2007) have suggested D/G intensity ratio is a measure of impurity, defect, and functionalization on CNTs. The increase of D/G ratio may suggest the attachment of substance to the defect sites of CNTs and the increase of impurity of CNTs. Thus, the increase of D/G intensity ratio with the increase of H_2S concentration may be relevant to the adsorptions of H_2S on the defects sites of CNTs.

(3) By integration of the result described in this chapter, the result obtained with CLSM fluorescence acquisition, the result obtained with the sulfur XANES and Raman

spectroscopy on the CNT-protein interaction, it can be concluded that H_2S can be absorbed on the CNTs in the presence of proteins. The Raman spectra study also provides more evidence to our hypothesis that H_2S is more likely absorbed on the defect sites of the CNTs and proteins are likely absorbed on the sidewall of CNTs. The measurement of H_2S with CNTs will not be disturbed by the adsorption of proteins.

(4) The increase of D/G intensity ratio of SWNTs is more apparent than that of MWNTs. This may suggest that SWNTs perform better than MWNTs for the adsorption of H_2S, which is in agreement of the results we obtained in Chapter 4. The change of D/G ratio seems relevant to the adsorption of H_2S on CNTs, and the relationship between D/G intensity ratio and H_2S concentration seems to be linear, this may provide us another method to measure the low concentration of H_2S in solutions.

CHAPTER 8: CONCLUSIONS AND RECOMMENDATION FOR FUTURE WORK

8.1 Conclusions

The overall objective of this thesis research was to study the mechanism which governs the interaction among key proteins in sera or blood, CNT, and hydrogen sulfide. There were four specific objectives that provide milestones for the overall objective, and they are: (1) examining the interactions between H_2S and CNT under the presence of proteins, (2) understanding the mechanism behind these interactions, (3) examining the difference with CNT structures in these interactions or sensing H_2S in sera, and (4) examining the interactions among hemoglobin, CNT, and H_2S.

These objectives were achieved by using the following tools: Raman spectroscopy, X-ray absorption spectroscopy (XAS) and confocal laser scanning microscopy (CLSM). After a thorough review of the literature in Chapter 2 and a description of general methods and materials employed in the study in Chapter 3, Chapter 4 described the study for Objective (1), Chapter 5 described the study for Objective (2), Chapter 6 described the study for Objective (3), and finally Chapter 7 described the study for Objective (4). This study can lead to the following conclusions:

(1) Both SWNT and MWNTs can be used to capture H_2S, and the relation between fluorescence intensity and H_2S concentration in sera is linear. The SWNT has a higher sensitivity than the MWNT. The measurement resolution in the serum can reach 10 μM.

(2) Two major proteins in sera, that is, albumin and globulin, can bind to non-functionalized CNTs, but their presence on CNTs do not affect fluorescence response under the specific incident wavelength (514 nm) and emission wavelength (530 to 580 nm).

(3) During the interaction of CNT with the serum which contains H_2S, carbon nanotubes do not desulfurize the proteins, so the fluorescence response of CNT treated with the solution that contains H_2S and the proteins is solely contributed by sulfur in H_2S but not in the proteins.

(4) The proteins are physically adsorbed on the sidewall of carbon nanotubes, while the sulfur element in H_2S is preferably attached to defects of the CNTs.

(5) The D/G intensity ratio may be a new probe to H_2S concentration in the serum and distilled water.

(6) The presence of hemoglobin and sulfhemoglobin (which is the product after hemoglobin reacts with H_2S) in sera will not affect fluorescence response of sulfur in H_2S in sera under the specific incident wavelength (514 nm) and emission wavelength (530 to 580 nm).

8.2 Contributions

(1) Provision of a further verification of the approach to measure H_2S in sera with non-functionalized CNT and fluorescence response. This includes the verification of accuracy (linearity), sensitivity and reliability of the approach. This approach is now well on the way to be applied to both research of and clinic measurement of endogenous H_2S. It is noted that in comparison with all the existing approaches in practice, this approach is least invasive, highest resolution (not compared with ISE) and of the simplest procedure.

(2) Provision of new evidence that the proteins (albumin and globulin) bind to non-functionalized CNT from two novel perspectives, that is, Raman spectrum and X-ray absorption spectroscopy. This provision helps to resolve the debate on whether functionalization of CNTs is a necessary condition for CNTs to bind with proteins.

(3) Finding that the proteins (albumin and globulin) bind to the sidewall of non-functionalized CNTs while the sulfur element binds to the defect site of non-functionalized CNTs. This may be true to other proteins as well as other sulfur-based elements while they interact with non-functionalized CNTs. More generally, this finding may help understand mechanisms which govern interaction behaviors among non-functionalized CNTs, proteins, and sulfur-based elements.

(4) Finding that SWNT is more sensitive to probe H_2S than MWNT while the size in diameter of MWNT may not be a significant factor that changes the performance of measuring H_2S with non-functionalized MWNT and fluorescence response. This finding may have a generalized implication to SWNT versus MWNT in the occasion where they interact with proteins and sulfur-based elements.

(5) Finding that the D/G ratio in Raman spectrum may be a new probe to H_2S in sera. The generalized implication is such that this probe may also be effective to other sulfur-based elements.

8.3 Recommendation for Future Work

(1) The current study shows that SWNT performs better than MWNT in terms of the sensitivity of H_2S measurement. We believe that the SWNT's significantly larger specific surface area may contribute to this result. The current study also suggests that H_2S be probably adsorbed on the defect sites of the carbon nanotubes. Thus, it may be hypothesized that the more defect sites are introduced on the SWNT, the better measurement performance would be. A further experiment to prove this hypothesis would be interesting.

(2) It has been shown that Raman spectroscopy is a powerful tool for the carbon nanotubes characterization. SWNT has some unique features such as radial breathing mode (RBM) and the split of G-band besides the common features shared with MWNT. In the study of protein interaction with CNTs, we observed the difference among the change of SWNT and MWNT in G-band and G'-band regarding their response to the interaction. We hypothesized that this may be due to the structural difference between SWNT and MWNT but the mechanism behind this warrants a further study.

(3) In the current study of protein interaction with carbon nanotubes, two proteins (albumin and globulin) were studied individually. They both are shown to be able to bind with CNTs. However, the situation where multiple proteins are co-

presented has not been studied, which is more close to a real situation in the biological environment. Wu *et al*. (2007) assumed that the albumin would form a film around CNT which prevents other proteins from being adsorbed to the CNT. However, the present study reveals that the both proteins can be adsorbed on CNTs. Therefore, a further study is needed to resolve this inconsistence. In particular, we propose a new hypothesis for the mechanism that may govern the interaction behavior when non-functionalized CNT interacts with the serum. The hypothesis is as this; when non-functionalized CNT interacts with the serum, albumin which counts 70% of the total proteins in the serum according to Fudenberg (1976) will first take to attach to the sidewall of CNTs. Two situations then follow this event: Situation I: after all the albumins attach to the CNT, there are still some free sidewall surfaces available; Situation II: the sidewall of the CNT is fully covered by the albumins. For Situation I, some other proteins may then take to attach to the CNT on those free sidewall surfaces. For situation II, there will be no other proteins that have an opportunity to attach to the CNT, as also noted that the attachment of albumins to the CNT is irreversible according to Chen *et al*. (2003, 2004). Nevertheless, whether there is a single protein in sera or are multiple proteins that may attach to non-functionalized CNTs will not compromise the effectiveness of the approach to measure H_2S in sera with the non-functionalized CNT and fluorescence response.

REFERENCES

Agency for Toxic Substances and Disease Registry (ATSDR). (2006). Toxicological profile for Hydrogen Sulfide. Atlanta, GA: U.S. Department of Health and Human Services, Public Health Service.

Abe K., Kimura, H. (1996). The possible role of hydrogen sulfide as an endogenous neuromodulator. *Journal of Neuroscience*, Vol 16, 1066-1071.

Akabayov, B., Doonan, C., Pickering, I., George, G., Sagi, I. (2005). Using softer X-ray absorption spectroscopy to probe biological systems. *Journal of Synchrotron Radiation,* 12(4), 392-401.

Alvarez, L., Righi, A., Guillard, T., Rols, S., Anglaret, E., Laplaze, D. (2000). Resonant Raman study of the structure and electronic properties of single-wall carbon nanotubes. *Chemical Physics Letters,* 316(3-4), 186-190.

Amos, W. B., White, J. G. (2003). How the confocal laser scanning microscope entered biological research. *Biology of the Cell,* 95(6), 335-342.

Arepalli, S., Nikolaev, P., Gorelik, O., Hadjiev, V. G., Holmes, W., Files, B. (2004). Protocol for the characterization of single-wall carbon nanotube material quality. *Carbon,* 42(8-9), 1783-1791.

Ascone, I., Messori, L., Casini, A., Gabbiani, C., Balerna, A., Dell'Unto, F., Castellano, A.C. (2008). Exploiting soft and hard X-ray absorption spectroscopy to characterize Metallodrug/Protein interactions: The binding of [trans-

RuCl4(im)(dimethylsulfoxide)][ImH] (im = imidazole) to bovine serum albumin. *Inorganic Chemistry, 47*(19), 8629-8634.

Attwood, D. (2007). *Soft x-rays and extreme ultraviolet radiation: Principles and applications*. Cambridge University Press.

Balavoine, F., Schultz, P., Richard, C., Mallouh, V., Ebbesen, T. W., Mioskowski, C. (1999). Helical crystallization of proteins on carbon nanotubes: A first step towards the development of new biosensors. *Angewandte Chemie International Edition,* 38(13/14), 1912-1915.

Bandosz, T. J. (2002). On the adsorption/oxidation of hydrogen sulfide on activated carbons at ambient temperatures. *Journal of Colloid and Interface Science,* 246(1), 1-20.

Baughman, R. H., Zakhidov, A. A., De Heer, W. A. (2002). Carbon nanotubes - the route toward applications. *Science,* 297(5582), 787.

Beauchamp, R. O., Bus, J. S., Popp, J. A., Boreiko, C. J., Andjelkovich, D. A., Leber, P. (1984). A critical review of the literature on hydrogen sulfide toxicity. *Critical Reviews in Toxicology,* 13(1), 25-97.

Bellacchio, E., McFarlane, K., Rompel, A., Robblee, J., Cinco, R.,Yachandra, V. (2001). Counting the number of disulfides and thiol groups in proteins and a novel approach for determining the local pKa for cysteine groups in proteins *in vivo*. *Journal of Synchrotron Radiation,* 8(3), 1056-1058.

Benoit, J., Buisson, J., Chauvet, O., Godon, C., Lefrant, S. (2002). Low-frequency Raman studies of multi-walled carbon nanotubes: Experiments and theory. *Physical Review B,* 66(7), 73417.

Brown, S., Jorio, A., Dresselhaus, M., Dresselhaus, G. (2001). Observations of the D-band feature in the Raman spectra of carbon nanotubes. *Physical Review B,* 64(7), 73403.

Canela, M. C., Alberici, R. M., & Jardim, W. F. (1998). Gas-phase destruction of H_2S using TiO2/UV-VIS. *Journal of Photochemistry and Photobiology A: Chemistry,* 112(1), 73-80.

Carroll, J. J. (1998). A Discussion of the Effect of pH on the Solubility of Hydrogen Sulfide. *http://www.telusplanet.net/public/jcarroll/ION.HTM,* Retrieved December 2009.

Chen, R. J., Bangsaruntip, S., Drouvalakis, K. A., Wong Shi Kam, N., Shim, M., Li, Y. (2003). Noncovalent functionalization of carbon nanotubes for highly specific electronic biosensors. *Proceedings of the National Academy of Sciences,* 100(9), 4984.

Chen, R. J., Choi, H. C., Bangsaruntip, S., Yenilmez, E., Tang, X., Wang, Q. (2004). An investigation of the mechanisms of electronic sensing of protein adsorption on carbon nanotube devices. *Journal of the American Chemical Society,* 126(5), 1563-1568.

Chen, R. J., Zhang, Y., Wang, D., Dai, H. (2001). Noncovalent sidewall functionalization of single-walled carbon nanotubes for protein immobilization. *Journal of the American Chemical Society,* 123(16), 3838-3839.

Corio, P., Jorio, A., Demir, N., Dresselhaus, M. (2004). Spectro-electrochemical studies of single wall carbon nanotubes films. *Chemical Physics Letters,* 392(4-6), 396-402.

Corio, P., Santos, P., Brar, V., Samsonidze, G. G., Chou, S., Dresselhaus, M. (2003). Potential dependent surface Raman spectroscopy of single wall carbon nanotube films on platinum electrodes. *Chemical Physics Letters,* 370(5-6), 675-682.

Dai, H. (2001). Nanotube growth and characterization. *Carbon Nanotubes,* 29-53.

Dai, H. (2002). Carbon nanotubes: Opportunities and challenges. *Surface Science,* 500(1-3), 218-241.

Datsyuk, V., Kalyva, M., Papagelis, K., Parthenios, J., Tasis, D., Siokou, A. (2008). Chemical oxidation of multi-walled carbon nanotubes. *Carbon,* 46(6), 833-840.

Dharap, P., Li, Z., Nagarajaiah, S., Barrera, E. (2004). Nanotube film based on single-wall carbon nanotubes for strain sensing. *Nanotechnology,* 15(3), 379-382.

Dombkowski, R. A., Russell, M. J., Olson, K. R. (2004). Hydrogen sulfide as an endogenous regulator of vascular smooth muscle tone in trout. *American Journal of Physiology- Regulatory, Integrative and Comparative Physiology,* 286(4), 678.

Dresselhaus, M., Dresselhaus, G., Jorio, A., Souza Filho, A., Saito, R. (2002). Raman spectroscopy on isolated single wall carbon nanotubes. *Carbon,* 40(12), 2043-2061.

Dresselhaus, M., Dresselhaus, G., Saito, R., Jorio, A. (2005). Raman spectroscopy of carbon nanotubes. *Physics Reports,* 409(2), 47-99.

Eto, K., Asada, T., Arima, K., Makifuchi, T., Kimura, H. (2002). Brain hydrogen sulfide is severely decreased in Alzheimer's disease. *Biochemical and Biophysical Research Communications,* 293(5), 1485-1488.

Ferraro, J. R., Nakamoto, K., Brown, C. W. (2003). *Introductory Raman Spectroscopy.* Academic Press.

Gao, C., Jin, Y. Z., Kong, H., Whitby, R. L. D., Acquah, S. F. A., Chen, G. (2005). Polyurea-functionalized multi-walled carbon nanotubes: Synthesis, morphology, and raman spectroscopy. *The Journal of Physical Chemistry B,* 109(24), 11925-11932.

Geng, B., Yang, J., Qi, Y., Zhao, J., Pang, Y., Du, J. (2004). H_2S generated by heart in rat and its effects on cardiac function. *Biochemical and Biophysical Research Communications,* 313(2), 362-368.

George, G. N., Gnida, M., Bazylinski, D. A., Prince, R. C., Pickering, I. J. (2008). X-ray absorption spectroscopy as a probe of microbial sulfur biochemistry: The nature of bacterial sulfur globules revisited. *Journal of Bacteriology,* 190(19), 6376.

George, G. N., Gorbaty, M. L. (1989). Sulfur K-edge X-ray absorption spectroscopy of petroleum asphaltenes and model compounds. *Journal of the American Chemical Society,* 111(9), 3182-3186.

George, G. N., Pickering, I. (2009), *Advanced Synchrotron X-ray Absorption Spectroscopy.* Lecture Notes, Department of Geological Sciences, University of Saskatchewan

Greyson, J. C. (1990). *Carbon, nitrogen, and sulfur pollutants and their determination in air and water.* CRC Press.

Grossman, M., Lee, M., Prince, R., Garrett, K., George, G., Pickering, I. (1999). Microbial desulfurization of a crude oil middle-distillate fraction: Analysis of the extent of sulfur removal and the effect of removal on remaining sulfur. *Applied and Environmental Microbiology,* 65(1), 181.

Guo, Z., Ding, J., Xiao, Y., Xing, D. (2007). Raman frequency shift in oxygen-functionalized carbon nanotubes. *Nanotechnology,* 18, 465706.

Hay, S. J., Metson, J. B., Hyland, M. M. (2004). Sulfur speciation in aluminum smelting anodes. *Industrial & Engineering Chemistry Research,* 43(7), 1690-1700.

Hemraj-Benny, T., Banerjee, S., Sambasivan, S., Balasubramanian, M., Fischer, D. A., Eres, G. (2006). Near-edge X-ray absorption fine structure spectroscopy as a tool for investigating nanomaterials. *Small,* 2(1), 26-35.

Hongwei, Z., Bingqing, W. (2008). Assembly and applications of carbon nanotube thin films. *Journal of Materials Sciences and Technology,* 24(04), 447-456.

Hosoki, R., Matsuki, N., Kimura, H. (1997). The possible role of hydrogen sulfide as an endogenous smooth muscle relaxant in synergy with nitric oxide. *Biochemical and Biophysical Research Communications,* 237(3), 527-531.

Hugh F.H. (1976). The plasma proteins: Structure, function, and genetic control: Second edition, volume 1, edited by frank W. Putnam. Academic press, New York, 1975. 481 pp., $37.50. *Clinical Immunology and Immunopathology,* 6(1), 123-123.

Iijima, S. (1991). Helical microtubules of graphitic carbon. *Nature,* 354(6348), 56-58.

Jalilehvand, F. (2006). Sulfur: Not a "silent" element any more. *Chemical Society Reviews,* 35(12), 1256-1268.

Jorio, A., Pimenta, M., Souza Filho, A., Saito, R., Dresselhaus, G., Dresselhaus, M. (2003). Characterizing carbon nanotube samples with resonance raman scattering. *New Journal of Physics,* 5, 139.

Jorio, A., Saito, R., Hafner, J., Lieber, C., Hunter, M., McClure, T. (2001). Structural (n, m) determination of isolated single-wall carbon nanotubes by resonant raman scattering. *Physical Review Letters,* 86(6), 1118-1121.

Kam, N. W. S., Dai, H. (2005). Carbon nanotubes as intracellular protein transporters: Generality and biological functionality. *Journal of the American Chemical Society,* 127(16), 6021-6026.

Kamoun, P., Belardinelli, M. C., Chabli, A., Lallouchi, K., Chadefaux-Vekemans, B. (2003). Endogenous hydrogen sulfide overproduction in down syndrome. *American Journal of Medical Genetics. Part A,* 116A(3), 310-311.

Kasrai, M., Brown, J., Bancroft, G., Yin, Z., Tan, K. (1996). Sulphur characterization in coal from X-ray absorption near edge spectroscopy. *International Journal of Coal Geology,* 32(1-4), 107-135.

Khan, S. U., Morris, G. F., Hidiroglou, M. (1980). Rapid estimation of sulfide in rumen and blood with a sulfide-specific ion electrode. *Microchemical Journal,* 25(3), 388-395.

Knezovich, J. P., Steichen, D. J., Jelinski, J. A., Anderson, S. L. (1996). Sulfide tolerance of four marine species used to evaluate sediment and pore-water toxicity. *Bulletin of Environmental Contamination and Toxicology,* 57(3), 450-457.

Koningsberger, D., Prins, R. (1988). X-ray absorption: Principles, applications, techniques of EXAFS, SEXAFS and XANES. *John Wiley and Sons New York*.

Lazar Research Laboratories, Inc. (2009). *Operating Instructions: The Lazar Model LIS-146AGSCM Micro Sulfide Ion Electrode (includes built in reference electrode).*

Liu, C., Fan, Y., Liu, M., Cong, H., Cheng, H., Dresselhaus, M. (1999). Hydrogen storage in single-walled carbon nanotubes at room temperature. *Science,* 286(5442), 1127.

Mills, D. M. (2002). Third-generation hard x-ray synchrotron radiation sources: Source properties, optics, and experimental techniques *Wiley-Interscience*.

Milby, T. H., Baselt, R. C. (1999). Hydrogen sulfide poisoning: Clarification of some controversial issues. *American Journal of Industrial Medicine,* 35(2), 192-195.

Miron, G., Kristensen, E. (1993). Behavioural response of three nereid polychaetes to injection of sulfide inside burrows. *Marine Ecology-progress Series,* 101, 147-147.

Olson, K. R. (2009). Is hydrogen sulfide a circulating "gasotransmitter" in vertebrate blood? *Biochimica Et Biophysica Acta (BBA) - Bioenergetics,* 1787(7), 856-863.

Pickering, I. J., Prince, R. C., Divers, T., George, G. N. (1998). Sulfur K-edge X-ray absorption spectroscopy for determining the chemical speciation of sulfur in biological systems. *FEBS Letters,* 441(1), 11-14.

Proctor, J. E., Halsall, M. P., Ghandour, A., Dunstan, D. J. (2006). High pressure raman spectroscopy of single-walled carbon nanotubes: Effect of chemical environment on individual nanotubes and the nanotube bundle. *Journal of Physics and Chemistry of Solids,* 67(12), 2468-2472.

Puacz, W., Szahun, W., & Linke, K. (1995). Catalytic determination of sulfide in blood. *The Analyst, 120*(3), 939-941.

Rao, A., Jorio, A., Pimenta, M., Dantas, M., Saito, R., Dresselhaus, G. (2000). Polarized raman study of aligned multiwalled carbon nanotubes. *Physical Review Letters,* 84(8), 1820-1823.

Reiffenstein, R. J., Hulbert, W. C., Roth, S. H. (1992). Toxicology of hydrogen sulfide. *Annual Review of Pharmacology and Toxicology,* 32(1), 109-134.

Rompel, A., Cinco, R. M., Latimer, M. J., McDermott, A. E., Guiles, R., Quintanilha, A. (1998). Sulfur K-edge x-ray absorption spectroscopy: A spectroscopic tool to examine the redox state of S-containing metabolites *in vivo*. *Proceedings of the National Academy of Sciences of the United States of America,* 95(11), 6122.

Roth, S. H., Skrajny, B., Reiffenstein, R. J. (1995). Alteration of the morphology and neurochemistry of the developing mammalian nervous system by hydrogen sulphide. *Clinical and Experimental Pharmacology and Physiology,* 22(5), 379-380.

Salvador-Morales, C., Flahaut, E., Sim, E., Sloan, J. (2006). Complement activation and protein adsorption by carbon nanotubes. *Molecular Immunology,* 43(3), 193-201.

Sarret, G., Connan, J., Kasrai, M., Bancroft, G. M., Charrie-Duhaut, A., Lemoine, S. (1999). Chemical forms of sulfur in geological and archeological asphaltenes from middle east, France, and Spain determined by sulfur K-and L-edge X-ray absorption near-edge structure spectroscopy. *Geochimica Et Cosmochimica Acta,* 63(22), 3767-3779.

Sheppard, C. J. R., Shotton, D. M., Sheppard, C. (1997). *Confocal laser scanning microscopy.* BIOS Scientific Publisher, Oxford, UK.

Shier, D., Lewis, R., Butler, J. (2002). *Hole's Human Anatomy & Physiology*, 9th ed., McGraw Hill.

Shim, M., Kam, N. W. S., Chen, R. J., Li, Y., Dai, H. (2002). Functionalization of carbon nanotubes for biocompatibility and biomolecular recognition. *Nano Letters,* 2(4), 285-288.

Sidorov, A. N., Pabba, S., Hewaparakrama, K. P., Cohn, R. W., Sumanasekera, G. (2008). Side-by-side comparison of raman spectra of anchored and suspended carbon nanomaterials. *Nanotechnology,* 19, 195708.

Skoog, D. A., Holler, F. J., Nieman, T. A. (1998). *Principles of instrumental analysis* (5th ed.). Philadelphia: Saunders College Pub.

Solomon, E. I., Hanson, M. A. (1999). *Inorganic electronic structure and spectroscopy* (pp. 106). New York: John Wiley & Sons.

Solomon, D., Lehmann, J., Martinez, C. E. (2003). Sulfur K-edge XANES spectroscopy as a tool for understanding sulfur dynamics in soil organic matter. *Soil Science Society of America Journal,* 67(6), 17-21.

Souza Filho, A., Jorio, A., Samsonidze, G. G., Dresselhaus, G., Saito, R., Dresselhaus, M. (2003). Raman spectroscopy for probing chemically/physically induced phenomena in carbon nanotubes. *Nanotechnology,* 14, 1130-1139.

Stöhr, J. (1992). *NEXAFS spectroscopy*. Springer, Heidelberg.

Sullivan, M. E., Klosterman, D., Palmese, G. R. (2007). Electron beam modification and functionalization of MWNT for covalent dispersion into polymeric systems. *Nuclear Instruments and Methods in Physics Research Section B: Beam Interactions with Materials and Atoms,* 265(1), 352-355.

Tang, X., Zhao, Y., Jiao, Q., Cao, Y. (2010). Hydrogenation of multi-walled carbon nanotubes in ethylenediamine. *Fullerenes, Nanotubes and Carbon Nanostructures,* 18(1), 14-23.

Thompson, A., Attwood, D., Gullikson, E., Howells, M., Kim, K., Kirz, J. (2001). X-ray data booklet. *Lawrence Berkeley National Laboratory,* 1–38.

Thomsen, C., Reich, S., Jantoljak, H., Loa, I., Syassen, K., Burghard, M. (1999). Raman spectroscopy on single-and multi-walled nanotubes under high pressure. *Applied Physics A: Materials Science & Processing,* 69(3), 309-312.

Ubuka, T. (2002). Assay methods and biological roles of labile sulfur in animal tissues. *Journal of Chromatography B,* 781(1-2), 227-249.

Wang, R. (1998). Resurgence of carbon monoxide: An endogenous gaseous vasorelaxing factor. *Canadian Journal of Physiology and Pharmacology,* 76(1), 1-15.

Wang, R. (2002). Two's company, three's a crowd: Can H_2S be the third endogenous gaseous transmitter? *The FASEB Journal,* 16(13), 1792.

Wang, R. (2003). The gasotransmitter role of hydrogen sulfide. *Antioxidants and Redox Signaling,* 5(4), 493-501.

Wang, R. (Ed.). (2004), *Signal Transduction and the Gasotransmitters: NO, CO, and H_2S in Biology and Medicine*, Humana Press, Totowa, N.J.

Wang, R. (2003). The gasotransmitter role of hydrogen sulfide. *Antioxidants and Redox Signaling, 5*(4), 493-501.

Whitfield, N. L., Kreimier, E. L., Verdial, F. C., Skovgaard, N., Olson, K. R. (2008). Reappraisal of H2S/sulfide concentration in vertebrate blood and its potential

significance in ischemic preconditioning and vascular signaling. *American Journal of Physiology- Regulatory, Integrative and Comparative Physiology,* 294(6), R1930.

Wu, D. Q. (2006). *An experimental study of the measurement of low concentration hydrogen sulfide in an aqueous solution.* Master's thesis, University of Saskatchewan.

Wu, X. C., Zhang, W. J., Sammynaiken, R., Meng, Q. H., Yang, Q. Q., Zhan, E. (2008). Non-functionalized carbon nanotube binding with hemoglobin. *Colloids and Surfaces B: Biointerfaces,* 65(1), 146-149.

Wu, X.C., Sammynaiken, R., Zhang, W., Wu, D., Yang, Q., Yang, W. (2007). Measurement of low concentration and nano-quantity hydrogen sulfide in aqueous solution. *Measurement Science and Technology,* 18, 1315-1320.

Wu, X.C., Zhang, W., Wang, R., Meng, Q., Wu, D., Sammynaiken, R. (2009). Measurement of low concentration and nano quantity hydrogen sulfide in serum using unfunctionalized carbon nanotubes. *Measurement Science and Technology,* 20, 105801

Wu, X.C., Zhang, W.J., Wu, D., Sammynaiken, R., Wang, R., Yang, Q. (2006). Using carbon nanotubes to absorb low-concentration hydrogen sulfide in fluid. *IEEE Transactions on NanoBioscience,* 5(3), 204.

Wu, X.C. (2007). *Measurement of low concentration and nano quantity hydrogen sulfide by carbon nanotube.* Doctoral dissertation, University of Saskatchewan.

Yagi, S., Matsumura, K., Nakano, Y., Ikenaga, E., Sardar, S. A., Syed, J. A. (2003). Adsorption behavior of sulfur-containing amino acid molecule on transition metal

surface studied by S K-edge NEXAFS. *Nuclear Instruments and Methods in Physics Research Section B: Beam Interactions with Materials and Atoms,* 199, 244-248.

Zhang H.H., B. Hedman and K. O. Hodgson (1999), in Inorganic electronic structure and spectroscopy, ed. E. I. Solomon and A. B. P. Lever, John Wiley & Sons, New York, vol. I, 513–517.

Zhao, X., Ando, Y., Qin, L. C., Kataura, H., Maniwa, Y., Saito, R. (2002). Radial breathing modes of multi-walled carbon nanotubes. *Chemical Physics Letters,* 361(1-2), 169-174.

APPENDIX A: Sulfur K-edge XANES Measurement for H_2S Water Solution

The appendix includes Sulfur K-edge XANES spectra of SWNT treated with H_2S water solution. Sulfur signal was observed in the spectra, which indicate the presence of sulfur on CNTs. The results provided the evidence of the adsorption of H_2S by CNT.

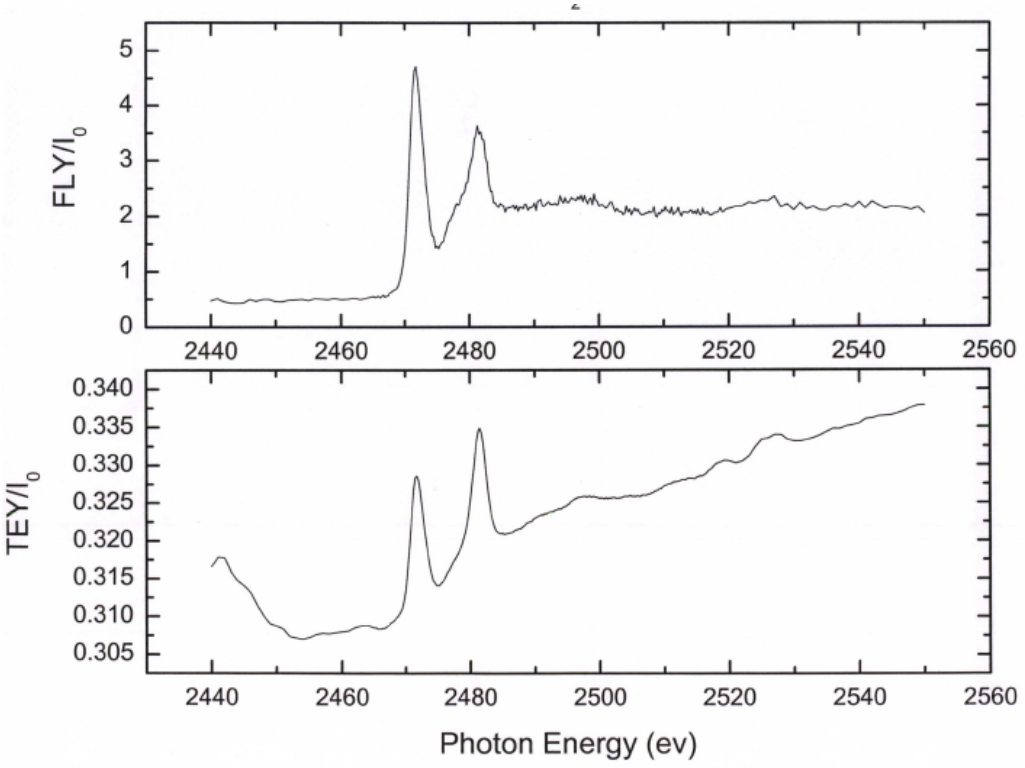

Figure A1. Sulfur K-edge XANES spectra of SWNT treated with 50 μM H_2S water solution.

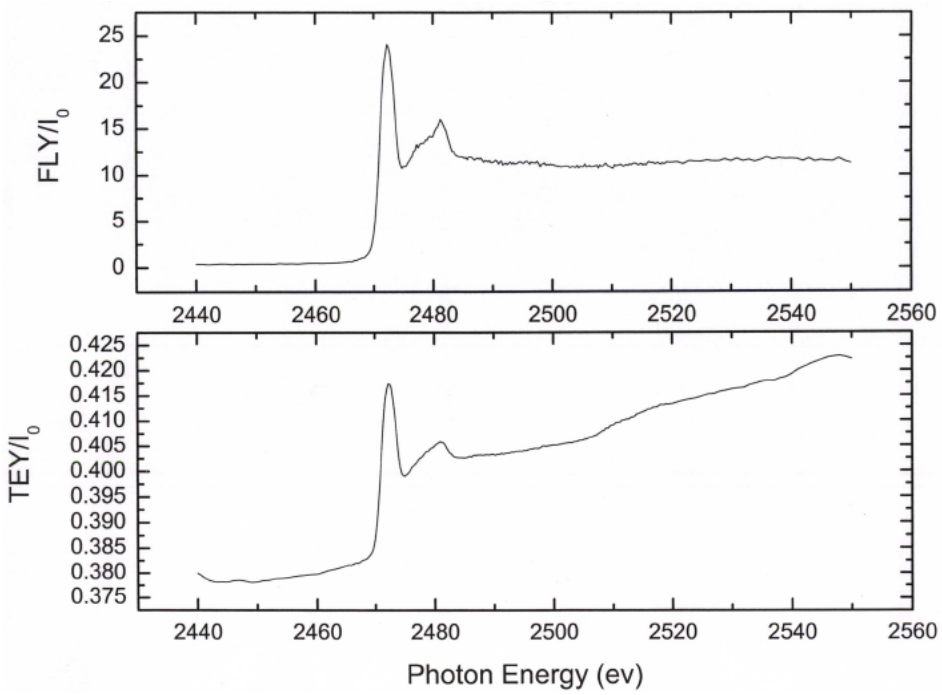

Figure A2. Sulfur K-edge XANES spectra of SWNT treated with 100 μM H_2S water solution.

Figure A3. The dried CNT samples were put on the carbon tapes before XANES measurement.

Figure A4. CNT samples were ready for XANES measurement.

Figure A5. High vacuum chamber at soft X-ray micro-characterization beamline (SXRMB) in Canadian Light Source (CLS).

Figure A6: Workstation at SXRMB for XANES data acquisition and analysis.

APPENDIX B: Nitrogen K-edge XANES for SWNT Treated with Serum

Nitrogen K-edge XANES measurement was performed on the SWNT samples treated with fetal bovine serum. It can be seen from Figure B1 that the spectrum of pure SWNT sample is almost featureless as expected of pure SWNT without nitrogen. A new peak appeared at around 403 eV in the spectrum of SWNT treated with the serum. The peak represents the existence of Nitrogen, and thus indicates the presence of proteins on SWNT.

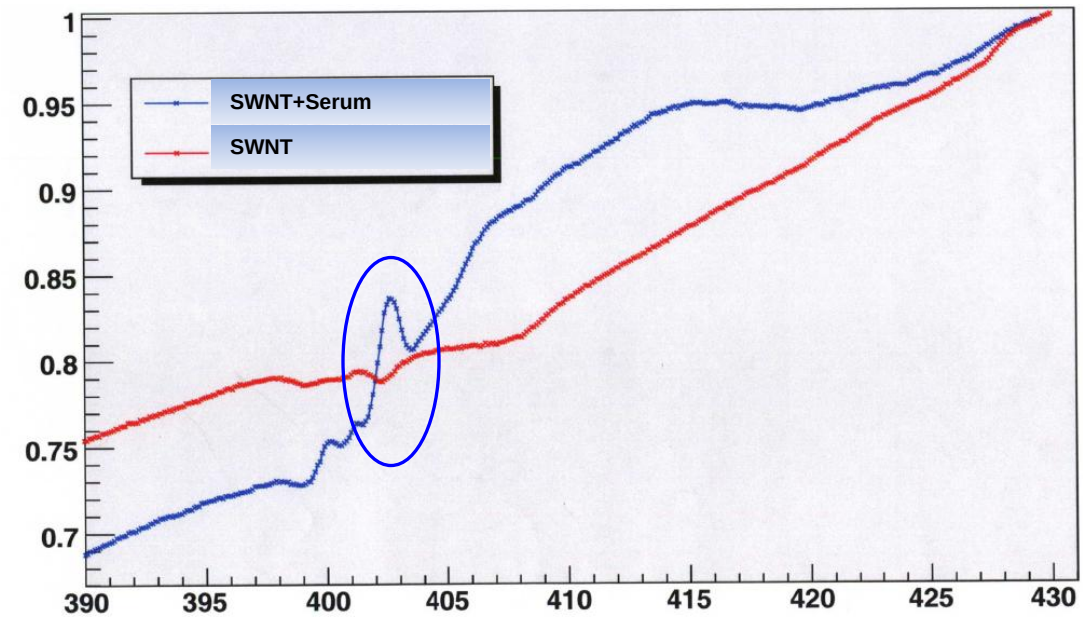

Figure B1. Nitrogen K-edge XANES spectra of pure SWNT, and SWNT treated with fetal bovine serum.

APPENDIX C: Raman Spectra of CNTs Treated with Serum

Raman spectra of SWNTs treated with fetal bovine serum were also obtained. It can been seen from Figure C1 and Table C1 that the spectra of SWNTs treated with the serum show the similar band shift as SWNT treated with BSA and globulin. This indicates that the proteins are adsorbed on SWNT in the serum. As discussed in Chapter 5, Raman spectra seem unable to differentiate the binding of BSA and globulin, because they both showed the same band shift, thus in the serum it is possible both of the proteins would bind to CNTs or one of the proteins, likely BSA, would be dominated since BSA has over twice amount as that of globulin.

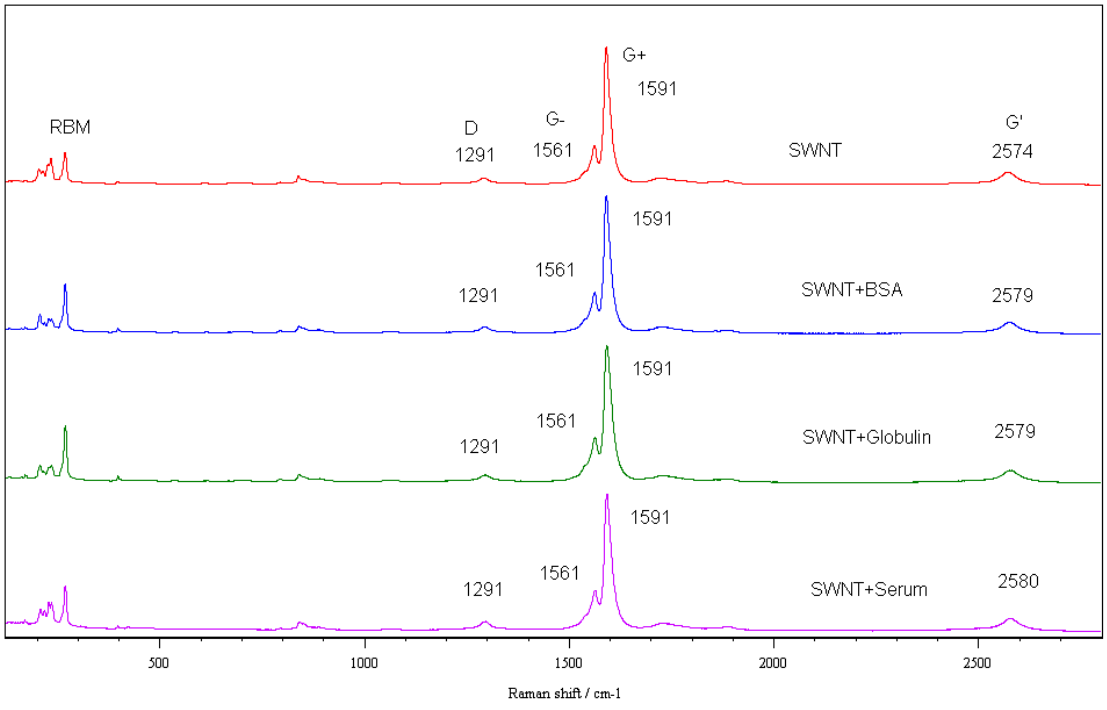

Figure C1: Raman spectra of SWNT treated with distilled water, BSA, globulin and serum.

Table C1. Band positions SWNT treated with distilled water, BSA, globulin and serum.

CNT	D	G-	G+	G'
SWNT 1	1291	1561	1591	2574
SWNT 2	1290	1561	1591	2573
SWNT 3	1291	1561	1590	2574
SWNT+BSA 1	1291	1561	1591	2580
SWNT+BSA 2	1292	1560	1590	2579
SWNT+BSA 3	1291	1561	1591	2580
SWNT+r-G 1	1291	1561	1591	2579
SWNT+r-G 2	1291	1560	1590	2579
SWNT+r-G 3	1290	1561	1591	2580
SWNT+serum 1	1290	1561	1591	2580
SWNT+serum 2	1291	1562	1592	2579
SWNT+serum 3	1292	1561	1591	2580